2017

Characterization of kinetics and performance in a microbial fuel cell supplied with synthetic landfill leachate

Zhimin Song
Michigan Technological University, zhimins@mtu.edu

CHARACTERIZATION OF KINETICS AND PERFORMANCE IN A MICROBIAL FUEL CELL SUPPLIED WITH SYNTHETIC LANDFILL LEACHATE

By

Zhimin Song

A THESIS

Submitted in partial fulfillment of the requirements for the degree of

MASTER OF SCIENCE

In Environmental Engineering

MICHIGAN TECHNOLOGICAL UNIVERSITY

2017

This thesis has been approved in partial fulfillment of the requirements for the Degree of MASTER OF SCIENCE in Environmental Engineering.

Department of Civil and Environmental Engineering

Thesis Advisor: *Dr. Jennifer Becker*

Committee Member: *Dr. Eric Seagren*

Committee Member: *Dr. Wen Zhou*

Department Chair: *Dr. David Hand*

Table of Contents

List of Figures

List of Tables

Acknowledgements

I would like to thank my advisor, Dr. Jennifer Becker, for offering me the opportunities to work on this project. This project cannot be finished without the excellent guidance and technical support from Dr. Becker during the past two years. Also, I would like to thank my committee members, Dr. Eric Seagren and Dr. Wen Zhou for the support and the guidance throughout my graduate studies.

I would like to thank my lab mates, Lindsey, Christa, Erinn, and Sara, for the help and assistance with my experiments whenever I need in the lab for the past two years. I really appreciate the help you gave, the assistance you offered, and the questions you took time to answer. As an international student from China, I really appreciate the friendship we build and the happiness I got after joining this great group.

I would also like to thank Rob Fritz for the construction of the reactors in this project. Special thanks are due to Mr. Dave Perram, who helps a lot in assisting the development and maintenance of the analytical equipment and also offering his expertise and guidance for the operation whenever I need.

Abstract

Biodegradable municipal solid waste (MSW) is rich in biochemical energy; however, much of this energy is sequestered in conventional landfills. Although bioreactor landfills enhance conversion of MSW to methane, the generated methane is a potent greenhouse gas and cannot be fully captured in landfills. Microbial fuel cells (MFCs) can directly convert the biochemical energy in MSW to electricity, treat leachate, extend landfill longevity, and minimize fugitive methane emissions. However, the electricity production from MFCs cannot yet meet the energy demands of treatment and improvements in the performance of leachate-fed MFCs are needed. Effective approaches for the design and operation of MFCs are currently lacking. Therefore, the goals of this study are to (1) improve our understanding of the effect of substrate concentration and organic loading rate on the performance of MFCs, and (2) estimate the kinetics parameters needed for the modeling of MFC-leachate treatment systems. These goals were achieved by generating synthetic leachate using a laboratory-scale bioreactor landfill filled with shredded paper, food waste, and dry dog food. The leachate was diluted to different substrate (chemical oxygen demand, COD) concentrations until steady-state current production was achieved at a given COD loading rate. Voltage in the MFC was measured continuously and, along with steady-state measurements of COD removal in the MFC, was used to estimate microbial kinetic parameters in the MFC and determine the optimal conditions for current production, the conversion of biochemical substrates to electricity (coulombic efficiency), and COD removal. This study will help inform the future design and operation of bioreactor landfill-

MFC treatment systems to achieve more effective leachate treatment as well as more efficient electricity generation.

Chapter 1: Introduction

1.1 Motivation

In 2012, around 135 million tons of municipal solid waste (MSW) were sent to landfills, which accounted for 54% of the total MSW generated in the United States [1]. The major categories of MSW in U.S. are shown in Figure 1.1. Most of the fractions are biodegradable, including paper, food waste and yard trimmings. Biodegradable MSW is rich in biochemical energy; however, much of this energy is sequestered in conventional landfills, which lack the moisture needed for efficient biological decomposition of MSW. Currently, there are two primary options for energy recovery from MSW. In the landfill-gas-to-energy approach, MSW is anaerobically converted to CH_4 in landfill bioreactors that incorporate leachate recycling to optimise biodegradation. The CH_4 generated is then combusted to produce electricity and, in some cases, thermal energy. In the waste-to-energy approach, MSW is combusted directly and used to power steam generators or thermally converted to combustible products. In addition to CH_4, anaerobic decomposition of biodegradable solid wastes in landfills produces the greenhouse gases (GHGs) carbon dioxide and nitrous oxide. Therefore, the current options for recovering energy from biodegradable MSW create concerns about greenhouse gas emissions (GHG) and air pollution, respectively.

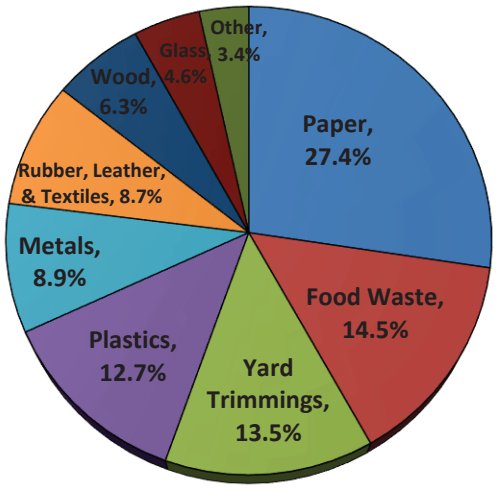

Figure 1.1 Composition of MSW generated in the United States in 2012 (before recycling) [1].

The leachate generated from landfills contains high concentrations of organic matter (both biodegradable and refractory), inorganic salts, and heavy metals [2-5]. Treatment of these complex and variable waste streams is technically challenging and comes at a high cost. It is estimated that the expenses associated with leachate treatment represent 50% to 67% of the total landfilling costs [6]. Given the size and importance of this industry, which generated an estimated annual revenue of $55 billion in 2011 [7, 8], improvements in the efficiency of treatment and energy usage in leachate treatment could significantly influence the economics and environmental impacts of MSW disposal.

Microbial fuel cells (MFCs) offer the potential to treat and recover energy from waste streams [9]. In MFCs, bacteria oxidize an electron donor substrate and transfer the electrons that are generated to an anode, which can be connected to an external circuit to do useful electric work [10-12]. A growing number of complex materials have been used

as a source of electron donors to fuel MFCs, including marine sediments [13], domestic wastewater [14], chocolate industry wastewater [15], meat processing wastewater [16], and urine [17]. In contrast to methanogenic biological processes, MFCs do not require heating, which consumes a large amount of thermal energy, nor do they produce the potent GHG methane. Consequently, there is growing interest in using MFCs to treat and recover energy from landfill leachate [18-23].

While several studies have examined leachate treatment using MFCs, to date, the electricity production has been low relative to the energy demands of treatment [24]. The underperformance of leachate-fed MFCs is largely due to the lack of knowledge about how to effectively design and operate MFCs. In contrast, extensive amounts of empirical data and a theoretical framework can be used to design effective treatment systems based on more mature biological technologies (such as activated sludge). Another challenge is that the concentration and biodegradability of organics and ammonia concentration in leachate change dramatically over time. This is important for MFCs because there is a trade-off between power production and the efficiency of conversion of biochemical energy to electricity (coulombic efficiency, CE) at different loading rates. For example, Ozkaya *et al.* [22] operated leachate-fed MFCs at different organic loading rate (OLR) and observed that a higher OLR resulted in a higher power output, but lower CE. Therefore, additional information is needed to understand how key parameters affect these performance criteria and design effective and efficient MFCs for treatment of leachate and other waste streams.

1.2 Project goal and objectives

The overall goal of this project is to determine how two key design parameters, the electron donor substrate concentration, and the loading rate, affect the treatment and electrochemical performance in an MFC treating synthetic landfill leachate.

Specifically, the objectives of this research project are to:

1) Characterize the relationships between leachate concentration and organic loading rate and the performance (measured as current density, coulombic efficiency, and COD removal of a continuous-flow MFC.
2) Determine the leachate concentration and organic loading rate that achieve optimal performance of a continuous-flow MFC supplied with synthetic landfill leachate.
3) Estimate the anode respiration kinetic parameters for modeling MFC-based leachate treatment systems.

Chapter 2: Literature Review

2.1 Introduction

This chapter includes a review of the literature on MFCs and landfill leachate characteristics and their treatment. Specifically, the following topics are discussed in this chapter: typical compositions of landfill leachate, landfill leachate treatment technologies, basic information about MFCs and their application to leachate treatment, and the state of the knowledge of MFC design.

2.2 MSW landfill leachate production and composition

In a conventional landfill, leachate is produced by the percolation of rainfall, surface water, and the liquid generated from the decomposition of the wastes. Table 2.1 summarizes some of the key constituents and their concentration ranges in conventional landfill leachate during the whole lifespan compiled by Kjeldsen *et al.* [3]. In anaerobic landfill bioreactors, water is generally added to the landfilled MSW to ensure that moisture levels are optimal for biodegradation and to help rapidly establish anaerobic conditions. The leachate is collected and recirculated through landfill bioreactors.

Table 2.1 Composition of conventional landfill leachate [3]

Parameter	Concentration range (Values in mg/L unless otherwise noted)
pH	4.5-9
Specific conductivity	2500-35,000 µs/cm
Total solids	2000-60,000
Heavy Metals	
Arsenic	0.01-1
Cadmium	0.0001-0.4
Chromium	0.02-1.5
Cobalt	0.005-1.5
Copper	0.005-10
Lead	0.001-5
Mercury	0.00005-0.16
Nickel	0.015-13
Zinc	0.03-1,000
Inorganic components	
Ammonium-N	50-2,200
Calcium	10-7,200
Chloride	150-4,500
Bicarbonate	610-7,320
Iron	3-5,500
Magnesium	30-15,000
Manganese	0.03-1,400
Potassium	50-3,700
Silica	4-70
Sodium	70-7,700
Sulphate	8-7,750
Total Phosphorous	0.1-23
Organic matter	
Biological Oxygen Demand (BOD_5)	20-57,000
Chemical Oxygen Demand (COD)	140-152,000
Organic nitrogen	14-2,500
Total organic carbon	30-29,000

As shown in Table 2.1, the composition of conventional landfill leachate is highly variable. It is influenced by several factors, including biological activity, the infiltration rate, the nature of the landfilled materials, climatic conditions and, especially, the landfill age/phase, as shown in Figure 2.1 [25-27].

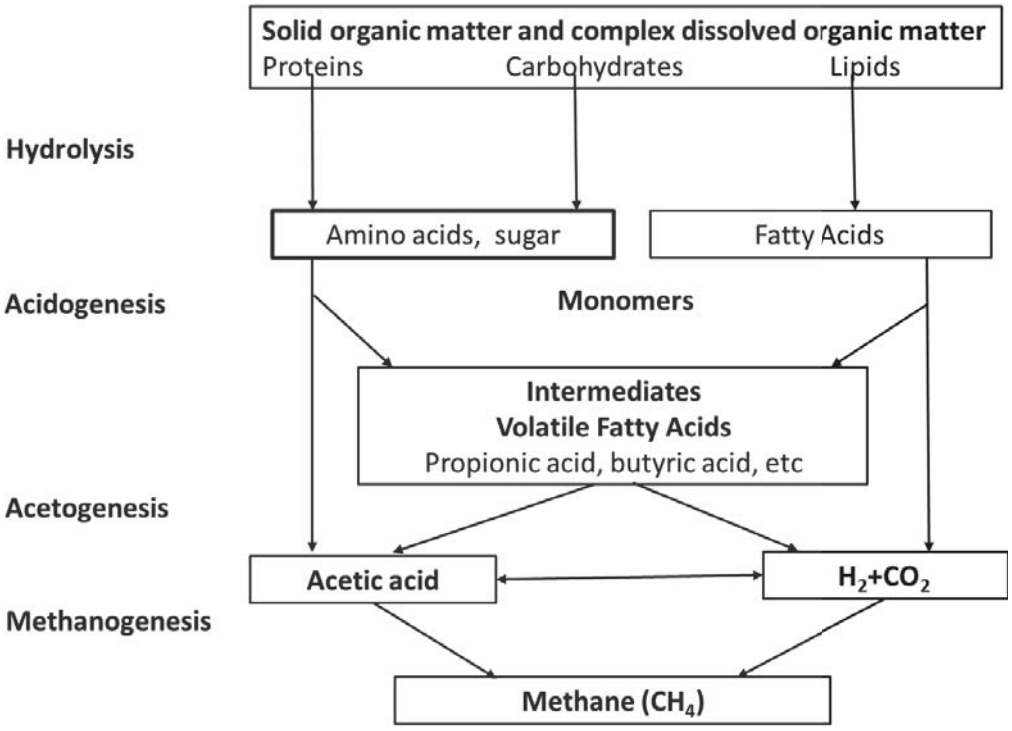

Figure 2.1 Degradation steps of an anaerobic digestion process. Adapted from [28].

The landfill age or phase impacts leachate composition through the biodegradation of MSW under anaerobic conditions. Typically, this leads to the formation of methane via four interrelated processes: hydrolysis, acidogenesis, acetogenesis, and methanogenesis, as shown in Figure 2.1 [28]. In hydrolysis, complex solid and aqueous organics are converted to monomers and polymers via hydrolytic reactions. At the acidogenesis stage, fermentative bacteria produce volatile fatty acids (VFAs) from the monomeric units, which

are converted into acetic acid, carbon dioxide, and hydrogen at the acetogenesis stage. In methanogenesis, acetate, H_2, and CO_2 are converted to methane [29].

Several changes in leachate composition are linked to these fermentative and methanogenic processes. Anaerobic conditions are established within a couple of months due to the depletion of oxygen by aerobic bacteria in Phase I (Fig. 2.2). The activity of acetogenic and fermentative bacteria generates VFAs, as noted above, causing the pH to drop (Phase II), and an increase in the biological oxygen demand (BOD) values in this phase [30]. During the initial methanogenic phase (Phase III), slow growth of methanogens occurs. In the stable methanogenic phase (Phase IV), methane production rates reach their maximum.

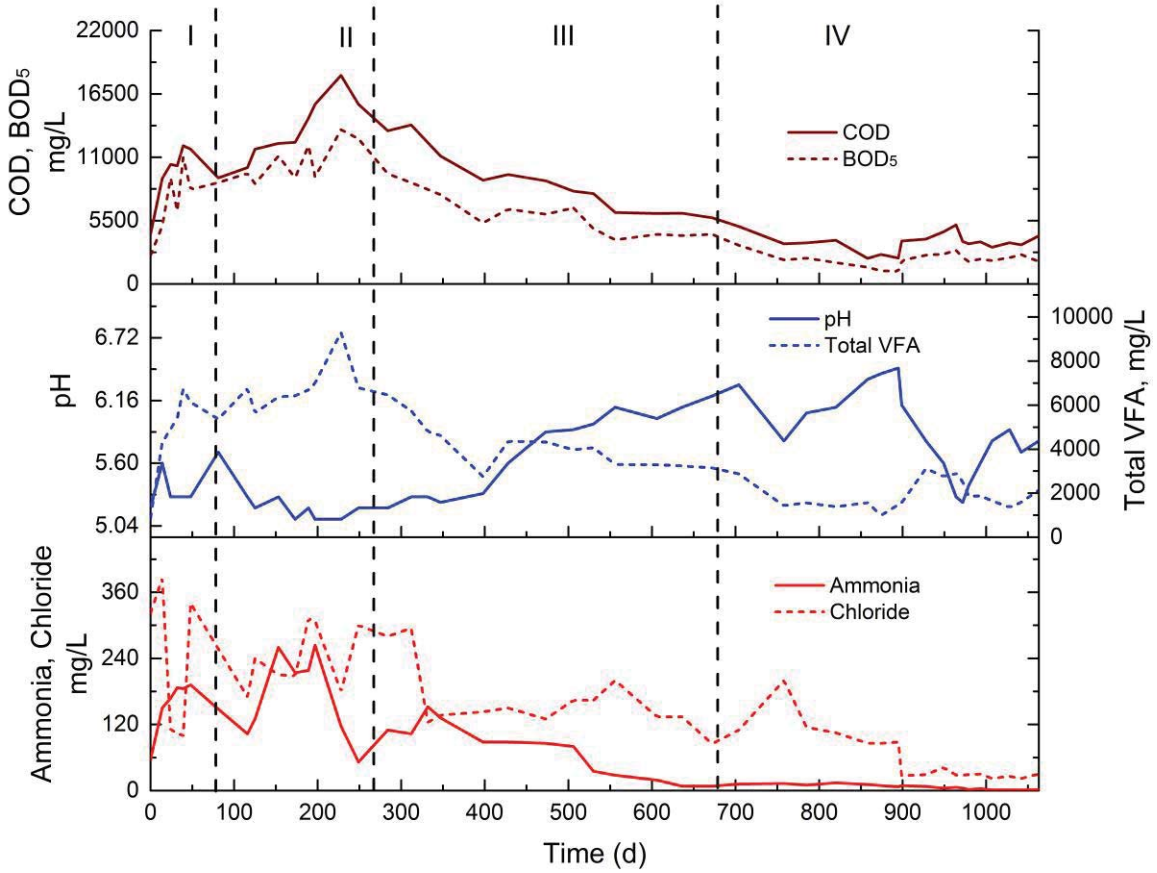

Figure 2.2 Generalized pattern of leachate COD, BOD5, total volatile fatty acid (TVFA) production, ammonia, chloride, and pH over time. Data were adapted from [31], and the graph was created by the author.

I. Initial aerobic phase, II. Anaerobic acid phase, III. Initial methanogenic phase, IV. Stable methanogenic phase.

2.3 Leachate management options

Currently, there are three major approaches for treating conventional landfill leachate: (1) recycling of leachate into the landfill, (2) treatment at a municipal wastewater treatment plant via aerobic and anaerobic biodegradation, and (3) treatment via physical and chemical

methods.[32, 33]. In many cases, combinations of these methods are used to achieve leachate treatment.

Each of these treatment approaches has drawbacks. Recycling of leachate increases the moisture content and waste biodegradation rate in landfill bioreactors [34]. But the high recirculation rates of the leachate may inhibit the anaerobic degradation and result in high concentrations of organic acids, which further affect the methanogenesis process [33, 35-37]. Municipal sewage treatment has low operating costs, but the leachate after treatment still contains hazardous heavy metals and low-biodegradable compounds.

The physical-chemical processes used in leachate treatment include adsorption, air stripping, chemical oxidation, coagulation, and flotation. These processes usually require significant inputs of chemicals and/or energy. The major concern associated with air stripping is the release of NH_3 during the treatment [32].

Biological processes have several advantages over physical-chemical processes because they achieve leachate treatment without adding chemicals or transferring pollutants to another phase. However, while aerobic biological processes are effective for COD removal, they are energy intensive and not suitable for treatment of high-strength leachate. Compared with aerobic processes, anaerobic treatment consumes less energy and is an effective method for high-strength waste treatment. Anaerobic treatment technologies include those based on methanogenic processes and MFCs. Both approaches offer the potential for energy recovery during treatment of leachate and other high-strength waste

streams. However, in methanogenic processes, a significant amount of the methane product is generally consumed in bioreactor heating. In contrast, in MFCs, the biochemical energy in wastewater is converted directly to electricity. Thus, the potential for GHG production is also lower with MFCs, compared with methanogenic processes. Theoretically, MFCs offer the potential to achieve energy neutral, or even energy positive, treatment [38].

Several researchers have examined the possibility of treating landfill leachate by MFCs [23, 39, 40]. For example, Puig et al. [41] found that MFCs can be used to treat leachate with a high nitrogen content (6033 mg N/L) and high salinity, corresponding to a conductivity of 73,588 μS/cm. The maximum power density is 344 mW/m^3 at a loading rate of 8.5 kg $COD/m^3 \cdot d$. You *et al.* achieved a power density of 6,817 mW/m^3 in a 40-mL, single-chambered, leachate-fed MFC [42].

2.4 Microbial fuel cells

2.4.1 Basics of current production in MFCs

Microbial fuel cells adopt certain bacteria to digest waste or biomass and at the same time produce electricity. Several different kinds of bacteria have been used in MFCs for the generating of electricity with different coulombic efficiencies, such as the *Geobacter sulfurreducens*, *Rhodoferax ferrireducens*, *Shewanella oneidensis* DSP10 [43]. Most of these bacteria can be found in wastewater, so wastewater can be used as inoculum. Almost all the biodegradable chemicals can be used as electron donors, which means MFCs can be used in treating swine wastewater [44], and landfill leachate [42] and sludge [45]. MFC is

also a possible denitrification technology that can quickly reduce the majority of NO_3^- in groundwater into N_2 with a low-maintenance and low-cost design [46].

2.4.2 Energetics of anode-respiring bacteria and MFCs

Respiratory bacteria oxidize electron donor substrates. The electron equivalents are transferred as hydrogen atoms via nicotinamide adenine dinucleotide (NADH) to an electron transport chain in the cell membrane. A proton gradient is created as the electrons flow through the respiratory chain and protons are transported outside the cell. The influx of protons back into the cell is coupled to the production of the energy storage molecule, adenosine triphosphate (ATP). The amount of energy that can be conserved by bacteria in the form of ATP is proportional to the difference in the potential of the electron donor, NADH, and the terminal electron acceptor in the respiratory chain. The greatest amount of energy can be conserved by bacteria respiring O_2 (Figure 2.3). Therefore, O_2 must be excluded from the anode compartment in order for anode respiration to occur. In the absence of O_2 and other soluble electron acceptors, anode respiring bacteria (ARB) will transfer electrons to a solid anode. In this mode of metabolism, the electrons leave the electron transport chain at a lower redox potential than that of O_2, e.g., at *cytochrome c* in *Paracoccus denitrificans* (Figure 2.3). Thus, the amount of energy conserved by *Paracoccus denitrificans* is proportional to the potential difference between NADH and *cytochrome c* (Figure 2.3). The fraction of the energy released by the oxidation of the electron donor substrate that is captured in the MFC is proportional to the potential difference between *cytochrome c* and O_2 [47].

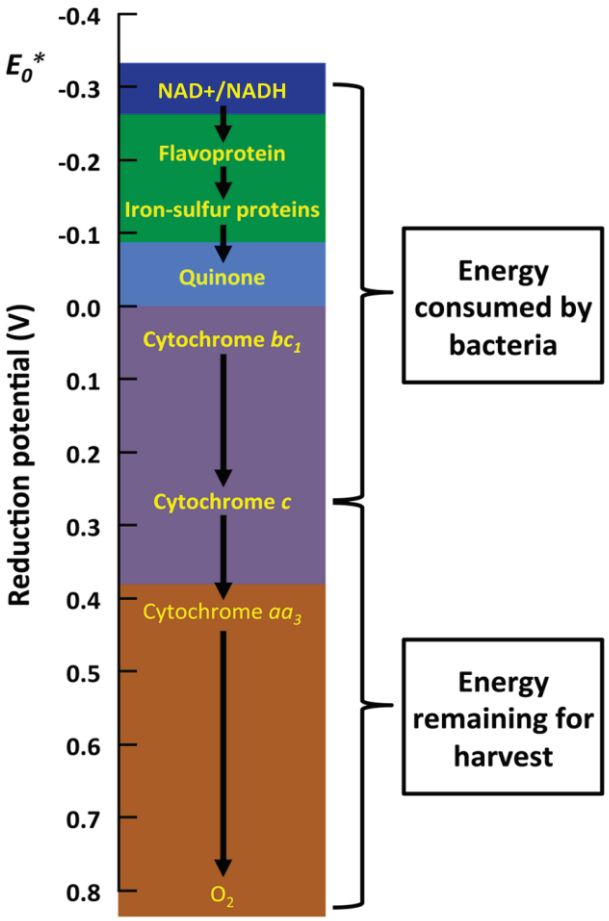

Figure 2.3 Theory of energy conservation by anode-respiring bacteria (ARB) and energy capture in MFCs illustrated using the respiratory chain of *Paracoccus denitrificans* [48, 49]. Other ARB may utilize other respiratory enzymes. Adapted from [48] drawn by the author.

The key components in an MFC include the anode, cathode, electrolyte, and an external circuit that connects the anode and cathode and provides external resistance, e.g., in the form or a resistor. The anode-respiring bacteria can oxidize the organic compounds and transfer electrons to the anode (Figure 2.4). The potential differences between the anode and the cathode then drive the electrons to move in the external circuit and generate

electricity. The system can be used as power sources (e.g., charge a battery, or electrically powered device (Figure 2.4). ARB oxidizes electron donor substrates and transfers electrons to the anode, as described above. The transfer of an electron to the anode is accompanied by the transport of a proton out of the anode compartment. Electrons flow through the external circuit to the cathode. At the cathode, H^+, electrons, and O_2 react with each other to produce water. The anode and cathode are separated by a proton exchange membrane (PEM). A multimeter and a computer can be used to record the voltage generated by the MFC [47]. Ferricyanide can replace O_2 as the electron acceptor at the cathode and may increase the power density 1.5 to 1.8 times compared with dissolved oxygen [47, 50].

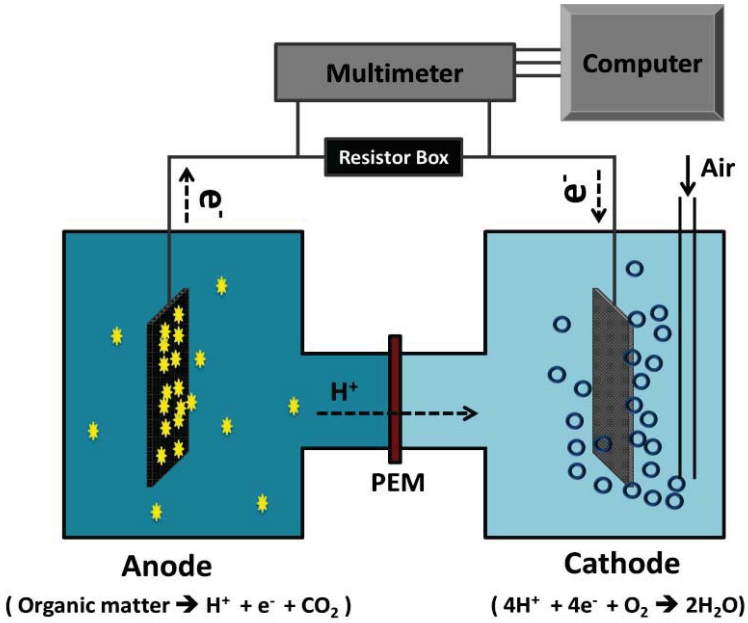

Figure 2.4 Key MFC components and processes. Adapted from [12] and drawn the by the author.

Using acetate as the electron donor, the reactions occurring at the MFC anode and cathode chamber are given by Equations 2-1 and 2-2, respectively.

$$CH_3COO^- + 3H_2O \rightarrow CO_2 + HCO_3^- + 8e^- + 8H^+ \quad (2\text{-}1)$$

$$2O_2 + 8e^- + 8H^+ \rightarrow CO_2 + HCO_3^- + H_2O \quad (2\text{-}2)$$

Reduction half-potentials (E'_H) of -0.28 V and +0.82 V were calculated for Reactions 2-1 and 2-2, respectively, assuming pH 7 and other conditions typical of an MFC environment, as described by Logan [12]. The highest total cell potential (E'_{emf}) in an MFC is achieved under open circuit (maximum resistance conditions). According to the balanced oxidation-reduction reaction:

$$CH_3COO^- + 2O_2 \rightarrow CO_2 + HCO_3^- + H_2O \quad (2\text{-}3)$$

the E'_{emf} that can be achieved under these conditions, the open circuit voltage (OCV), is theoretically +1.1 V. However, in practice, limitations at the cathode prevent the $E'_{H,cathode}$ of +0.82 V from being achieved. Therefore, the OCV of MFCs fed with acetate is always less than 1.1 V. So far, the largest OCV obtained from an MFC with oxygen as an electron acceptor is 0.83 mV [12, 51].

2.4.3 Internal resistance and its measurement

In addition to cathode limitations, several other losses prevent the theoretical E'_{emf} from being achieved in MFCs. The actual cell potential (E_{cell}) measured with the multimeter can be described by Equation 2-4:

$$E_{cell} = OCV - IR_{int} \tag{2-4}$$

where R_{int} is the internal resistance in the MFC. Clearly, R_{int} plays a critical role in determining the performance of an MFC. With a high R_{int}, the MFC will have low output. There are several ways to reduce R_{int}, such as using an electrolyte with higher ionic conductivity [47], increasing the surface area of the carbon electrodes [12], and reducing the spacing between the anode and cathode [52].

As described by Logan [12], there are several methods that can be used to determine R_{int}, including the polarization slope method, power density peak method, electrochemical impedance spectroscopy (EIS), and the current interrupt method. The polarization slope and power density peak methods are described briefly below.

Polarization curves can be obtained either by changing the resistance of the external circuit and observing the current output or by using the linear sweep voltammetry (LSV) method with a low scanning range of the voltage [40, 53-55]. As shown in Figure 2.5, the internal resistance is calculated as the slope of the linear region of the polarization curve.

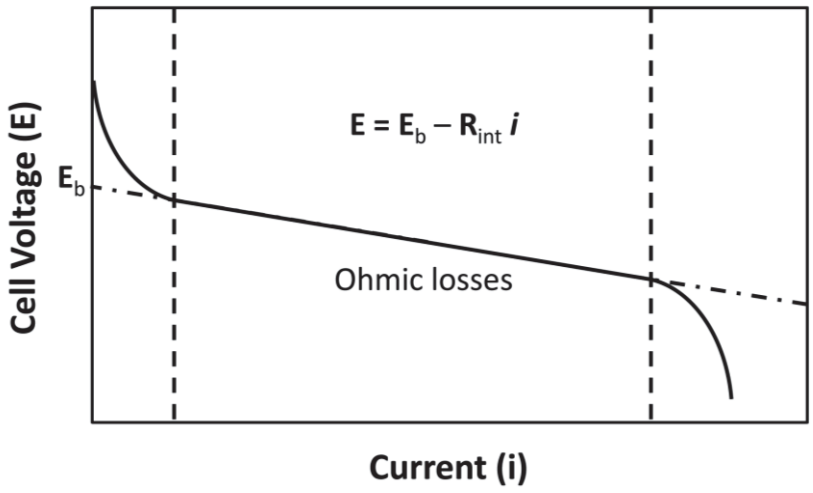

Figure 2.5 Idealized polarization curve.

The maximum power ($P_{\max}$) that can be output by an MFC is given by:

$$P_{\max} = \frac{OCV^2 R_{ext}}{\left(R_{\text{int}} + R_{ext}\right)^2} \tag{2-5}$$

where R_{ext} is the external resistance.

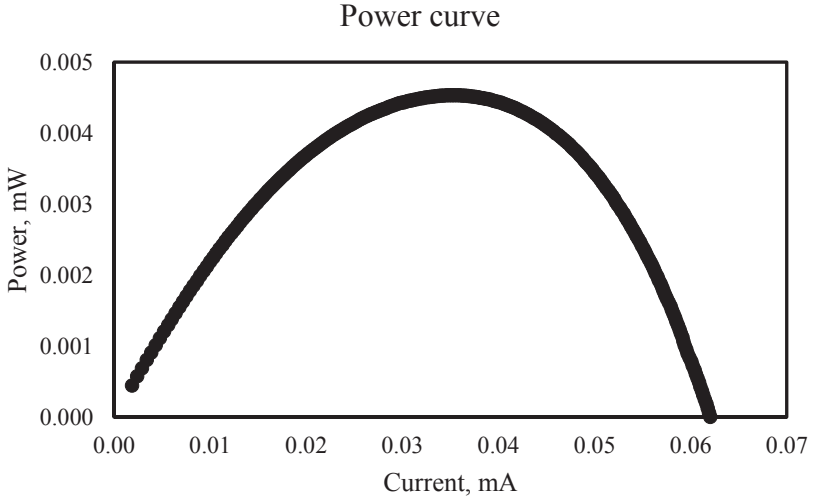

Figure 2.6 Example of power curve obtained from a leachate fed batch-MFC in this project.

According to Equation 2-5, P_{max} can be expected when $R_{int} = R_{ext}$. The R_{ext} applied when P_{max} is applied is known based on the experimental procedures. Therefore, R_{int} can be assumed to equal the R_{ext} corresponding to the P_{max} value obtained from the power curve.

2.5 MFC materials and operation

2.5.1 Electrode materials

Both the anode and cathode of the MFC should be highly conductive, stable, durable and cost effective. Materials used for MFC anodes are usually carbon based, such as carbon cloth, carbon paper, or carbon foams, because of their high electron conductivity and high surface areas. A high surface area is needed to increase the amount of active microorganisms that can attach to the anode. Graphene has 37 times more surface area than carbon fiber and 58,600 times more than carbon cloth [56]. Modifications of carbon anodes can also be used to improve the performance of the anode. Common anode modification methods include ammonia treatment [51], heat plus acid treatment [57], and electrochemical oxidation [58]. Heat-treated carbon fiber brush anodes exhibited a 15% increase in power density compared to untreated anodes [59]. Ammonia gas treatment of anodes achieved a nearly 50% increment in power density and a 20% increase in coulombic efficiency [51]. Unfortunately, the sophisticated treatment environment and equipment needed for ammonia treatment will make its use in scaled-up applications difficult [56].

The cathode materials are also typically carbon cloth or carbon paper containing Pt catalyst [12, 51, 60-62]. At the cathode, a catalyst is often used to lower the activation energy for oxygen reduction. Platinum is the most commonly used catalyst, although it is expensive. Several studies have evaluated platinum alternatives. Cheng *et al.* [63] found that when cobalt tetramethylphenylporphyrin (CoTMPP) was used as the cathode catalyst, the power density was only 12% lower than that obtained with Pt (0.5 mg/cm^2). In another study, hydrothermally synthesized, nanostructured MnO_2 was employed as the cathode catalyst in an air-cathode MFC [18]. The power density generated with MnO_2 was 119.07 mW/m^2 (or 5950 mW/m^3 based on a 50-mL anode volume) using leachate as the electron donor. This power density is close to the value obtained by You *et al*. [42] (6817 mW/m^3) using platinum as the cathode catalyst in a 40-mL, leachate-fed air-cathode MFC.

2.5.2 Inoculum methods

A variety of heterogeneous materials have been used to inoculate MFC anode compartments with ARB, including wastewater, anaerobic digester sludge, and sediment [64]. However, one potential disadvantage of using anaerobic digester sludge, as the inoculum is that it contains highly varied microbial communities. Therefore, it also introduces methanogens and other fermentative bacteria into the anode compartment, which can reduce power output and coulombic efficiency. Li *et al.* [65] evaluated the use of different waste streams, including acidic food waste leachate, domestic wastewater, anaerobic sludge, and activated sludge, as MFC inocula for the treatment of the acidic food waste leachate. They found that acidic food waste leachate itself could serve as an MFC

inoculum. Co-addition of the other inoculum sources could accelerate the MFC start-up process. The highest power and coulombic efficiency were obtained with anaerobic digester sludge as inoculum. Kim *et al.* [64] reviewed the effectiveness of a variety of inocula and procedures. They found that an MFC inoculated using biomass harvested from an existing MFC achieved a higher power density than an MFC of the same design that was inoculated with anaerobic digester sludge.

In addition to the inoculum source, the potential at which an MFC is operated also can affect the start-up time needed until steady current production is achieved because the anode potential affects the theoretical energy gained by bacteria [66]. Wang *et al.* reported that applying 0.2 V (vs. Ag/AgCl) to the working electrode can reduce the MFC start-up time [67].

2.5.3 Conductivity

As noted above, the R_{int} of an MFC plays a critical role in determining its performance, and mass transfer limitations are generally a significant component of R_{int}. The most important mass transfer limitations appear to be the transport of protons across the PEM and transport of protons to the cathode [12].

Theoretically, the use of high salinity/conductivity media should result in relatively fast proton transfer rates. Several studies have experimentally demonstrated that increasing the conductivity of the anolyte and catholyte could improve the MFC power output, but high salinity in the system can also induce adverse effects. [68-70]. Liu *et al.* [71] found

that the power output increased by 85% when 17.5 g/L NaCl was added to the anolyte. Miyahara *et al.* [72] studied the effect of NaCl concentration on anode microbes and determined the optimum NaCl concentration of 5.8 g/L by balancing salt tolerance of exoelectrogens and the solution conductivity. Lefebvre *et al.* [73] evaluated the effect of NaCl concentration on the performance of a two-chambered MFC supplied with acetate medium. They found that 20 g/L NaCl improved power output by 30%, but the highest CE was found at 5 g/L NaCl. The CE started to decrease with further increases in the NaCl concentration. Li *et al.* [69] evaluated the performance of a leachate-fed MFC supplied with 0 to 8.8 g/L NaCl. The MFC supplied with 5.8 g/L NaCl achieved the highest P_{max} and lowest R_{int}. In sum, the optimum NaCl concentration for high power density and lower internal resistance is around 5 g/L, and deviation is expected based on the different MFC configuration and medium concentrations.

2.6 Microbial fuel cell design

2.6.1 Treatment goals

Microbial fuel cell aims at a high-efficient and environmental-friendly treatment of waste water using electrochemical active bacteria, and at the same time transforming the chemical energies inside organic compounds and producing positive electricity output. So far, the application of MFCs is limited due to its relatively low power density (a few Watt per m^3) compared with batteries and chemical-based fuel cells. To increase the current and energy density of MFCs, a systematic design of the MFC configuration and operation parameters

is needed. An efficient MFC configuration should optimize the waste treatment as well as the power generation.

The anode anaerobic chamber is the key link for biochemical treatment and electrochemical power generation. Therefore, seeking the best operation parameters and studying the respiration kinetics at the anode side would be highly informative for optimizing the design of MFCs with high treatment efficiencies and maximum power generation.

2.6.2 Key design parameters

2.6.2.1 Substrate concentration

Substrate concentrations at the anode chamber directly affect the performance of the whole MFC. In general, low substrate concentrations limit the biological activities of the bacteria in the anode chamber, while high substrate concentrations may saturate the anode and impede the chemical reactions at the cathode [42]. Depending on the operation mode of the MFC (either batch or continuous), the effect of substrate concentration on the MFC performance will be different. For batch mode MFCs, the substrate concentration will reduce with the increase of operation time; however, for continuous mode MFCs, the effective substrate concentration also depends on the retention time. Several previous studies of batch MFCs treating leachate are summarized in Table 2.2.

Table 2.2 Summary of the performance of leachate-fed batch MFCs under different leachate concentration

Reactor type	Volume (mL)	Leachate concentration (mg COD/L)	Max. Power density	Max. COD or BOD removal (%)	CE [a] (%)	Reference
Dual chamber plastic bottle	125	9800	2060 mW/m^3	NR	NR	[42]
Single chambered air cathode	40	4900	6817.4 mW/m^3	98	21.2	[42]
Single chambered	934	2130±907	31 mW/m^2	27±16	17.4±15	[74]
Single chambered bucket	1890	2386	NR	74	5	[74]
Two chamber	600	1022	4200 mW/m^3	78	NR	[75]
Single chambered air cathode	300	1412-20800 mg BOD/L	NR	86	NR	[21]
Cylindrical air-cathode	570	12033±3974	49.2±2.3 mW/m^2	74.7±5.5	0.58±0.11	[23]

*a CE= coulombic efficiency; *b NR= not reported

You, *et al* [42] used single-chambered batch MFC to study the effect of leachate concentration on the performance of the MFC. A Monod-type relationship between the output power density and leachate COD concentration was observed. The maximum power density was around 5920 mW/m^3 with a COD concentration around 4900 mg/L and an external resistance of 500 Ω.

Gil, *et al* [76] used a two-chambered batch MFC to study the effect of wastewater concentration on the current output. The relationship showed similar saturation kinetics. The maximum current density increased with the wastewater concentration up to 50 mg/L, while the CE increased linearly with the concentration up to 400 mg/L.

2.6.2.2 COD loading rate

For continuous mode MFCs, the organic loading rate is another key parameter in determining the COD removal, current density, and coulombic efficiency. In general, higher organic loading rates result in the increase in current output and COD removal but decrease in coulombic efficiency [22], while further increase organic loading rate may decrease the COD removal.

Rabaey, *et al* [77] studied the effect of glucose feeding rate on the power generation and electron recovery. The removal rate of the glucose to electricity increased up to a loading rate of 3 g COD L^{-1} d^{-1}. The bacterial external electron transfer reduced when the loading rate was higher than 3.5 g L^{-1} d^{-1}. The coulombic efficiency, however, reduced from 89 % to 10 % when the loading rate increased from 0.5 to 5 g L^{-1} d^{-1}.

He, *et al* [78] used up-flow MFC to investigate the influence of organic loading rate on the power generation, soluble COD (SCOD) removal efficiency, VFA, and coulombic efficiency. The maximum power density 92.9 mW/m^2 was reached at a COD loading rate of 2.0 g COD L^{-1} d^{-1} with no further increase under higher loading rate. The coulombic

efficiency, however, reduced from 7.1 to 0.7%. The SCOD removal increased with the loading rate, with a maximum value of 97% at 3.4 g COD L^{-1} d^{-1}.

Key features of previous studies of continuous MFCs treating leachate are summarized in Table 2.3.

Table 2.3 Summary of the performance of leachate-fed continuous MFCs under different organic loading rate

Reactor type	Volume (mL)	OLR (gCOD/L· d)	HRT (d)	Power density mW/m^2 (mW/m^3)	COD (BOD) removal (%)	CE [a] (%)	Ref.
Two chambered acrylic cubic	230	0.9-1.4	5	158	NR[b]	NR	[5]
Two chamber	275	67	0.5	900(2250)	43	1	[22]
Single chambered air cathode	900	4.17	4.68	1.82	31	NR	[79]
Single chambered air cathode	176	24.4	0.15	(344)	37	2	[41]

*a CE= coulombic efficiency; *b NR= not reported

2.6.3 Kinetics of anode respiration

2.6.3.1 Models of substrate utilization and current density at the anode

The kinetics of the anode respiration bacteria (ARB) are highly related to the power generation and substrate utilization of an MFC. Because of the complicity of the anode biofilm, several models have been developed to estimate the kinetic parameters for ARB.

The two factors that should be taken into consideration for the determination of kinetic parameters are the gradient in substrate concentration and the potential difference between terminal electron acceptor and the anode [80].

The most widely used model is the Monod model (Equation 2-6), in which a single substrate limit the growth of the bacteria [80-82]. The Nernst-Monod model also accounts for the effects of the potential difference on microbial growth (Equation 2-7) [80]. When the limiting substrate is self-inhibitory, microbial growth can be described using Andrews Kinetics (Equation 2-8) [83]. The substrate inhibition may result from a high osmotic pressure from the substrate or the substrate toxicity. The Han-Levenspiel model is used to describe microbial growth that stops completely when a critical inhibitor concentration (S_m) is reached and accounts for different types of inhibition (competitive, uncompetitive, or non-competitive) [83].

Monod model: $$r = r_{\max} \frac{S}{K_s + S} \qquad 2\text{-}6$$

Nernst-Monod model: $$r = r_{\max} \frac{S}{K_s + S} \left(\frac{1}{1 + \exp\left[-\eta \frac{F}{RT} \right]} \right) \qquad 2\text{-}7$$

Andrews kinetic model: $$r = r_{\max} \frac{S}{K_s + S + S^2 / K_{IH}} \qquad 2\text{-}8$$

Han-Levenspiel model: $$r = r_{\max}\frac{S(1-S/S_m)^n}{S+K_s(1-S/S_m)^m} \quad \text{2-9}$$

where r is the substrate utilization rate (g/L·d), the maximum output current density (mA/m^2) or maximum power density (mW/m^2), or voltage (mV) at each substrate concentration;

r_{max} is the maximum substrate utilization rate (g/L·d), maximum output current (mA/m^2) or maximum power density (mW/m^2), or voltage (mV) among all range of substrate concentration; S is the substrate concentration (mg/L); K_s is the half-saturation coefficient (mg/L); η is the difference in the potential of the anode at a given S and anode potential at the half-maximum current density, where η= $E_{anode} - E_{KA}$; E_{anode} is the anode potential (V); E_{KA} is the anode potential at the half-maximum current density (V); R is the ideal gas constant (8.3145 J/mol·K); T is the temperature (K); F is the Faraday constant (96,485 J/V·mol); K_{IH} is the self-inhibition coefficient (mg/L); S_m is the critical inhibitory concentration above which growth stops (mg/L); and n/m is empirical constants that are used to account for different types of inhibition.

2.6.3.2 Estimation of anode respiration kinetic parameters

Lee, *et al* [39] adopted the Monod model to estimate the kinetic parameters for the growth of *S. putrefaciens* bacteria in leachate-fed MFC reactors. The K_s value of bacteria in leachate-fed MFC reactor was 214.6 mg/L, with a growth yield coefficient around 0.65. Zhang, *et al* [83] considered the substrate inhibition and adopted four different models to estimate the kinetic parameters of substrate degradation based on the relationship between

substrate concentration and the substrate degradation rate, power density, and output voltage in an anodic denitrification MFC (AD-MFC). The Han-Levenspiel model was found to be the best model to fit the substrate degradation in the AD-MFC. The critical inhibitory concentration of COD was found to be approximately 20g/L. Liu, *et al* [81] also adopted the Monod model to fit the performance of the acetate/butyrate-fed MFCs. The model fitting showed the maximum power densities were 661 mW/m^2 for an acetate-fed MFC and 349 mW/m^2 for a butyrate-fed MFC; the K_s value was around 141 mg/L and 93 mg/L for the acetate-fed and butyrate-fed MFC, respectively. For leachate-fed MFCs, studies on the kinetics of leachate degradation and electricity generation are still needed. The kinetics parameters will be informative to optimize the MFC design and performance.

Chapter 3: Methods and Materials

3.1 Experimental Approach

Leachate was collected from laboratory-scale landfill bioreactors loaded with shredded paper, vegetable matter, and dried dog food. The leachates were diluted to different chemical oxygen demand (COD) concentrations. A continuous flow, single-chambered, bottle-type MFC reactor was filled with diluted or undiluted leachate and operated until the MFC reached steady state. The output voltage of the MFC reactor was monitored continuously. At the end of each experiment, the leachate properties (COD, BOD, Ammonia, VFA, pH, and conductivity) were characterized to determine the treatment and coulombic efficiencies of the MFC reactor. By comparing the coulombic efficiencies of the MFCs, we can evaluate the effect of leachate strength and loading on MFC performance and estimate the Monod kinetic parameters for the anode-respiring bacteria (ARB).

Two landfill bioreactors HYD1 and HYD2 were built to compare the recipes of the synthetic MSW. Every two weeks, 450 mL leachate was collected from the reactor effluent lines using 60 mL disposable syringes (Becton-Dickson). The leachate removed by sampling was replaced with 450 mL of synthetic rainwater to maintain liquid levels and the solid waste degradation process. This sampling regimen was initiated on day 5 and continued until day 68 or the effluent chemical oxygen demand (COD) concentration was lower than 5000 mg/L.

Once the optimum recipe was decided, six new landfill reactors were built following the same method. 1000 mL synthetic rainwater was added to each reactor to produce more leachate on day 10. The reactors were shut down on day 19 and all the leachate were collected in a media bottle anaerobically and stored at 4°C to avoid compositional changes prior to use.

3.2 Materials

3.2.1. Synthetic solid waste

In this study, synthetic MSW (a mixture of shredded office paper and food waste) was loaded into the landfill bioreactor. The preparation of synthetic MSW follows the recipe (HYD 2) shown in Table 3.1. In detail, office paper and cardboard were shredded into 5 mm × 20 mm using a paper shredder and stored at ambient temperature. Dog food (Hill's Science Diet), vegetables and fruits were purchased from Walmart and stored at 4^{o}C before loading into the landfill bioreactor. The food scraps were cut into chunks of approximately 1.25 cm to 2.50 cm by hand. The wet weight of the MSW components was recorded before they were mixed thoroughly by hand and separated into 6 portions. The reactor was loaded in layers of one portion of waste mixture plus 50 mL of inoculum per layer. Each layer was lightly compacted by hand before a new layer was added. Another recipe of the synthetic MSW was also used (HYD 1, shown in Table 3.2) and the two recipes were compared with real landfill reactor in terms of the variations in ammonia/COD concentration versus time, to determine which recipe is better for lab-scale simulation of real landfill reactor.

Table 3.1 Recipe of synthetic MSW used in landfill bioreactor (HYD2).

Categories	Materials	Percent by wet weight (%)	Wet weight (g)
Paper	Office paper	9.95	150
	Cardboard	4.97	75
Dog food	Dog food	4.97	75
Food scraps	Carrots	17.77	268
	Lettuces	19.89	300
	Tomatoes	30.24	456
	Potato	12.20	184
Total		100.00	1508

Table 3.2 Recipe of synthetic MSW used in Landfill bioreactor (HYD1).

Categories	Materials	Percent by wet weight (%)	Wet weight (g)
Paper	Office paper	21.94	252.2
	Cardboard	4.46	51.3
Yard wastes	Yard trimmings	9.44	108.5
Food scraps	Carrots	13.47	154.8
	Lettuces	19.56	224.8
	Tomatoes	31.14	357.9
Total		100.00	1149.5

3.2.2. Synthetic rainwater

During the study, synthetic rainwater was prepared to simulate the inorganic chemical composition of precipitation [84, 85]. The solution was added to the landfill bioreactor as

needed to replace leachate removed for sampling purposes and through evaporation to ensure that there was sufficient landfill leachate. The composition of the synthetic rainwater is shown in Table 3.3. The rain water was prepared by DI water, and the pH of the synthetic rainwater was adjusted to 6 to 6.5 with 1 M NaOH and 1 M HCl.

Table 3.3 Composition of synthetic rainwater used in this study

Chemicals	Concentrations (μM)	Concentrations (mg/L)
$MgSO_4$	0.420	0.051
K_2SO_4	0.425	0.074
$CaSO_4$	0.635	0.086
$CaCl_2$	0.235	0.026
$NaC_2H_3O_2$	0.540	0.044
NH_4NO_3	3.070	0.246
NaCl	1.220	0.071
HNO_3	0.560	/
HCl	0.800	/

3.2.3. Inoculum and media

3.2.3.1 Landfill reactor

To ensure that abundant hydrolytic and fermentative bacteria were present in the landfill bioreactor, the bioreactor was inoculated with anaerobic bacteria collected from the solid waste in a previous landfill reactor.

The bacterial inoculum was prepared with 300g solid waste collected from a previous hydrolysis reactor following the procedures described by Beaster (2013) [86]. The inoculum was stored at 4°C before adding into the landfill bioreactor together with the synthetic MSW and synthetic rainwater.

3.2.3.2 MFC reactor

The MFCs were inoculated based on previously reported procedures [54, 55, 70, 87]. A 2.05 L air cathode MFC that has been previously described [86] and maintained continuously for three years on the leachate derived from a synthetic solid waste hydrolysis reactor was used as a source of anode-respiring bacteria to inoculate the MFCs operated in the current study. This "mother" MFC was originally inoculated with anaerobic digester sludge from the Portage Lake Wastewater Treatment Plant (Houghton, MI).

Three methods of inoculating the H-style MFCs using bacteria from the mother MFC were tested before an approach was selected. In the first approach, a small portion of carbon fiber was cut from the graphite brush anode in the mother MFC reactor and transferred to a new MFC that was filled with leachate. In the second approach, a carbon fiber cut from the graphite brush anode was used to prepare an inoculum solution. The carbon fiber was added to 50 mL of anaerobic phosphate buffer solution (NaCl, 10 g/L; KCl, 1 g/L; 7.2 g/L $Na_2HPO_4 \cdot 7H_2O$, 13.6 g/L; KH_2PO_4, 1.2 g/L). The solution was mixed thoroughly by stir plate for half hour to form a suspension of microbes. Then the solution was aseptically added to 100 mL of autoclaved and anaerobic media. The media was adapted from a recipe described by Timmis et al. [88] and contained: Fe(III)-Citrate, 13.7 g/L; $NaHCO_3$, 2.5 g/L;

NaH_2PO_4, 0.6 g/L; KCl, 1 g/L; CH_3COONa, 6.8 g/L; and 10 mL each of trace metal (Table 3.4) and vitamin (Table 3.5) solutions. The inoculum solution was incubated at 30˚C for 5 days before being transferred to an MFC under anaerobic conditions. Neither of the methods involving the use of graphite brush fibers as a source of inoculum reliably resulted in current production.

Because of the inconsistent results obtained with the inoculum procedures described above, they were abandoned in favor of using effluent from the mother MFC as the source of anode-respiring bacteria, when starting up new MFCs. The following approach was used. First, 150 mL of effluent from the mother MFC was anaerobically collected and then combined in a 1:1 (v/v) ratio with sterile and anoxic sodium acetate feed solution. The sodium acetate feed solution was adapted from a recipe describe by Kim et al. [89] and contained: sodium acetate, 1g/L; NH_3Cl, 0.31g/L; KCl, 0.13g/L; $NaH_2PO_4 \cdot H_2O$, 2.69g/L; $Na_2HPO_4 \cdot 7H_2O$, 8.04g/L; and 10mL/L each of metal and vitamin solutions. Table 3.4 shows the recipe for the metal solution [12]. The vitamin solution (Table 3.5) was developed to sustain the growth of anode-respiring *Geobacter* strains and was prepared according to the instructions given for DSMZ Medium 579 [90].

Table 3.4 Composition of trace metal solution

Constituent	Concentration (g/L)	Constituent	Concentration (g/L)
NaCl	8.8	$MnSO_4 \cdot H_2O$	0.005
$MgCl_2 \cdot 6H_2O$	0.303	NH_4Cl	0.0031
KH_2PO_4	0.014	KCl	0.002
$CaCl_2 \cdot 2H_2O$	0.364	$CoCl_2 \cdot 6H_2O$	0.001
K_2HPO_4	0.021	$ZnCl_2$	0.001
$Na_2HPO_4 \cdot 7H_2O$	0.056	$CuSO_4 \cdot 5H_2O$	0.0001
$FeSO_4 \cdot 7H_2O$	0.01	H_3BO_3	0.0001
Na_2MoO_4	0.00025	$NiCl_2 \cdot 6H_2O$	0.00024
EDTA	0.001	$NaHCO_3$	0.1

Table 3.5 Composition of Vitamin solution

Constituent	Concentration (mg/L)	Constituent	Concentration (mg/L)
Folic acid	2	Vitamin B_{12}	0.1
Pyridoxine-HCl	10	D-Ca-pantothenate	5
Thiamine-HCl·$2H_2O$	5	p-Aminobenzoic acid	5
Riboflavin	5	Lipoic acid	5
Nicotinic acid	5	Biotin	2

3.2.4. Electrodes and proton exchange membrane (PEM)

Carbon cloth (carbon content = 99%, Fuel Cell Store, Inc., Texas) was subjected to various treatments before being used as an MFC cathode or electrode. The cross-sectional area of the anodes was 25 cm^2 The carbon cloth used to prepare the anodes was heat-treated in a

muffle furnace at 450 ºC for 30 minutes to increase the effective surface area [57, 91], as previously described. The cross-sectional area of the cathodes was 5.7 cm^2 in the single bottle air-cathode MFC and 25 cm^2 in the H-style MFC. The Same pretreatment was used for the single bottle air-cathode MFC and the H-style MFC. The carbon cloth was waterproofed by soaking it in a 100mL of 30% polytetrafluoroethylene (PTFE) dispersion in water (Sigma Aldrich) for 60 minutes, dried completely at room temp, and baked at 370ºC for 30 minutes. Then the carbon cloth was treated following methods modified from Cheng et al [92] and Middaugh et al. [93]. On one side of the cathode, a carbon layer was applied by applying a mixture of 1.56 mg of carbon black powder (Vulcan XC 72R, Fuel Cell Store, Woburn, MA), 18.72 uL of a 40% PTFE solution, and 40 uL of isopropyl alcohol every 1 cm^2 of carbon cloth. The isopropyl alcohol as a dispersing agent is used to thoroughly mix the carbon black solution. The volume of isopropyl alcohol can be adjusted as needed and they will be evaporated off after application. The purpose of this layer was to minimize water loss from, and oxygen diffusion into, the anode chamber. The mixture was applied to the cloth with a paintbrush at ~1.56 mg/cm^2, allowed to dry at room temperature, and then baked at 370°C for 30 minutes. On top of the carbon layer, four layers of a 60% (by weight) PTFE dispersion in water (Sigma Aldrich) were applied to the cloth using a paintbrush to provide additional waterproofing. After the carbon cloth was air-dried at room temperature, it was baked at 370°C for 15 minutes. The anode side of the cathode carbon cloth was coated with a platinum catalyst layer. The catalyst was prepared as follows. 0.5g of a 20:80 (w/w) platinum: carbon mixture (Fuel Cell Store, Inc., Texas)

was dispersed in 10 mL of isopropanol and ultrasonicated for 30 min. Then 2.5g of 5% Nafion solution (Ion Power, Inc.) was added to the mixture. The mixture was then p with an air brush on the anode side of the carbon cloth at a rate of approximately 0.5 mg/cm^2 and dried using a hair dryer set at low to prevent the catalyst from passing through the carbon cloth. The MFC electrodes are shown in Figure 3.1. All electrodes were soaked in distilled water for 1 day before being used. Copper wire (18 Gauge, Coleman Cable, Inc., IL) was bonded with the electrodes using a Silver conductive epoxy (8331 Silver Conductive Epoxy, MG Chemicals, Surrey, British Columbia, Canada).

The PEM was made of Nafion 117 (Fuel Cell Store, Inc., Texas). The effective area of the PEM was 5.7 cm^2. The PEM was pretreated by boiling it for 1 hour successively in each of the following: a 30% (by volume) aqueous H_2O_2 solution at 80°C, 0.5 M H_2SO_4, and DI water. The PEM was stored in DI water until used [94, 95].

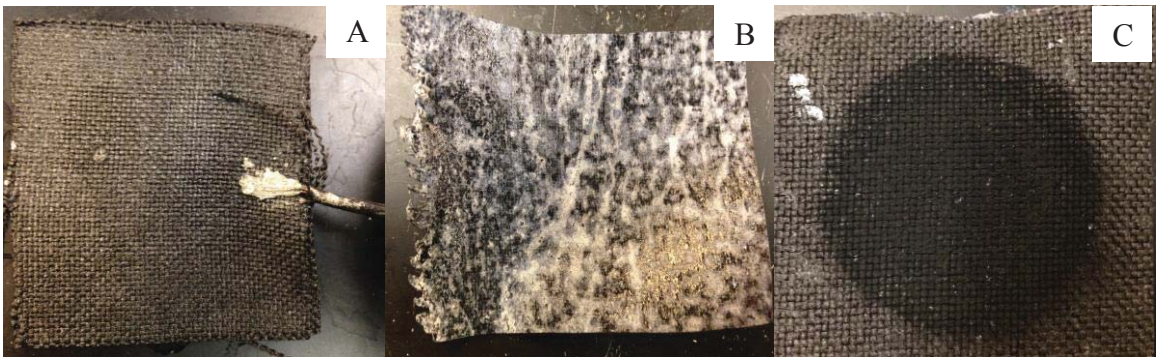

Figure 3.1 MFC Electrodes
A) Carbon cloth for anode electrode; B). The air side of the cathode after the carbon base layer and 4 diffusion layers were applied, and C) The platinum/carbon catalyst applied to the anode side of the cathode.

3.2.5 Landfill bioreactor start-up procedure

After the synthetic MSW, the bacterial inoculum, and 2 L of synthetic rainwater were loaded into a landfill bioreactor, the leachate from the reactor was recirculated through Tygon lab tubing(L/S 15, Cole-Parmer) at a rate of 10 to 12 mL/min using a peristaltic pump (7520-40, Masterflex). The landfill bioreactors were operated at a room temperature of 20 ± 3°C. An example of a loaded landfill bioreactor is shown in Figure 3.2.

Figure 3.2 Photograph of synthetic municipal solid waste loaded into the landfill bioreactor.

3.3 Reactor configurations and operation

Three different reactor designs were used in this study. Landfill bioreactors were used to achieve hydrolysis of the synthetic solid waste and generate leachate that fueled the MFCs. Two-compartment, "H-style", batch MFCs were used in preliminary assays. The two-compartment MFCs were subsequently modified to create a single-bottle air cathode MFC for the primary experiments. The design and construction of all three types reactor are described below.

3.3.1 Laboratory-scale landfill bioreactor

Two laboratory-scale landfill bioreactors were used in this study. The same basic design, which was developed by Tristan Beaster [86], was used for both reactors. Tristan Beaster constructed one hydrolysis reactor, and Zhimin Song constructed the second hydrolysis reactor. Figure 3-3 gives a schematic image of the hydrolysis reactor build by Tristan Beaster. The detailed description of the reactor can be found in his thesis. To prevent blocking the effluent port, a 3 cm layer of sand wrapped with synthetic geotextile cloth was loaded at the bottom (Fig. 3.3g). To better distribute the liquid, a similar sand layer was placed at the top of the solid waste (Fig. 3.3e).

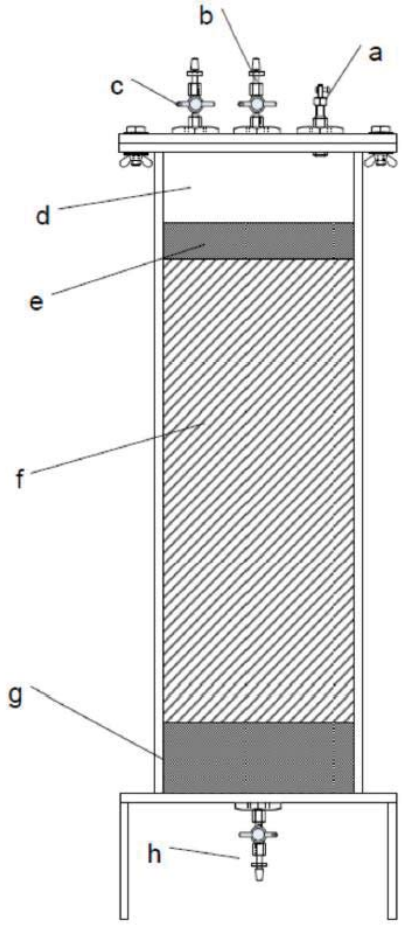

Figure 3.3 Landfill bioreactor schematic.

Components labeled are (a) headspace gas sampling valve, (b) recycle flow return valve, (c) influent feed valve, (d) headspace, (e) sand layer to disperse influent, (f) solid waste layer, (g) sand drainage layer, and (h) effluent control valve. Adapted from Beaster (2013)[86].

3.3.2 Two-chambered H-style MFCs

The two-chambered H-style MFCs used in the preliminary experiments are shown in (Figure 3.4). Each MFC was constructed using two of the modified media bottles (each with a 330 mL capacity). One bottle formed the anode compartment, and the other bottle

comprised the cathode compartment. The cathode chamber of each H-style MFC was filled with DI water and aeration was initiated by bubbling house air into the chamber. The PEM was sandwiched between the flanged ends of the side-arm tubes with a rubber O-ring (source) on each side and held in place with a clamp. The distance between the electrodes was approximately 14 cm.

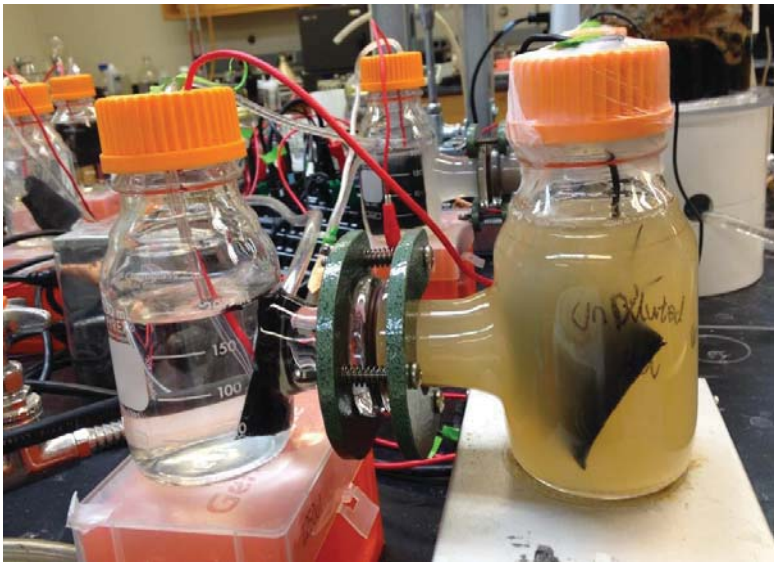

Figure 3.4 The H-style MFC components.
The anaerobic anode chamber (right) and an aerobic cathode chamber (left) are clamped together. Their contents are separated by a Nafion PEM. The cathode chamber was sparged with air to provide dissolved oxygen at the cathode.

3.3.3. Single bottle air-cathode MFC

The MFC reactor used in this study was a single-chambered, air cathode MFC, similar to that described by Logan, Cheng et al [96]. A photograph of the MFC is shown in Figure 3.5A. The anode was constructed from a 250-mL Pyrex media bottle that had been modified by a glassblower. A flanged glass side arm (inner diameter = 27 mm, outer

diameter = 33 mm) was added to the bottle to permit incorporation of a cathode and resulted in a total volume of 330 mL for the anode compartment. A rubber O-ring (Chemglass Inc., New Jersey) was placed in a groove in the flange. The cathode was then sandwiched between the O-ring, rubber sheet and a 5.5mm thick plexiglass plate with a 32 mm hole centered over the cathode, and the whole assembly was clamped together (Figure 3.5A and 3.5E). Rubber sheet was fitted to prevent leakage.

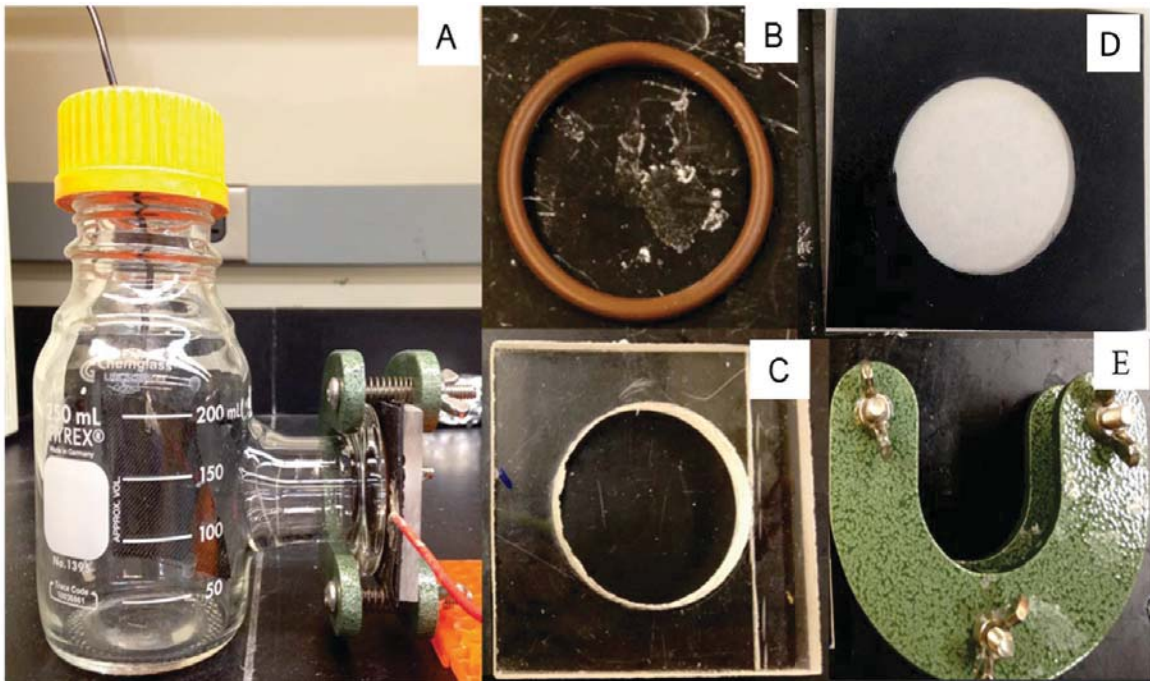

Figure 3.5 The Single bottle-style MFC configuration.
A) Photograph of the assembled MFC. B) O-ring. C) Custom made **plexiglass** plate D) Rubber sheet E) Horseshoe-shaped clamp (Chemglass Inc., New Jersey)

3.3.4 MFC operation

3.3.4.1 Start up

The mixture of MFC effluent and sodium acetate solution was anaerobically transferred into the anode compartment of two single-bottle MFCs. On each MFC, a resistor box (Elenco Electronics Inc., Illinois) was used to maintain an external resistance of 50 Ω between the anode and cathode and close the circuit. Whenever the voltage fell below 1 mV, 10 mL of sodium acetate (33 g/L) was added to the anode compartment of the MFC to bring the concentration of sodium acetate back up to 1 g/L. The MFCs were maintained on sodium acetate for 30 to 60 d, and the voltage was monitored continuously across the external resistor during this start-up period. A voltage > 10mV was taken as evidence that an active anode respiration bacteria population had been developed on the anode carbon cloth. MFCs that produced a stable voltage were used in the kinetic experiments, as described below.

3.3.4.2 Kinetic study

After achieving repeatable maximum current, the MFCs were ready for use in a kinetic experiment. The effect of the substrate loading rate on the kinetic characteristics of the MFCs, treatment performance, and coulombic efficiency was evaluated by using solid waste leachate that was collected from the landfill bioreactor and diluted with DI water to achieve a COD ranging from 10 to 25,000 mg /L. The pH of the leachate was adjusted to 6.8 to 7.2 using 5 M NaOH and 5 M HCl. The conductivity of the mixture of 1L raw leachate with 50mM buffer solution (introduced by adding 8.04 g $Na_2HPO_4 \cdot 7H_2O$ and

3.04 g $NaH_2PO_4 \cdot 2H_2O$ per liter leachate) was measured to be 11~ 12 mS/cm. The conductivity of the diluted leachate was also measured, and various salt amounts were added to achieve a constant conductivity of 11 to 12 mS/cm. For conductivities ≤4 mS/cm a high-strength (100 mM) phosphate buffer was introduced to the 1L solution by adding 16.09 g $Na_2HPO_4 \cdot 7H_2O$ and 6.08 g $NaH_2PO_4 \cdot 2H_2O$. For conductivities > 4 mS/cm, a low-strength (50 mM) phosphate buffer (8.04 g/L $Na_2HPO_4 \cdot 7H_2O$ and 3.04 g/L $NaH_2PO_4 \cdot 2H_2O$) was used. Finally, NaCl solid was added to adjust the conductivity of all leachate solutions to 11 to 12 mS/cm.

For each experiment, the pair of MFCs received the same concentration of leachate. However, one MFC was operated in a fed-batch mode in a single bottle MFC, which only was operated for a week. 330 mL of liquid was removed and replaced with an equal amount of the diluted leachate at different concentration every day, which yielded a retention time (HRT) of 1 day. Six different concentrations were tested in the fed-batch MFC. The other MFC was converted to a continuous-flow, air cathode configuration, which is shown in Figure 3.6. Diluted leachate was pumped into the MFC at a flow rate of 0.73 mL/min to yield an HRT of 7.6 h.

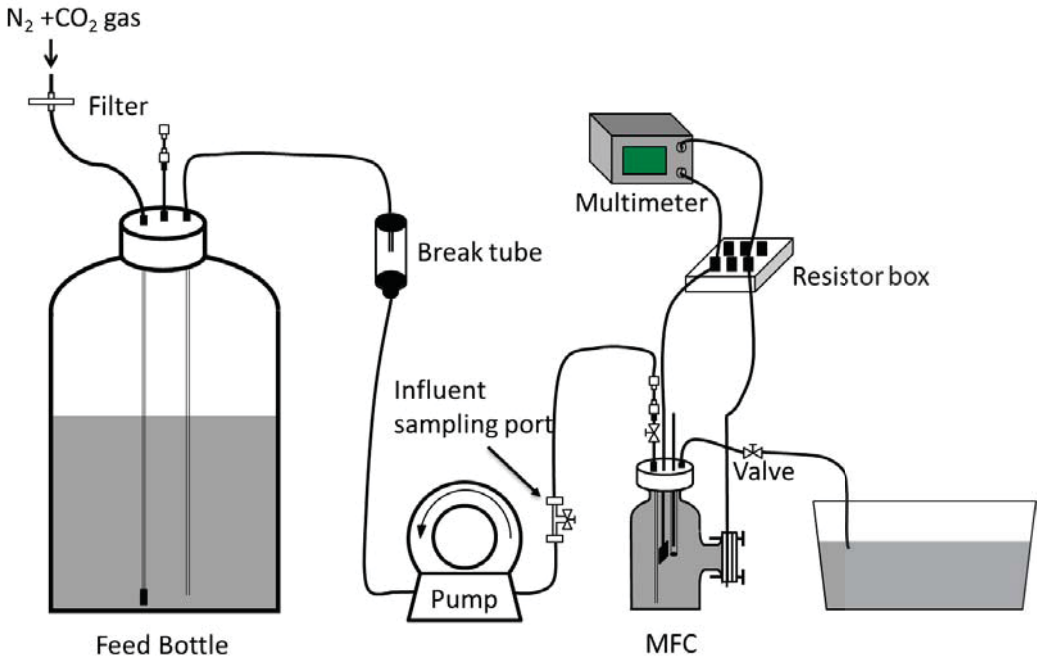

Figure 3.6 Process diagram of Continuous-flow MFC

After adjusting the conductivity and pH of the diluted leachate, it was autoclaved for 0.5 hr in a 5 L media bottle (Pyrex) and fitted with a threaded cap (GL 45, Valco instruments) containing four straight threaded fittings. The configuration of the bottles follows the description in the thesis of Sara Klemm [97]. The media was kept under anaerobic conditions by maintaining it under positive pressure achieved with N_2/CO_2 (80:20, v/v) supplied at 20 mL/min. Oxygen was removed from the gas by passing it through a heated copper catalyst. The feed bottle was connected to the MFC via 20 cm pump tubing (L/S 14, Cole-Parmer) and 70 cm polyfluoroethylene tubing (1/8" OD, Cole-Parmer) covered with Viton tubing (1/8" ID, Cole-Parmer). A glass break tube prevented back-growth of bacteria into the feed bottle. A peristaltic pump (Masterflex L/S) was used

to deliver the feed to the MFC. To ensure the leachate concentration in the MFC bottle was homogenous distributed, it was continuously stirred using a stir plate and magnetic stirrer.

3.4 Sampling and Analytical Methods

3.4.1 Sampling procedures

3.4.1.1 Landfill bioreactor

Leachate was sampled on a weekly basis throughout this study to characterize the pH, temperature, conductivity, sodium sulfide, soluble chemical oxygen demand (COD), 5-day biological oxygen demand (BOD_5), and volatile fatty acid (VFA) concentration of the leachate. Liquid samples (8-mL) were collected from polycarbonate stopcock valves (Cole Parmer) in the recycle flow line of the landfill bioreactor using a 10-mL B-D™ disposable Luer-lock syringe and transferred to a test tube. An Accumet XL 50 meter (Fisher Scientific) was used to measure the pH, temperature, and conductivity of the leachate samples. Next, 3 mL of leachate was transferred to a 10-mL Falcon tube and centrifuged for 15 min at 10,000g. After centrifuging, 1 mL of supernatant was used for soluble sulfide analysis. The remaining 2 mL of supernatant was filtered through a 0.45 μm syringe filter (13mm, polyethersulfone, Millipore) for analysis of soluble COD and VFA. The sodium sulfide and COD analyses were performed immediately. The VFA samples were stored at -20°C until analyzed. Gas samples (1 mL) were collected from the headspace of the hydrolysis reactor using a gas-tight syringe (1 mL, Valco Instruments Co., Inc.), whenever leachate samples were collected.

3.4.1.2 Batch MFC

The batch MFC was sampled every day when feeding new diluted leachate solution. The COD, pH, and conductivity of the influent and effluent were measured to determine the columbic efficiency and COD removal at different leachate concertation.

3.4.1.3 Continuous-flow MFCs

Influent and effluent samples were collected from continuous-flow air cathode MFCs and analyzed for COD, BOD_5, NH_3-N, VFAs, pH, and conductivity to characterize the treatment and coulombic efficiencies of the MFCs under steady-state conditions. An MFC was considered to be at steady state when the current density was stable (exhibited <10% variation) for three hydraulic retention times.

3.4.2 Analytical Methods

3.4.2.1 Liquid analysis

COD and soluble sulfide were determined following the USEPA-approved reactor digestion method (EPA 5220 D, Hach TNT 821/822/823,) and the methylene blue method (Hach 8131), respectively [98]. A Hach DRB200 reactor was used to digest the samples. Ammonia nitrogen was quantified using the salicylate method (Hach 10031). A Hach DR 6000 spectrophotometer was used for all colorimetric assays. The total BOD_5 was measured using HACH BODTrak II respirometric BOD apparatus (P/N 2952400).

A high-performance liquid chromatorgraphy (HPLC) system (Hewlett Packard 1100 series) with diode array detection (DAD) and Agilent ChemStation software was used for

VFA analysis. Phosphoric acid (1%, by volume) was used as the eluent and prepared by adding 1 mL pure phosphoric acid (>99.5% purity) to as 18 MΩ water to make a 1 L solution. The eluent flow rate was 1.0 mL/min. The total running time was 18 min for each sample. The sample injection volume was 100 μL. A Shodex KC-811 column (8.0*300 mm) equipped with a guard column was used for separation of organic acids. The column temperature was kept at 50°C, and the wavelength of the detector was set to 205 nm.

Sample VFA concentrations were determined based on comparison with a standard curve. The standard solutions were prepared using the sodium salts of acetate (>99% purity, Mallinckrodt Chemicals), propionate (>99% purity, Alta Aesar) and butyrate (>99% purity, Alta Aesar), with distilled water as the solvent. The standards were filtered with a 0.45-μm syringe filter (PES, 13mm, Millex), aliquoted into auto-sampler vials (Fisher Scientific) with screw-cap, and frozen at -20°C.

One set of standard vials was removed from the freezer, thawed, and analyzed each time samples were analyzed. Duplicate injections were analyzed for each standard and the average concentration was used in the calibration curves. Calibration curves for each organic acid were created by plotting the peak area vs. the known concentration (in mg/L) of the organic acid. The peak area was determined by the valley-to-valley integration method. The retention times for acetic, propionic, and butyric acid were found to be 10.4, 12, and 14.3 min, respectively. The sum of the concentrations of these three VFAs in samples was reported as the total VFAs.

3.4.2.2 Gas analysis

Headspace methane concentrations were analyzed using a gas chromatograph (GC, Hewlett Packard 6890 series), equipped with a 1% SP-1000, 60/80 Carbopack column (8.0 ft × 1/8 in. × 2.1 mm; Supelco) and a flame ionization detector (FID). The carrier gas was helium, which was supplied at a flow rate of 40 mL/min. Hydrogen (40 mL/min) and air (400 mL/min) were supplied as detector gases. The inlet temperature was 200°C, and the temperature of the detector was 250°C. The column temperature was maintained at an initial temperature of 60°C for 2 minutes. Then, the temperature was increased to 150°C at a rate of 15°C/min). It was maintained at 150°C for 7 minutes.

Standards were prepared by first flushing Teflon gas bags (1L, SKC) with N_2 gas (99.999%, American Welding&Gas) for 5 minutes and then empty the bags. The known quantities of CH_4 gas (>99.9%, Praxair, Inc., Danbury, CT USA) and N_2 (99.999%, American Welding & Gas) were added using gas-tight syringes (1.0 mL (VICI), 10mL (Hamilton 81656) and 100mL (Hamilton 86346)) with concentrations from 50.4 μmol/L to 40,207 μmol/L). The calibration curve was prepared by plotting peak area as a function of the mass (in moles) of injected methane. The average retention time for methane was 0.42 min. The total amount of methane ($M_{(CH4)}$) in the headspace was calculated using the mass of methane ($m_{(CH4)}$) determined from the calibration curve by the GC response factor, and the ratio of the volume of headspace (V_{head}) to the volume of sample (V_{sample}):

$$M_{(CH_4)} = m_{(CH_4)} \frac{V_{head}}{V_{sample}} \tag{3-1}$$

The headspace volumes were estimated based on volumetric graduation marks labeled on the landfill reactor. The atmospheric pressure was assumed in the headspace.

3.4.2.3 Electrochemical analyses

A resistor box (50Ω, Elenco Electronics Inc., Illinois) was used to connect the carbon anode with the air cathode to close the electrical circuit. A Keithley 2701 digital multimeter (Keithley Instruments Inc., Ohio) was used to continuously measure the voltage across the resistor box. Data were collected every 20 mins and automatically downloaded to an Excel spreadsheet using Excelinx.

Linear sweep voltammetry (LSV) was carried out using a potentiostat (Interface 1000, Gamry Instruments). Polarization and power density curves for the MFCs were following previously described methods [47, 54, 99]. The MFC was disconnected from the data acquisition system and let it sit for 2 hrs to reduce possible hysteresis effect on the LSV measurement. The MFC cathode was used as both the counter and reference electrode. The MFC anode served as the working electrode. The voltage ranged from the open circuit voltage (OCV), which was approximate -780 mV, to -0.1 mV and was conducted at a scan rate of 0.2 mV/s. The total internal resistance (R_{int}) [Ω] was estimated by measuring the slope of the linear region of the polarization curve according to:

$$R_{\text{int}} = \frac{\Delta U}{\Delta I} \tag{3-2}$$

where, ΔU = the potential difference in the linear region of LSV curve [V], and ΔI = the current difference in the linear region of LSV curve [A].

LSV was also performed to evaluate cathode performance. The scanning voltage ranged from -0.5 V to 0.4 V. The scan rate was 1 mV/S. A new anode carbon cloth was used as the counter electrode. The cathode was used as the working electrode, and Ag/AgCl acted as the reference electrode. LSV was performed in 50 mM phosphate buffer.

Electrochemical impedance spectroscopy (EIS) was used to characterize the internal resistance of the MFCs. EIS was conducted after half hours of LSV test at the OCV at frequencies ranging from 0.01 Hz to 100 kHz. The amplitude was 10 mV. There are four components of total internal resistance (Eqn. 3-3): the solution resistance ($R_{solution}$) [Ω], charge transfer resistance (R_{charge}) [Ω], the diffusion resistance ($R_{diffusion}$) [Ω], and other resistance (R_{other}) [Ω].

$$R_{\text{int}} = R_{solution} + R_{charge} + R_{diffusion} + R_{other} \tag{3-3}$$

The solution resistance (Figure 3.7, point A) was determined from the first x-intercept in the high-frequency region. The charge transfer resistance was obtained based on the diameter of the first circular section (Figure 3.7, curvature AB) in the Nyquist plot by circle fit [54, 55]. The diffusion resistance and all other internal resistance were calculated by subtracting the solution resistance and charge transport resistance from R_{int} [100].

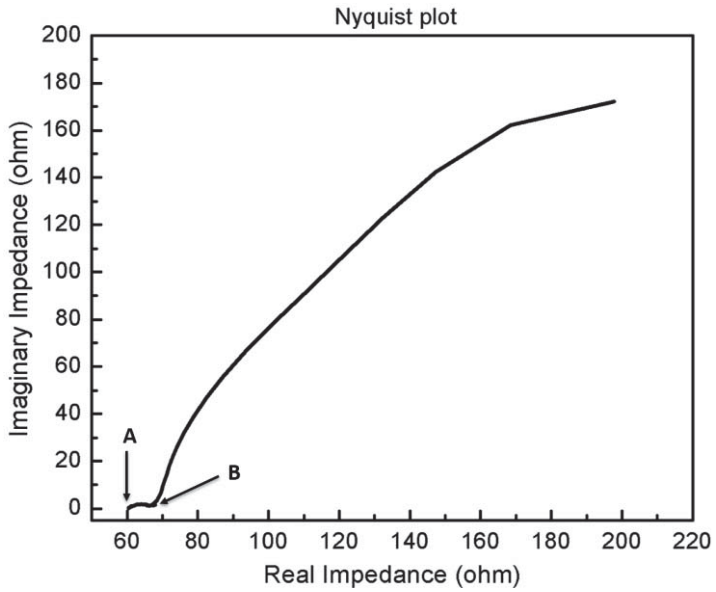

Figure 3.7 Nyquist plot of electrochemical impedance spectroscopy

Cyclic voltammetry (CV) was used to characterize the performance of the anode. A three-electrode system was used for the CV tests (Figure 3.8). The MFC anode served as the working electrode, Ag/AgCl as the reference electrode, and the MFC cathode served as the counter electrode. First-derivative CV curve was obtained using the OriginLab software. First, the differential function in the software was used to calculate the derivative of the voltage-current data. The transformed data are then plotted against the voltage to get the first-derivative CV curve.

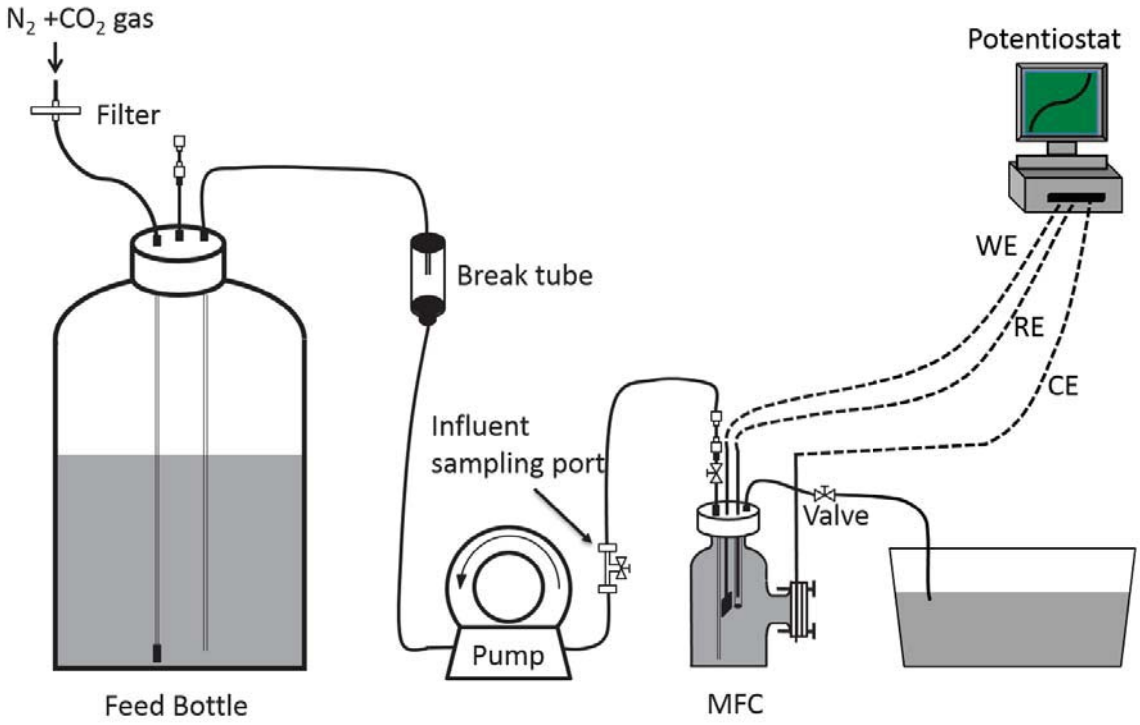

Figure 3.8 MFC three-electrode connection during the electrochemical test. MFC: Microbial fuel cell; WE: working electrode; RE: Reference electrode; CE: Counter electrode.

3.4.2.4 Microbial Fuel Cell performance evaluation

Current flow (*I)* [mA] in the MFCs was calculated according to Ohm's law:

$$I = \frac{U}{R_{ext}} \tag{3-4}$$

where, U is the voltage [mV], and R_{ext} is the applied external resistance [Ω].

Power (P) [W] was calculated according to:

$$P = I \times U \tag{3-5}$$

Current density ($I_{d,}$) [A/m^2] and power density (P_d) [W/m^2] were calculated by normalizing *I* and *P*, to the projected cathode surface area ($A_{cathode}$) [m^2] according to Equations 3-6 and 3-7, respectively:

$$I_d = \frac{I}{A_{cathode}} = \frac{U}{R_{ext} A_{cathode}} \tag{3-6}$$

$$P_d = \frac{P}{A_{cathode}} = \frac{U^2}{R_{ext} A_{cathode}} \tag{3-7}$$

Coulombic efficiency (C_E) of the MFC is defined as the percent of electrons in the starting organic matter recovered as current [12, 47]. In batch MFCs, C_E is calculated according to:

$$C_E = \frac{M \int_0^{t_b} I dt}{Fb \upsilon_{An} \Delta COD} \tag{3-8}$$

where M is molecular weight of oxygen [g/mol], F is Faraday's constant [C/mol e^-], b is the mole of electrons per mole of oxygen [e^-], ν_{An} is the volume of liquid in the anode compartment [L], and ΔCOD is the change in COD [g/L] over a period of time (t_b) [s] for each cycle. In continuous-flow MFCs, CE is calculated according to:

$$CE = \frac{M \int_0^{t_b} I dt}{FQt_b \Delta COD} \tag{3-9}$$

where Q is the flow rate of leachate into the MFC reactor [L/s].

The relationship between Current (I) and the aqueous substrate concentration [mg COD/L] was modeled using a Monod-type relationship [80, 101, 102]. Two sets of Monod parameters were estimated. $I_{d,max,app,}$ the maximum current density [A/m^2], and $K_{s,app}$ [mg COD/L], the apparent half-maximum rate coefficient, incorporate the limitations caused by substrate diffusion and the anode overpotential [80] and were fit to measurements of substrate concentrations and current across R_{ext} in the continuous-flow MFC, according to:

$$I_d = I_{d,\max,app} \frac{S^0}{K_{s,app} + S^0} \tag{3-10}$$

$$I_d = I_{d,\max,app} \frac{S}{K_{s,app} + S} \tag{3-11}$$

$$I_d = I_{d,\max,anode} \frac{S}{K_{s,anode} + S} \tag{3-12}$$

where S is the substrate concentration at steady-state [mg COD/L]. The maximum current density through the anode, $I_{d,max,\ anode}$ [A/m^2], and $K_{s,anode}$ the anode half-maximum rate coefficient [mg COD/L] were estimated by fitting current data obtained from CV curves to Equation 3-12.

The user-defined function was used to write Equations 3-11 and 3-12 in OriginLab. Then, K_S and I_{max} were estimated by using nonlinear, orthogonal distance regression method to fit Equation 3-11 or 3-12 to the I_d data obtained from steady-state measurements of U across R_{ext} or from the CV curves, respectively.

Chapter 4 Results and Discussion

4.1 Hydrolysis reactor performance

4.1.1 Comparison of synthetic MSW recipes

Two bench-scale hydrolysis reactors were packed with different combinations of substrates, as described in Section 3.2.1. The concentrations of two key constituents, ammonia, and COD, in the leachate generated from these hydrolysis reactors were monitored over the course of a batch cycle, which consists of four distinct phases (Figure 2.1), to determine which recipe yielded leachate properties that are the most like full-scale landfill leachate. Because of the differences in the scale, a batch cycle is completed in approximately 70 days in bench-scale hydrolysis reactor; 3 years may be required before all four phases are completed in a full-scale landfill cell [3]. Therefore, to facilitate the comparison of the COD concentrations and ammonia levels over time in the bench-scale reactors and full-scale landfill, the overall operation time for each system was normalized into the range from 0 to 1 according to:

$$T_{new} = \frac{T - T_{\min}}{T_{\max} - T_{\min}} \tag{4-1}$$

Where T_{new} is the normalized value; T is the original time; T_{max} and T_{min} are the maximum and minimum value of time, respectively.

The COD and ammonia concentrations for the full-scale landfill were obtained/estimated from Kjeldsen et al. 2002 [3] and plotted along with the data from the bench-scale

hydrolysis reactors as a function of normalized time in Figure 4.1. Inspection of the plotted COD and ammonia levels suggests that the degradation patterns in HYD2 more closely followed those in the full-scale landfill reactor compared to HYD1. Most likely this is because the dog food contains a high percentage of protein, which resulted in the lower C/N in HYD2 than HYD1. Therefore, all subsequent experiments were conducted with leachate produced using the HYD2 solid waste recipe.

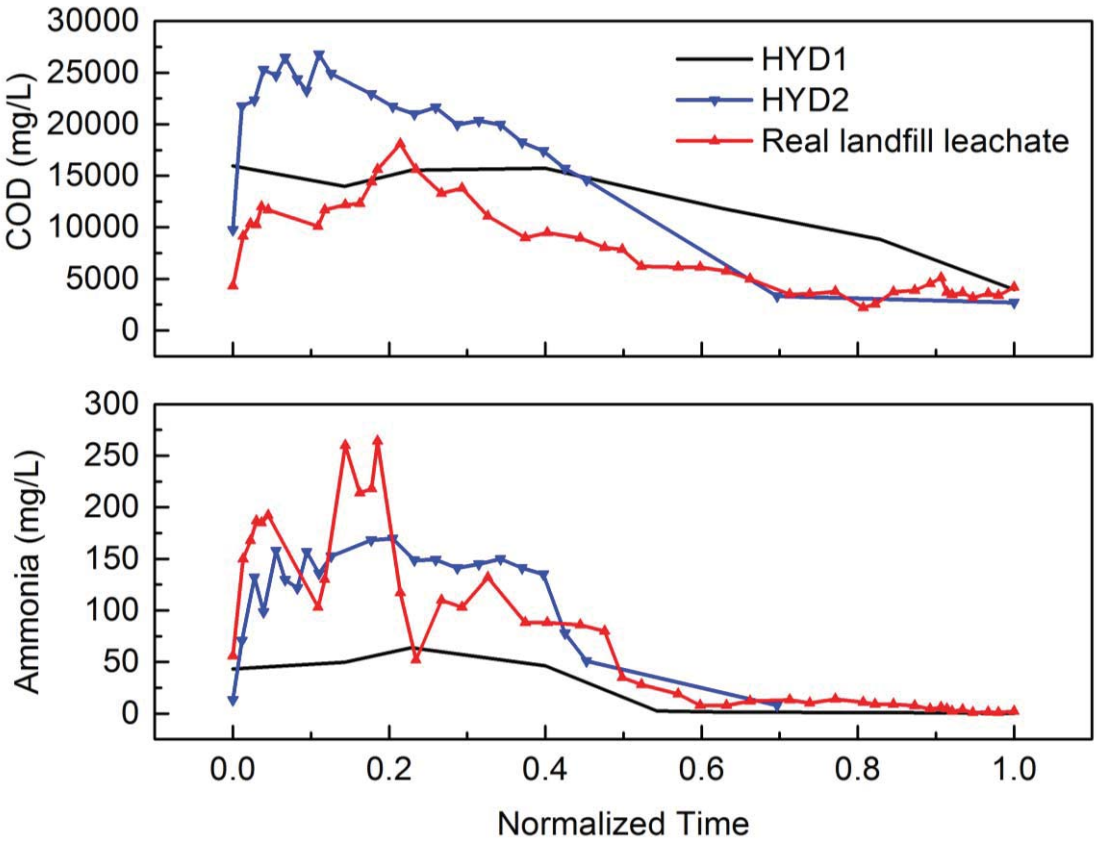

Figure 4.1 Ammonia and COD concentrations in two bench-scale hydrolysis reactors (HYD1 and HYD2) and a full-scale landfill bioreactor as a function of normalized time. Full-scale leachate data were estimated based on data reported in [3].

4.1.2 Detailed characterization of HYD2 leachate

HYD2 leachate was needed to conduct the experiments evaluating the effect of substrate concentration and loading rate on MFC performance. To facilitate comparison of the results obtained in different experiments, leachate collected during a period of steady hydrolysis reactor operation was needed. It is theoretically impossible to achieve a true steady state in a batch system. Therefore, a detailed characterization of the HYD2 leachate was performed to identify a period of "pseudo-steady-state" operation. Specifically, COD and BOD, pH, ammonia, and cumulative CH_4 production in the HYD2 leachate were measured. The data are presented in Figure 4.2.

The COD, BOD, and ammonia concentrations increased steeply during the initial aerobic phase. As expected, the pH dropped below 5.5 during this phase because of volatile fatty acid production. The COD concentration followed a gradual decline from day 30 as readily biodegradable substrates were depleted. After day 50, a rapid increase in methane production was observed, indicating that the initial methanogenic phase had begun. The pH value started increasing slowly until day 100 because volatile fatty acids were converted to methane and carbon dioxide at the initial methanogenic phase and only recalcitrant compounds were left at stable methanogenic phase.

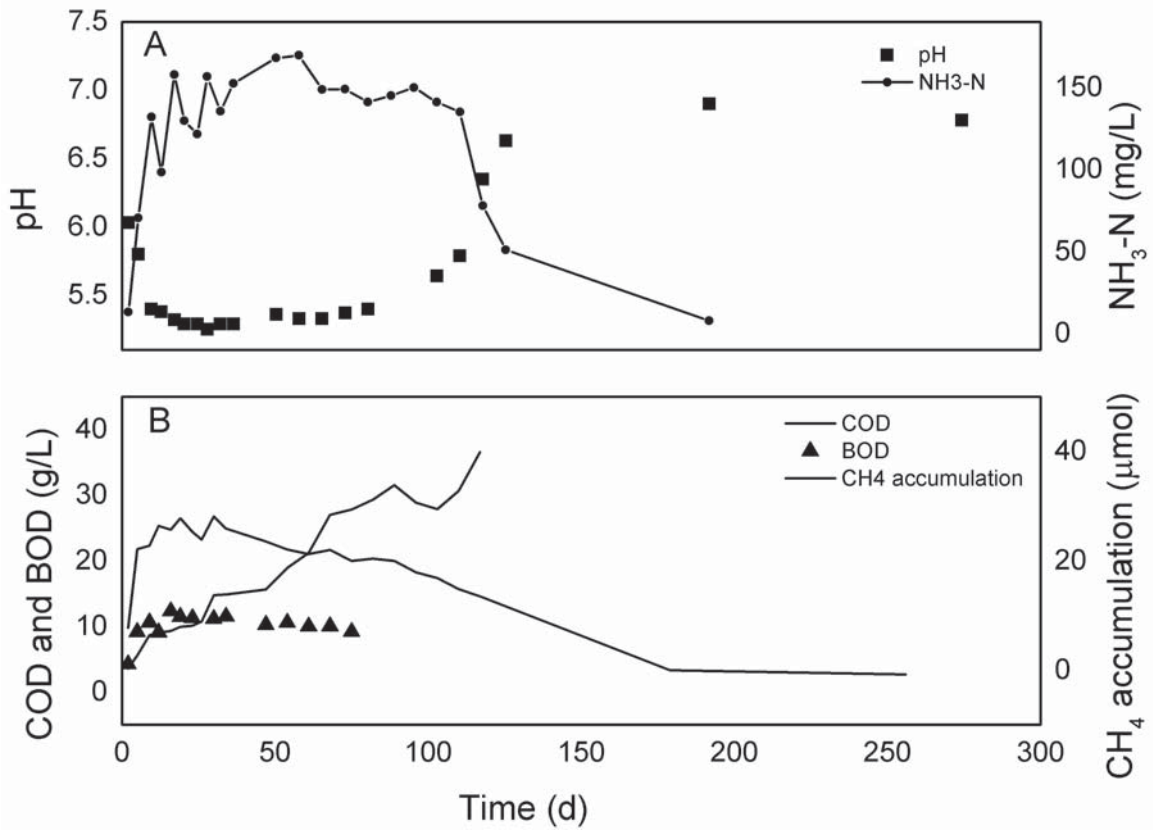

Figure 4.2 Concentrations of key constituents in the HYD2 leachate as a function of time: (a) pH and NH_3-N, and (b) COD, BOD and cumulative CH_4 production.

The decrease in methane accumulation between days 89 and 103 presumably represent the loss of gas through sampling and, perhaps, leakage because the hydrolysis reactor is not completely gastight. However, because this study was focused on the performance of the MFC under different operating conditions and the hydrolysis reactor was primarily needed to generate the leachate supplied to the MFC, no adjustment was made to the hydrolysis reactor design.

Stable methane production was not observed during the first 100 days of operation of the hydrolysis reactor. However, the concentrations of all other leachate constituents

were fairly constant or at a pseudo-steady-state between approximately days 15 and 50. Therefore, leachate was collected from HYD2 for the MFC performance studies on day 19.

4.1.3 Raw leachate characterization

The characteristics of the leachate collected from HYD2 on day 19 are shown in Table 4.1. Importantly, the BOD/COD ratio is 0.63, implying the leachate collected during this period is highly biodegradable.

Table 4.1 Characteristics of the leachate collected from HYD2 on day 19

Parameter	Value
pH	5.24
Conductivity	7.14 mS/cm
COD	24,852 mg/L
BOD	15,713 mg/L
NH_3-N	176.7 mg/L
Acetic acid	4,996 mg/L
Propionic acid	1,201 mg/L
Butyric acid	6,743 mg/L

4.2 Batch MFC experimental results and kinetic parameter estimation

There were a few problems with the two-chambered H-style MFCs. The water in the cathode chamber became turbid after running for a long time and diffused to the anode chamber. In addition, the membrane is expensive and increases the internal resistance. As results, single-chambered MFC was used in the batch and continuous MFC experiment.

The batch MFCs were inoculated and supplied with repeated additions of sodium acetate (33 g/L) when the voltage dropped to < 1 mV. This pattern was maintained until the maximum voltage measured during a given batch cycle did not exceed the maximum voltage measured in the previous cycle. The performance of a typical batch MFC maintained at R_{ext} = 50 Ω during the start-up period is shown in Figure 4.3. A maximum potential of 174 mV, which corresponds to a maximum power density of 1.06 W/m^2 based on the nominal cathode surface area, was achieved during the fourth cycle. The maximum voltage during the fifth cycle is lower than that achieved in the fourth cycle, which may be due to biofouling of the cathode catalyst layer.

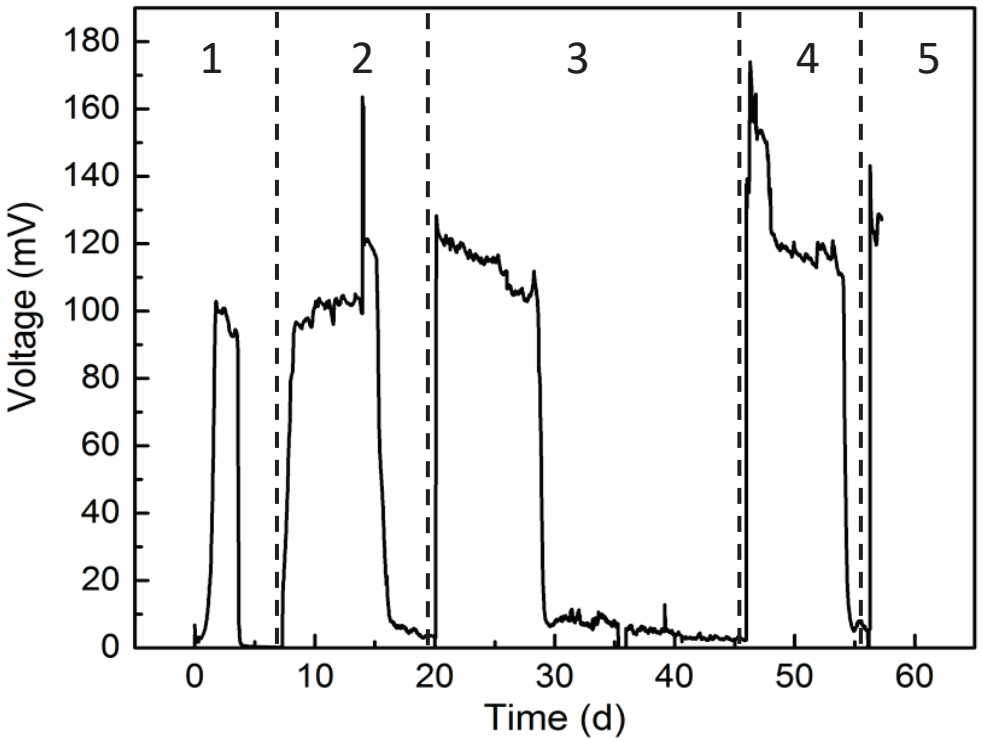

Figure 4.3 Voltage of MFC during start up.

At the end of the start-up phase, each batch MFC was supplied with leachate diluted to have a COD concentration ranging from 9 to 800 mg COD/L and operated for approximately 1 day. The current densities were monitored over time and are summarized in Figure 4.4. The maximum current densities ranged from 0.035 A/m^2 at the lowest leachate concentration (9.17 mg COD/L) to 6.28 A/m^2 at the highest strength leachate (789 mg COD/L). The maximum current measured at each leachate concentration during this time period was used for the kinetic parameter estimation. Two observations suggest that the substrate concentration in the most dilute leachate was too low to maintain the positive net growth of the ARB. First, the current density began dropping immediately and never rebounded. Second, negative COD removal was observed (Table 4.2), presumably due to the release of soluble products of endogenous cellular decay.

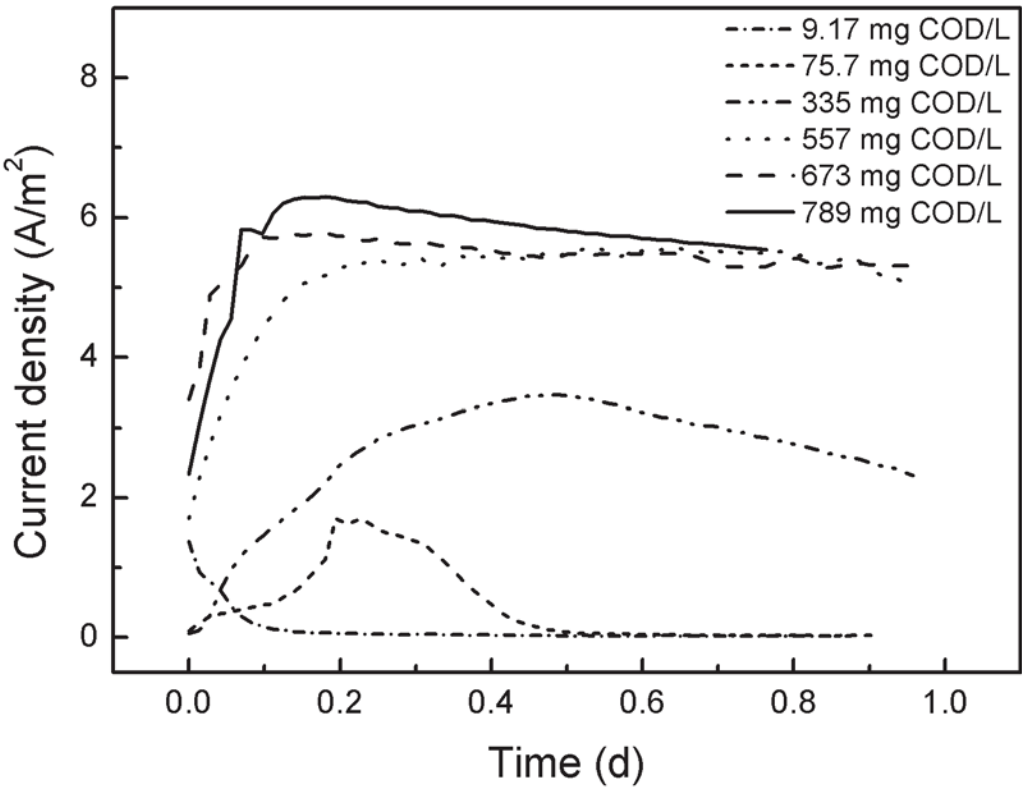

Figure 4.4 MFC current density measured in batch, air cathode MFCs during operation with leachate diluted to different initial COD concentrations

Table 4.2 COD removal, columbic efficiency (CE), and maximum current density ($I_{d,max}$) measured in batch, air cathode MFCs during operation with leachate diluted to different initial COD concentrations

	9.17 mg COD/L	75.7 mg COD/L	335 mg COD/L	557 mg COD/L	673 mg COD/L	789 mg COD/L
CE (%)	NA	13.54	29.58	33.45	40.11	NA
COD removal (%)	-115	58.5	34.33	36.6	27	NA
$I_{d,max}$ (A/m^2)	0.035	1.71	3.44	5.58	5.79	6.28

NA: Not Available.

The data collected during the operation of the batch air-cathode MFCs at various leachate COD concentrations were used to estimate Monod kinetic parameters for leachate utilization (Equation 3-10). P_d and voltage density have been used to estimate kinetic parameters in most of the published research related to the substrate utilization kinetics in MFCs [42, 81, 83]. As explained by Lee *et al.* 2009, only I_d, and not P_d or voltage density, should be used to estimate kinetic parameters because the voltage is a function of thermodynamics, not kinetics, and estimates of K_s were 85% larger when P_d was used for estimation rather than I_d [80]. The best fit of the Monod model (Equation 3-10) to the data was obtained with K_s and I_{max} values of 665.1 ± 280.2 mg COD/L and 11.6 ± 2.6 A/m^2, respectively (Figure 4.5). You *et al.* used P_d values to estimate the kinetics of a leachate-fed single-chambered MFC. A K_s value of 251.39 mg/L was obtained with a $P_{d,max}$ value around 5920.96 mW/m^3 [42]. Because the kinetic parameters were fit to P_d values in the study by You et al. [42], it is hard to compare their results directly with the parameter estimates obtained in our study. Therefore, we recalculated the I_d data based on their P_d values as the function of S. The results are shown in Figure 4.6, and the best fit K_s and I_{max} values are 73.1 ± 13.21 mg COD/L and 3.4 ± 0.1 mA/m^3, respectively. The modified K_s value is lower than that observed in our work, which may due to the use of real leachate in the study conducted by You et al. [42], and the use of synthetic leachate in the current study.

.

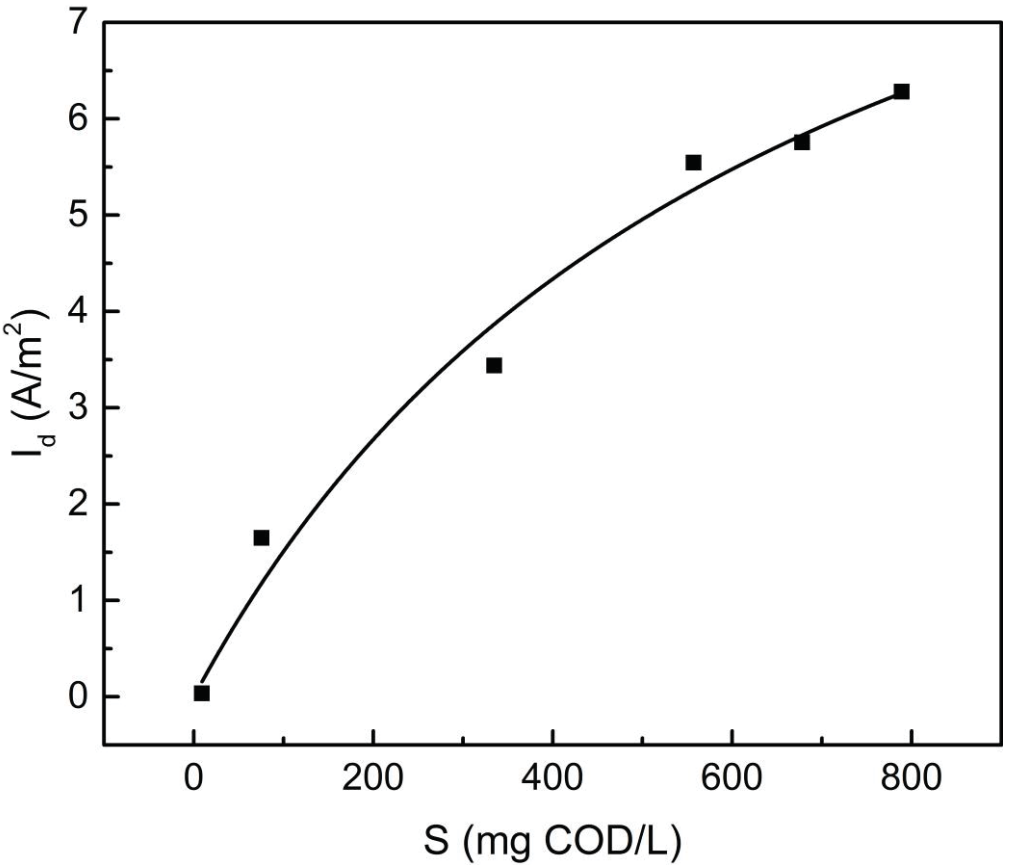

Figure 4.5 Maximum current measured in batch, air-cathode MFCs operated on leachate diluted to different initial COD concentrations. Each data point represents the maximum current density measured in a single-chamber MFC. The solid line represents the best fit of the Monod model to the data.

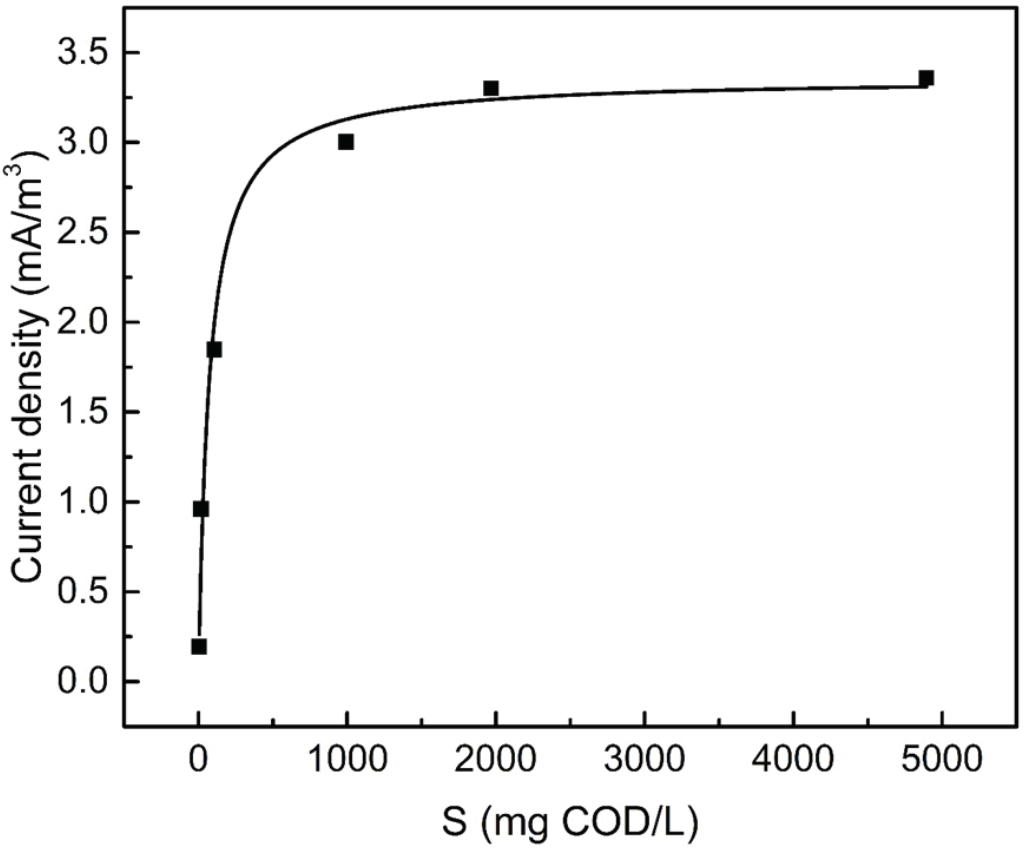

Figure 4.6 Current density as a function of S for leachate in single chamber MFC (data from You, et al. 2007) [42]. Each data point represents the maximum current density at given S (mg COD/L). The solid line represents the best fit of the Monod model to the data.

4.3 Continuous MFC experimental results and parameter estimation

Two sets of continuous-flow MFC experiments were conducted. The overall goals of these experiments were to: (1) obtain I_d measurements at different OLRs so that apparent kinetic parameters could be fit to the data, and (2) relate MFC performance in terms of COD removal, C_E, and P_{max} to the OLR. In each set of experiments, the influent COD

concentration (S°) was varied by changing the concentration of leachate in the feed. OLR changes with S°, according to:

$$OLR = \frac{S^{\circ} Q}{V} = \frac{S^{\circ}}{HRT} \qquad 4\text{-}2$$

where, Q is the flow rate of leachate into the MFC reactor [L/d], and V is the volume of the anode chamber [L]. The first set of experiments (Trial 1) was conducted with a single cathode at S° values ranging from 27 to 789 mg COD/L. At an HRT of approximately 0.316 d, these S° correspond to OLRs ranging from 0.085 to 2.5 g COD/L·d. The second set of continuous-flow experiments (Trial 2) was conducted using a new cathode to provide replication of the results obtained in Trial 1. Because a new cathode was used in Trial 2, comparison of the results of the two trials also provided insight into the impact of cathode fouling on kinetic parameter estimates. The Trial 2 experiments were conducted with S° values ranging from 56 to 562 mg COD/L, which correspond to OLRs ranging from 0.18 to 1.78 g COD/L·d. Two sets I_d measurements were made in each trial. First, I_d through the external circuit (whole MFC) was determined using Ohm's Law (Eqn. 3-2) and the U measured across R_{ext} using the multimeter. Second, CV was applied to characterize I_d (and the electron transport mechanisms) at the ARB biofilm-anode interface.

4.3.1 I_d Results of Trial 1 Continuous-Flow MFC Experiments

Figure 4.7 shows I_d calculated based on U measured across R_{ext} in the Trial 1 MFC operated at various OLR. As expected, I_d increased with the substrate concentration. This makes

sense because when the ARB were supplied with a higher concentration of electron donors, they metabolized the substrate, and thus transferred electrons to the anode, at a higher rate.

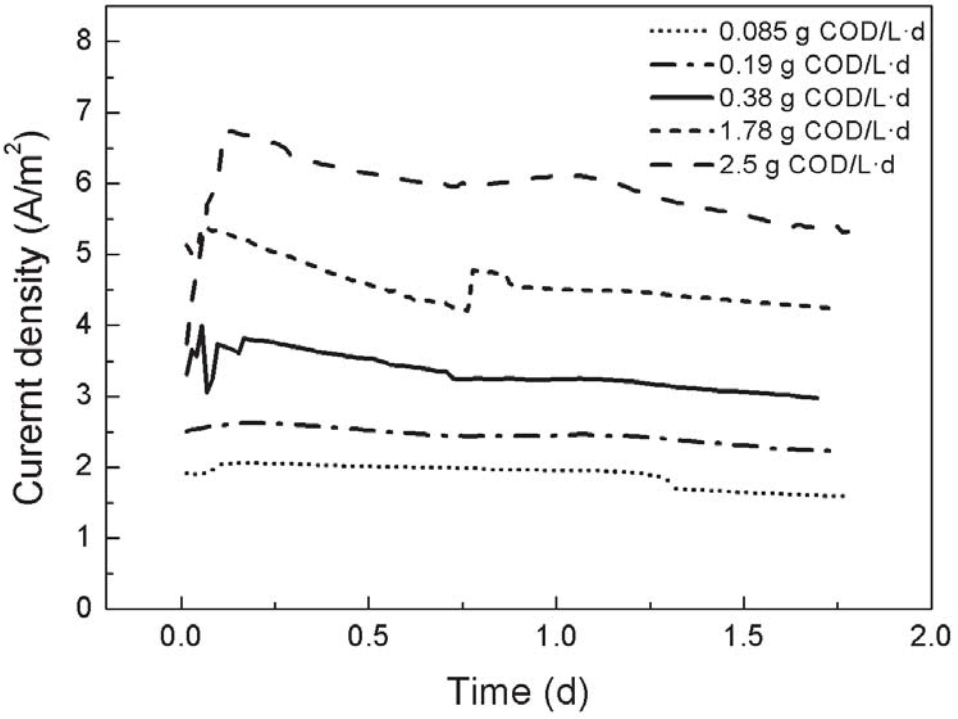

Figure 4.7 I_d of the whole MFC measured based on E across R_{ext} at different OLR during Trial 1

The current density curves obtained using CV analysis of the anode at various OLR are shown in Figure 4.8. Consistent with the determination of I_d based on measurement of the potential across the external resistor, the I_d measured via CV at -0.1 V increased with the OLR. A dominant inflection point is observed at ~0.37 ± 0.01 V at all the OLR, which suggests that a single oxidation/reduction reaction limited the rate of electron transfer to the reactor under all operating conditions tested [103]. For CV test, the anode is used as the working electrode. The current-voltage curve shows exactly the relationship between

anode potential (vs. reference electrode) and the current flow through the anode. CV analysis at low scan rates is most used to evaluate the performance of bacteria at steady-state. The current density obtained from the multimeter, however, is related to both the voltage difference between the anode and cathode and R_{ext}. Therefore, fitting the current densities obtained from CV curves to the Monod model (Equation 3-12) provides a more accurate estimate of the kinetics of the bacteria [104, 105]. On the other hand, fitting the current densities acquired from external circuit offers kinetic information of the whole MFC under its operational condition.

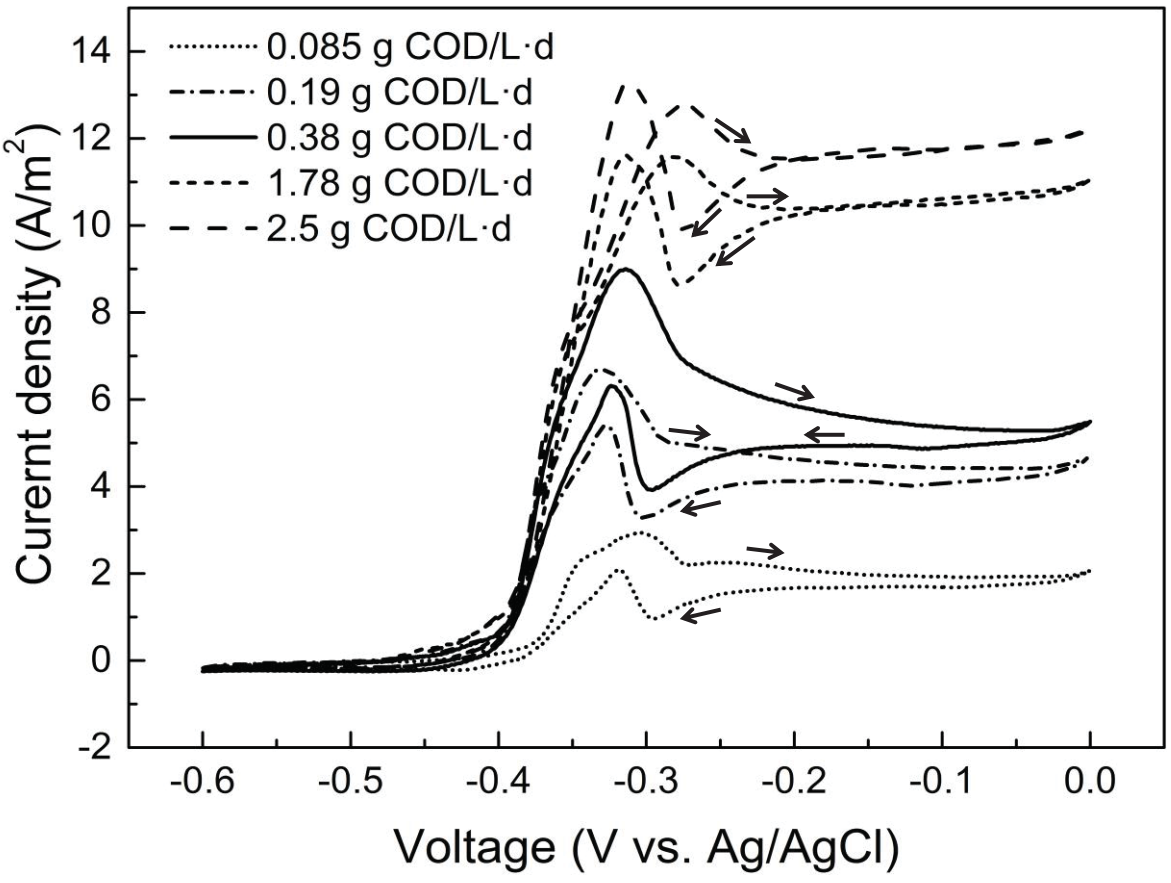

Figure 4.8 I_d of the whole MFC measured via CV at different OLR during Trial 1.

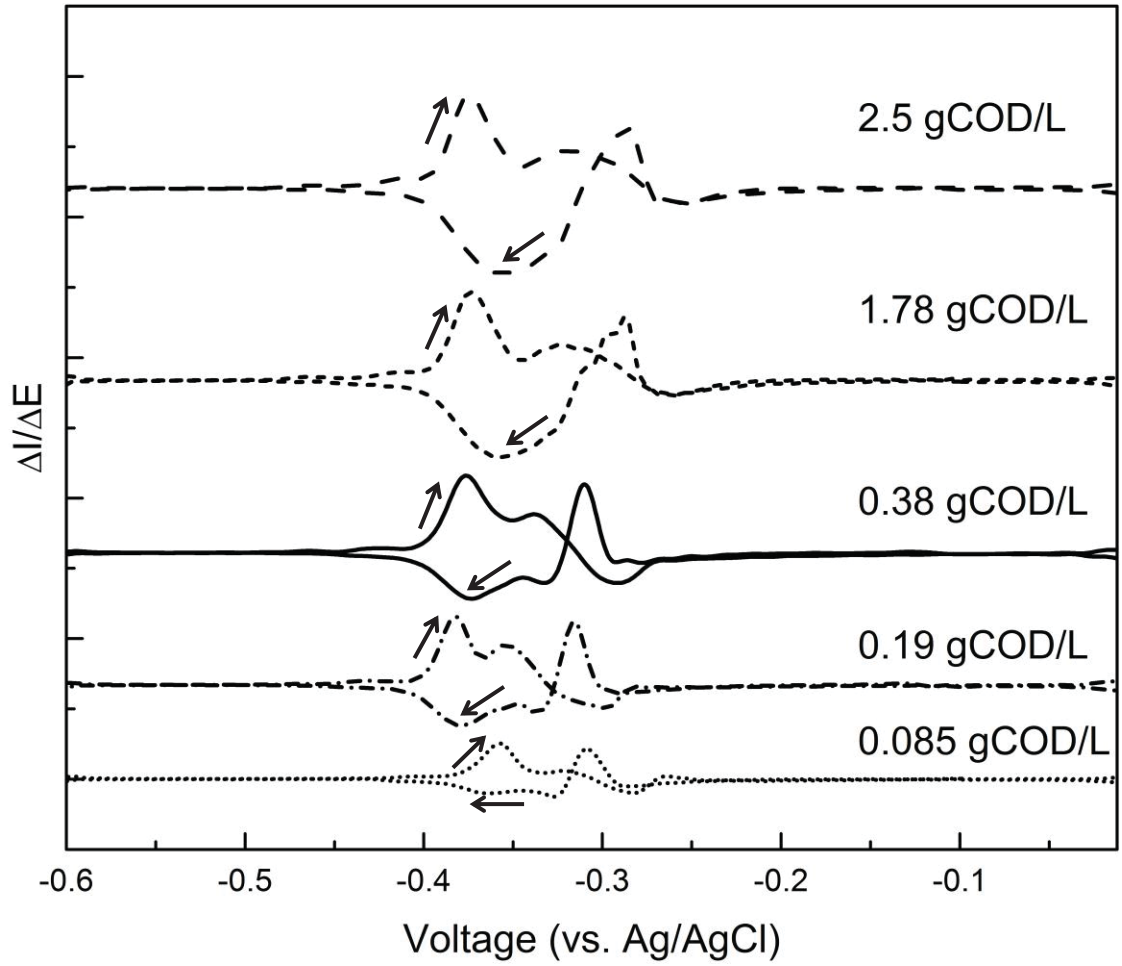

Figure 4.9 First derivatives of cyclic voltammograms obtained via CV analysis of the anode operated at different OLR during Trial 1. The midpoint potential detectable in catalytic waves of the anode biofilm is shown.

The I_d values obtained based on E across R_{ext} and CV analysis of the anode at each OLR were plotted as a function of the steady-state COD concentration, S, and used to obtain estimates of the apparent Monod model parameters, $K_{s,app}$ and $I_{max,app}$, and the anode electron-transfer kinetic parameters, $K_{s,anode}$ and $I_{max,anode}$, respectively. The whole MFC kinetic parameters ($K_{s,app}$ and $I_{max,app}$) were estimated based on the average I_d values during

steady-state operation. The MFC was considered to be at steady-state when I_d varied less than 10% at a given OLR, which generally occurred after 1 day (Figure 4.7). The fitted curve is shown in Figure 4.10 and the parameter estimates are given in Table 4.3.

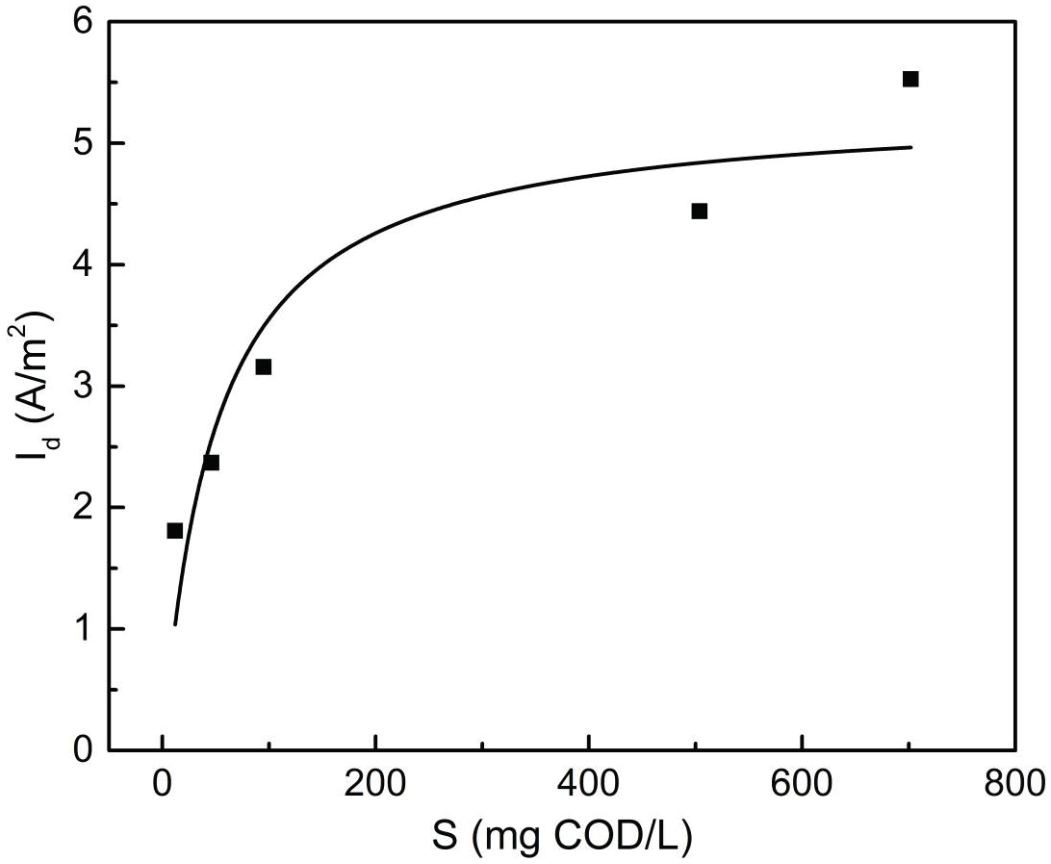

Figure 4.10 I_d as a function of S in the continuous-flow MFC during Trial 1. Each data point represents the average steady-state I_d at a given OLR. The solid line represents the best fit of the Monod model to the data.

The anode I_d values measured via CV at -0.1 V (vs. Ag/AgCl) are plotted as a function of S in Figure 4.11 and the best-fit Monod parameters are reported in Table 4.3. Although the kinetics of electron transfer at the anode by the ARB are not directly

comparable to the whole MFC kinetics estimated based on E across R_{ext}, it is interesting to note that the estimated K_S and I_{max} values estimated using the two approaches are of similar magnitude.

Table 4.3 Summary of best-fit kinetic parameters [a]

		Ks (mg COD/L)[b]	I_{max} (A/m^2) [c]
	Batch Experiment	665 ± 280	11.6 ± 2.6
External	Trial 1 continuous-flow	50 ± 22	5.3 ± 0.6
Circuit	Trial 1 & Normalized Trial 2	46 ± 24	5.0 ± 0.6
	Trial 1 & Trial 2	37 ± 19	5.8 ± 0.6
	Trial 1 continuous-flow	120 ± 27	13.3 ± 0.9
CV	Trial 1 & Normalized Trial 2	129 ± 35	13.1 ± 1.1
	Trial 1 & Trial 2	116 ± 37	14.3 ± 1.3

[a] Values represent the average value ± the standard error.

[b] Estimates obtained in batch experiments and by measuring U across R_{ext} in continuous-flow experiments represent $K_{S,app}$ values. Estimates obtained via CV analysis of the anode in continuous-flow experiments represent $K_{S,anode}$ values.

[c] Estimates obtained in batch experiments and by measuring U across R_{ext} in continuous-flow experiments represent $I_{max,,app}$ values. Estimates obtained via CV analysis of the anode in continuous-flow experiments represent $I_{max,anode}$ values.

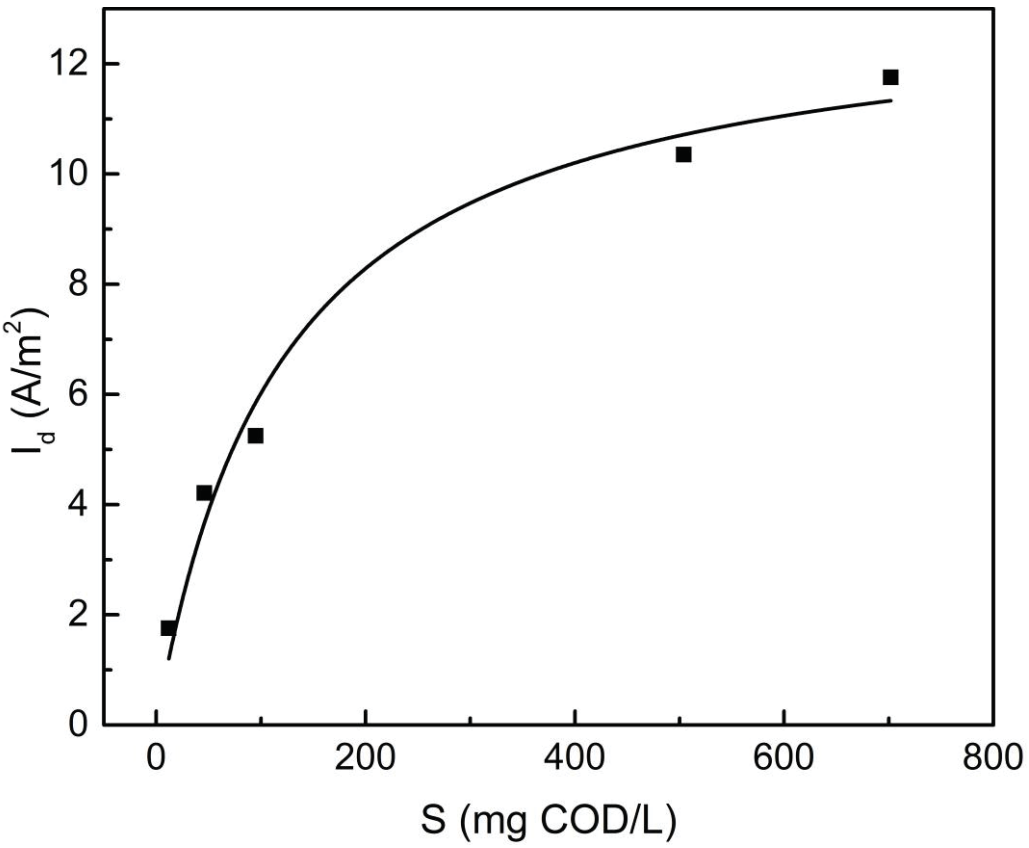

Figure 4.11 Anode Id measured via CV as a function of S in the continuous-flow MFC during Trial 1. Each data point represents the Id measured at -0.1 V (vs. Ag/AgCl) at a given OLR. The solid line represents the best fit of the Monod model to the data.

4.3.2 I_d Results of Trial 2 Continuous-Flow MFC Experiments

Attempts to conduct additional experiments at higher OLR with the cathode used in Trial 1 were unsuccessful because the I_d dropped to 1.8 A/m^2 and could not be restored (data not shown). Therefore, the cathode was replaced and three additional experiments were conducted at various OLRs in Trial 2 with the new cathode. The Trial 2 results are shown in Figure 4.12. The overall trends in the I_d obtained based on the characterization of the external circuit and CV analysis of the anode was the same in Trial 2 as in Trial 1. I_d in the whole MFC increased as the OLR and S rose (Figure 4.12A). Similarly, CV analysis of the

anode showed that the I_d increased with the OLR, and the oxidation-reduction mechanism involved in electron transfer was constant at different OLRs because the inflection point of the ascending I_d-applied voltage curves was the same (Marsili et al., 2008; Figure 4.12B). However, the Id values obtained with the new cathode were much higher in Trial 2 than in Trial 1. For example, at an OLR of 1.78 g COD/L·d, the maximum I_d was approximately 7.5 A/m^2 in Trial 2, compared to approximately 5.4 A/m^2 in Trial 1.

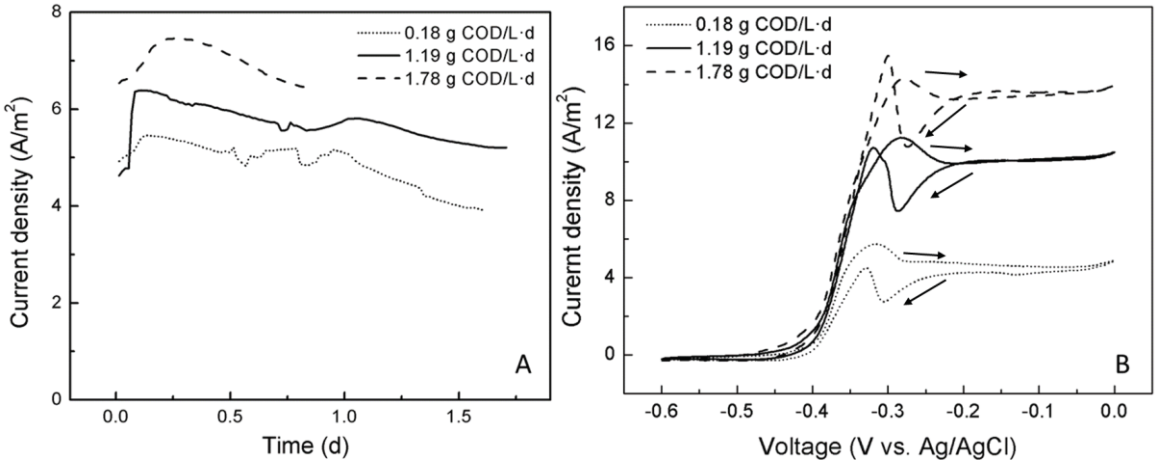

Figure 4.12 I_d measurements made in the continuous-flow MFC at different OLR during Trial 2.

A: Whole MFC values based on E across R_{ext}; B: Anode values measured via CV.

The change in response to the I_d to OLR with the new cathode raised two key questions: (1) What is the best way to combine the results of the two continuous-flow MFC trials (and is this even feasible)?; and (2) What caused the change in the I_d response to OLRs and did this impact the magnitude of the kinetic parameter estimates?

4.3.3 Integration of the Trial 1 and 2 Data for Estimation of the Monod Model Parameters

Two methods of combining the data from the two continuous-flow experiments for the purpose of fitting the Monod model parameters were compared. The first involved normalizing the Trial 2 results to the Trial 1 data using the "min-max" normalization method [105]. The other approach involved fitting the Monod model to the untransformed data obtained in the two trials.

The min-max normalization method transforms the original value (v) to an adjusted value (v') according to Equation 4-3:

$$v' = \frac{v - \min}{\max - \min}\left(\max_{new} - \min_{new}\right) + \min_{new} \qquad (4\ 3)$$

where min and max are the minimum and maximum values in the original dataset (Trial 1); $\max_{new}$ and $\min_{new}$ are the minimum and maximum values in the transformed data set (Trial 2).

To normalize the data in Trial 2 (v) to Trial 1 (v´) using equation (4-1), the parameters *min*, *max*, max_{new}, and min_{new} have to be identified first. In our case, we assumed the data in Trial 1 and Trial 2 followed the same trend for OLRs ranging from 0.19 to approximately 1.78 g COD/L·d. The steady-state I_d values obtained at the minimum and maximum OLRs of 0.19 g COD/L·d and 1.78 g COD/L·d in Trial 1 were set equal to the values of *min* and *max*, respectively.

The values of max_{new} and min_{new} in Trial 2 were obtained by assuming the current densities at 1.78 g COD/L·d and 0.18 g COD/L·d in Trial 2 can be transformed into the corresponding current densities in Trial 1 using Equation 4-1. Based on this assumption, two equations with two unknowns, max_{new} and min_{new}, can be obtained. The value of max_{new} and min_{new} were determined by solving the simple binary equations.

After the values of max_{new} and min_{new} were obtained, the I_d at 1.19 g COD/L·d in Trial 2 was normalized to the corresponding value in Trial 1 following Equation 4-1. The normalized current density at 1.19 g COD/L·d from Trial 2 combined with the I_d values from Trial 1 were used to obtain estimates of $K_{s,app}$ and $I_{max,app}$, as shown in Figure 4.13.

The Monod model (Equation 3-10) was also fit to the combined and untransformed I_d values from Trials 1 and 2, as shown in Figure 4.14. The best-fit kinetic parameters obtained using the two methods are summarized in Table 4.3. In both cases, the parameter estimates obtained using the combined data sets were similar in magnitude to the parameter estimates obtained based on the Trial 1 continuous-flow data alone. The average values of $K_{s,app}$ and $I_{max,app}$ estimated based on measurement of U across R_{ext} for the three data sets in Table 4-3 were 44 ± 22 mg COD/L and 5.4 ± 0.6 A/m^2, respectively. The $I_{max,app}$ values are generally lower than the $I_{max,anode}$ values obtained from the CV curves. Presumably, this is because I_d values obtained from CV curves directly reveal the activity of the ARB, while I_d values obtained based on measurement of U across R_{ext} reflect the additional R_{int} and R_{ext} associated with the entire MFC.

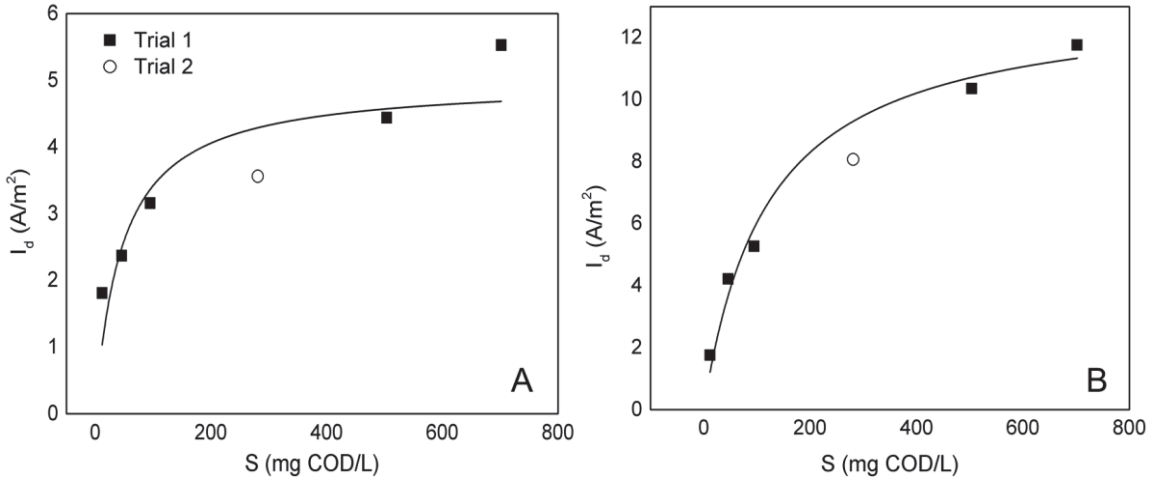

Figure 4.13 I_d as a function of S in the continuous-flow MFCs during Trials 1 and 2, after normalizing the Trial 2 data to the Trial 1 data set using the min-max normalization method, as described in the text. (A) I_d values were obtained by measuring U across R_{ext}. (B) I_d values were obtained from CV curves. Each data point represents the average steady-state I_d at a given OLR. The solid line represents the best fit of the Monod model to the data.

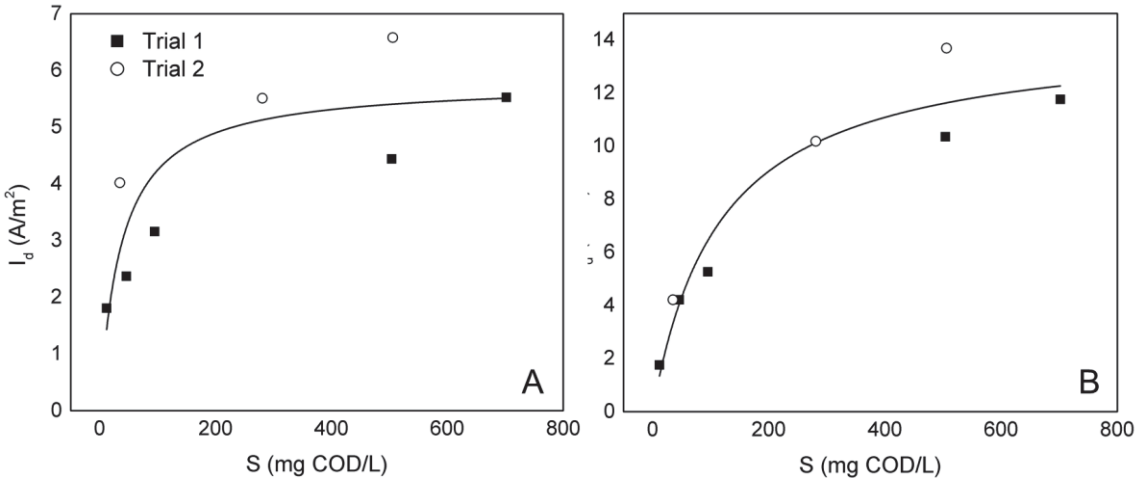

Figure 4.14 I_d as a function of S in the continuous-flow MFCs during Trials 1 and 2. The two data sets were combined without transformation. (A) Id values were obtained by measuring U across Rext. (B) Id values were obtained from CV curves. Each data point represents the average steady-state Id at a given OLR. The solid line represents the best fit of the Monod model to the data.

4.3.4 Effects of leachate on the performance of the MFC anode and cathode

As noted above, I_d measurements made in Trials 1 and 2 suggested that cathode poisoning by some leachate constituent(s) led to the decrease of MFC performance in Trial 1. Therefore, a set of separate experiments was conducted to specifically test whether exposure to high-strength leachate from the hydrolysis reactor negatively impacted electron transfer at the cathode.

4.3.4.1 Effects of high-strength leachate on current production and CV curves in continuous-flow MFCs operated with low-strength leachate

First, a continuous-flow MFC maintained at an HRT of 0.316 d was fitted with a new cathode and the I_d was monitored while it was supplied with a low substrate concentration (110 mg COD/L) from day 0 to day 4 and then switched to an influent consisting of undiluted leachate. The underlying rationale was that if a constituent of the leachate was inhibitory to the cathode performance, the current should drop after switching from diluted to undiluted leachate. As shown in Figure 4.15, the current increased continuously while the MFC was supplied with diluted leachate. However, when the influent was changed to raw leachate after 4.5 days, the current immediately dropped to nearly 0 from a previous high of 2.3 mA, which suggests that a constituent of the leachate inhibited the performance of the anode or the cathode. To test this, a CV test was performed to evaluate the activity of the ARB after switching to the undiluted leachate feed (Figure 4.16). There were no obvious peaks in the forward and reverse CV curves, indicating that no electron transfer to

the anode and no redox reactions took place after exposure to the full-strength leachate. There were abundant electron donors in the undiluted leachate. Based on the results of this experiment, it seems highly likely that some constituent of the leachate suppressed the activity of the ARB when present at high concentrations.

The experiment described above was next repeated to evaluate whether the inhibitory effects of the leachate occurred at lower concentrations (higher dilutions) that were similar to those used in Trial 1. The MFC was supplied with 321 mg COD/L from day 0 to day 2 and then leachate diluted to 2130 mg COD/L after day 2. After switching to the higher strength leachate, the current recovered briefly after an initial drop but then declined steadily (Figure 4.17), which suggests that the MFC performance was negatively impacted even by leachate diluted to ~2000 mg COD/L. However, CV analysis of the ARB showed clear reduction and oxidation peaks (Figure 4.18), which indicates the performance of the anode is still good at this leachate dilution. Consequently, the declining I after switching to the higher strength leachate apparently was the decreased cathode performance. This suggests that the leachate might contain multiple inhibitory constituents that may negatively impact MFC performance via more than one mechanism. A constituent of undiluted leachate appeared to completely inactivate ARB, while lower strength leachate allowed ARB to be active but negatively impacted cathode performance.

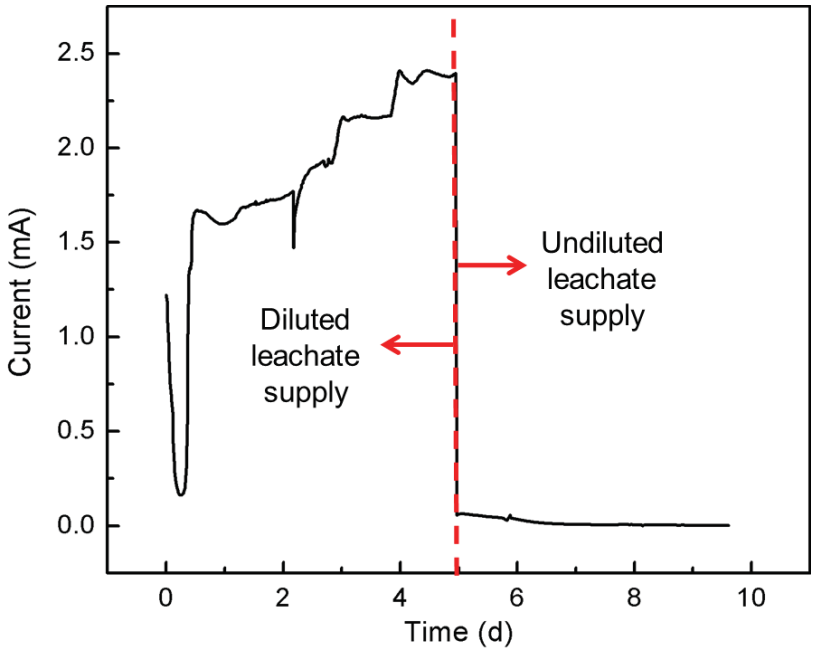

Figure 4.15 Evaluation of the effect of inhibitory constituents on current (I) in a continuous-flow MFC fitted with a new cathode and supplied with diluted and undiluted leachate. Diluted leachate (110 mg COD/L) was supplied from day 0 to 4.5 d. Undiluted leachate (24,852 mg COD/L) was supplied after 4.5 d.

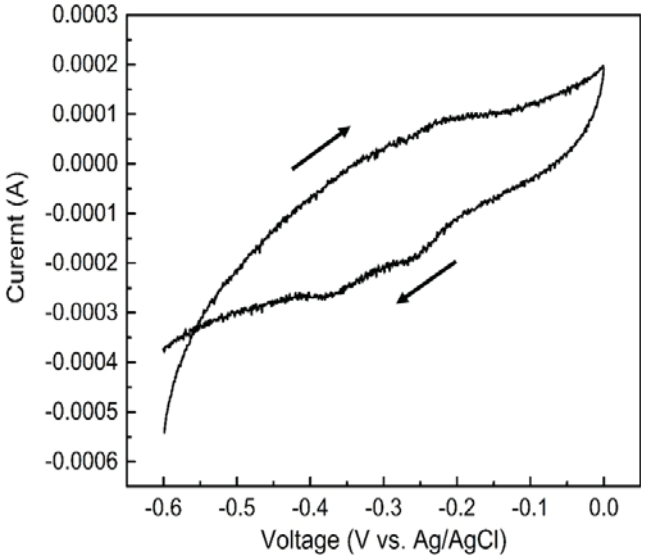

Figure 4.16 Anode cyclic voltammetry curve obtained in the continuous-flow MFC fed with undiluted leachate on day 9 in Figure 4.15.

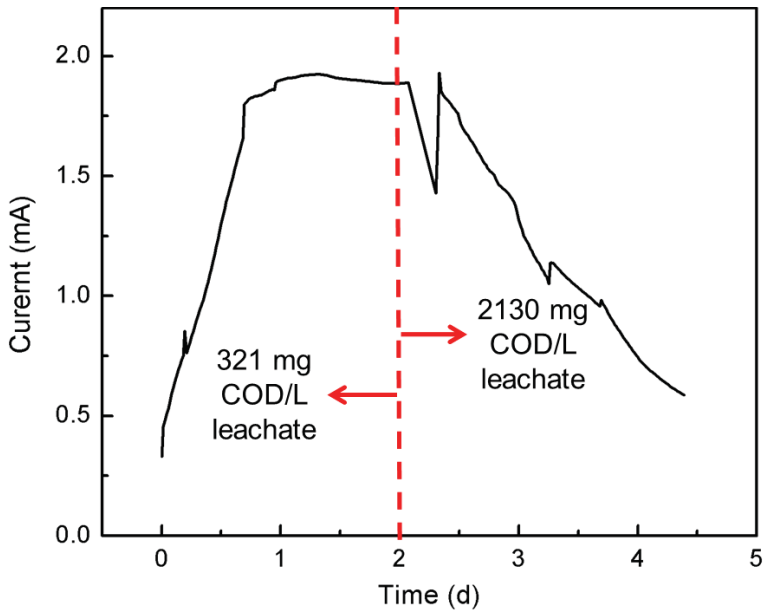

Figure 4.17 Evaluation of the effect of inhibitory constituents on current (I) in a continuous-flow MFC fitted with a new cathode and supplied with diluted leachate. Diluted leachate (321 mg COD/L) was replaced with another diluted leachate (2130 mg COD/L) after 2 d.

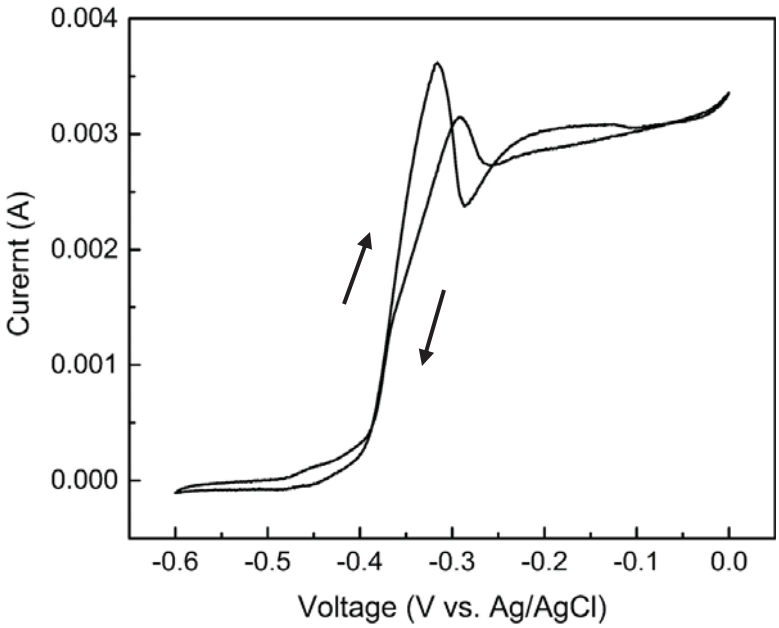

Figure 4.18 Anode cyclic voltammetry curve obtained in the continuous-flow MFC fed with 2130 mg COD/L diluted leachate on day 4 in Figure 4.17.

4.3.4.2 Use of LSV analysis to evaluate the effects of leachate concentration and time of exposure to leachate concentration on cathode performance in continuous-flow MFC performance

To better understand how exposure to leachate constituents affected cathode performance in the continuous-flow MFCs, LSV was performed on a new cathode prior to the start of Trial 2 and following exposure to a series of different substrate concentrations. The LSV curve for a new cathode was first obtained to obtain baseline information. Then this cathode was consecutively exposed to leachate diluted to 562 mg COD/L, 56 mg COD/L, 377 mg COD/L, and 1013 mg COD/L. The cathode was operated at each concentration for 1 to 2 d. An LSV curve was acquired at each concentration before switching to a new substrate concentration. The LSV curves are shown in Figure 4.19. In general, the LSV curves shifted to the upper left with each new concentration. This trend suggests increasing the time of exposure to the landfill leachate affected cathode performance. However, the shifts in the LSV curves with each new exposure to landfill leachate were relatively minor until the MFC influent was switched to 1013 mg COD/L. This was a much higher-strength leachate than was used at the previous time points, and the change in the LSV curve relative to the baseline was also much greater than for more modest changes in leachate strength. Therefore, it is difficult to completely rule out the possibility that exposure to high-strength leachate, rather than the total length of time of exposure to leachate caused the shift in LSV curves.

Previous studies provide evidence that both total exposure time, and the strength of the MFC influent, can negatively impact cathode performance. He *et al.* [106, 107] found that water pressure in an MFC operated in continuous-flow mode could cause the cathode to flood could cause the flood of the cathode, which will prevent oxygen from diffusion into the air side of the cathode, and consequently a decline in MFC performance over time. In another study, the elevated levels of salt in high-strength leachate supplied to an MFC reduced the catalytic activity of the cathode [108]. Therefore, it is possible that both exposure to high water pressure over time, and exposure to high-strength leachate, reduced the performance of the cathode.

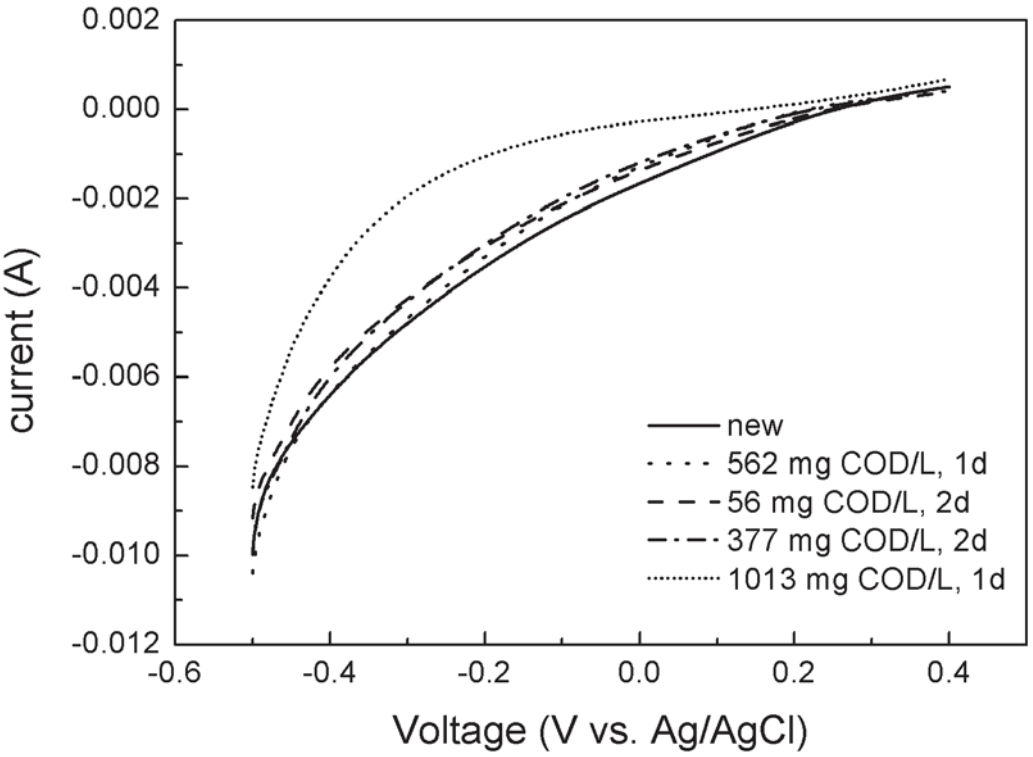

Figure 4.19 Cathode LSVs obtained in 50 mM phosphate buffer after running in the continuous-flow MFC fed with different concentrations of leachate.

4.3.4.3 Use of CV analysis to evaluate the effects of cathode age on cathode performance in continuous-flow MFC performance

The last study undertaken to gain insight into the effects of high-strength leachate on MFC performance involved comparing the CV curves obtained with new and used cathodes at the same leachate strength in continuous-flow MFCs. Five pairs of CV curves were obtained and are shown in Figure 4.20.

Although the CV curves are obtained by characterizing the ARB at the anode, the performance of the cathode can also influence the CV curves. At leachate concentrations of around 350 and 560 mg COD/L (Figure 4.20, panels D and E), the plateaus of the CV curves and the voltage outputs (showed in the legend) increased after changing from an old to a new cathode. However, for the MFCs operated at approximately 50, 100, and 1000 mg COD/L, the current plateaus of the CV curves at a given influent leachate concentration did not change when a new cathode was used.

The following conceptual model was formulated to explain the different apparent responses to cathode age at different influent substrate concentrations. At low leachate strengths (below 100 mg COD/L), the anode performance and current output are limited by the substrate concentration and therefore the condition of the cathode has little impact on overall MFC performance. When the leachate concentration increased further, to around 350 ~ 560 mg COD/L, the substrate concentration no longer limiting, and .the cathode condition becomes the limiting factor for the overall current flow through the MFC. Therefore, higher current plateaus were observed for the MFC after switching to a new

cathode when operated at these intermediate leachate strengths. At the highest leachate strength (1013 mg COD/L), the anode performance limits the current through the MFC because of the increase in the concentrations of inhibitory constituents associated with high-strength leachate. In this case, substrate concentration again became the limiting factor instead of cathode condition. Thus there was no big change in the current plateau when a new cathode was used.

Cathode limitations were obvious in this study because of the low ratio of cathode area-to-anode area. Previous studies have shown that increasing the ratio of cathode surface area to the anode area can improve the performance of the MFC and the power output [109]. As a result, the voltage output is highly sensitive to the condition of the cathode, which is why the different voltage outputs were observed when a new cathode was used (at intermediate leachate strengths). As shown in Figure 4.19, the cathode condition might change over time. Biofilm formation and salt precipitation on the interior and exterior of the cathode may have further reduced the cathode performance over time [110].

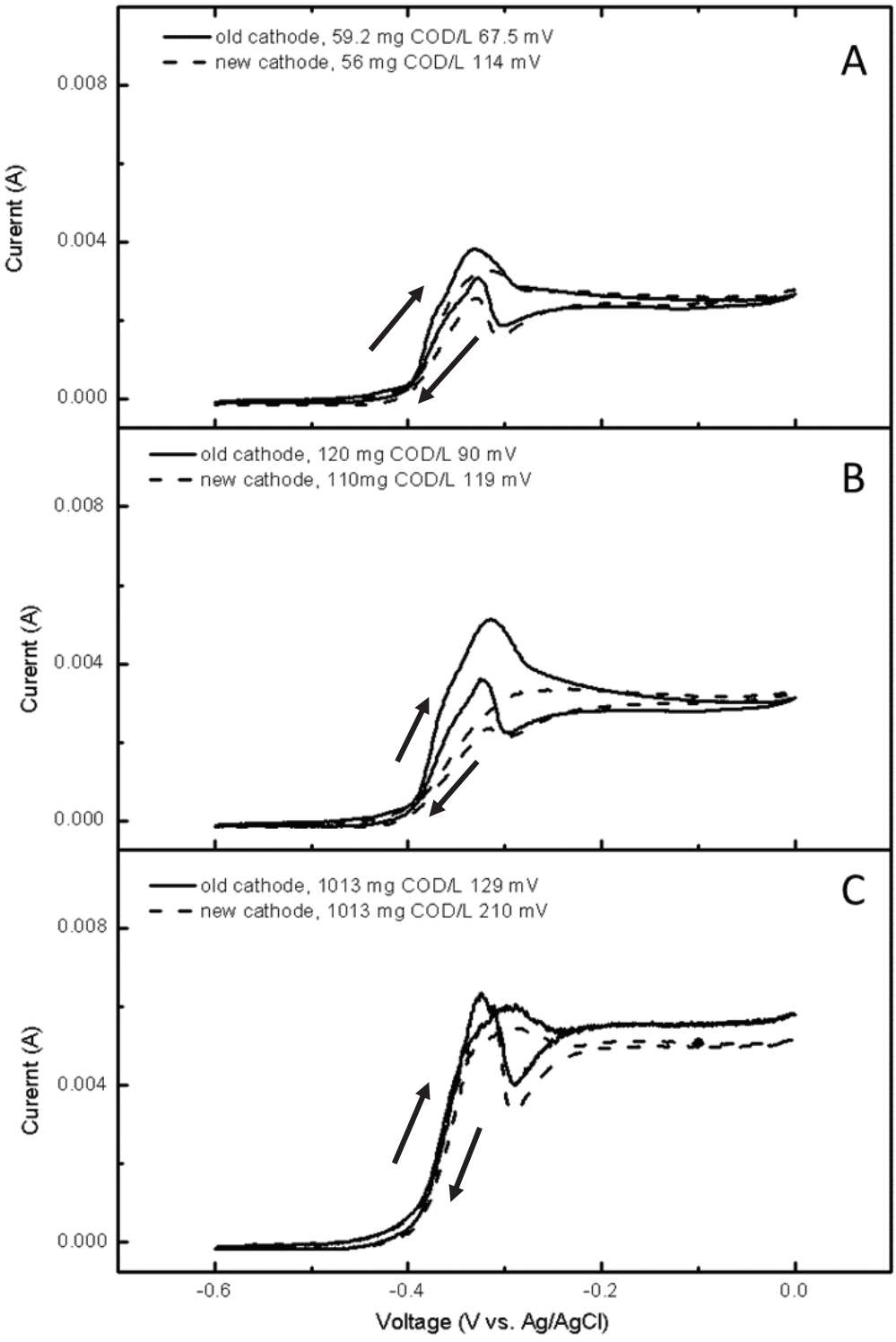
old cathode, 59.2 mg COD/L 67.5 mV
new cathode, 56 mg COD/L 114 mV
A
old cathode, 120 mg COD/L 90 mV
new cathode, 110mg COD/L 119 mV
B
old cathode, 1013 mg COD/L 129 mV
new cathode, 1013 mg COD/L 210 mV
C
Curernt (A)
0.008
0.004
0.000
-0.6
-0.4
-0.2
0.0
Voltage (V vs. Ag/AgCl)

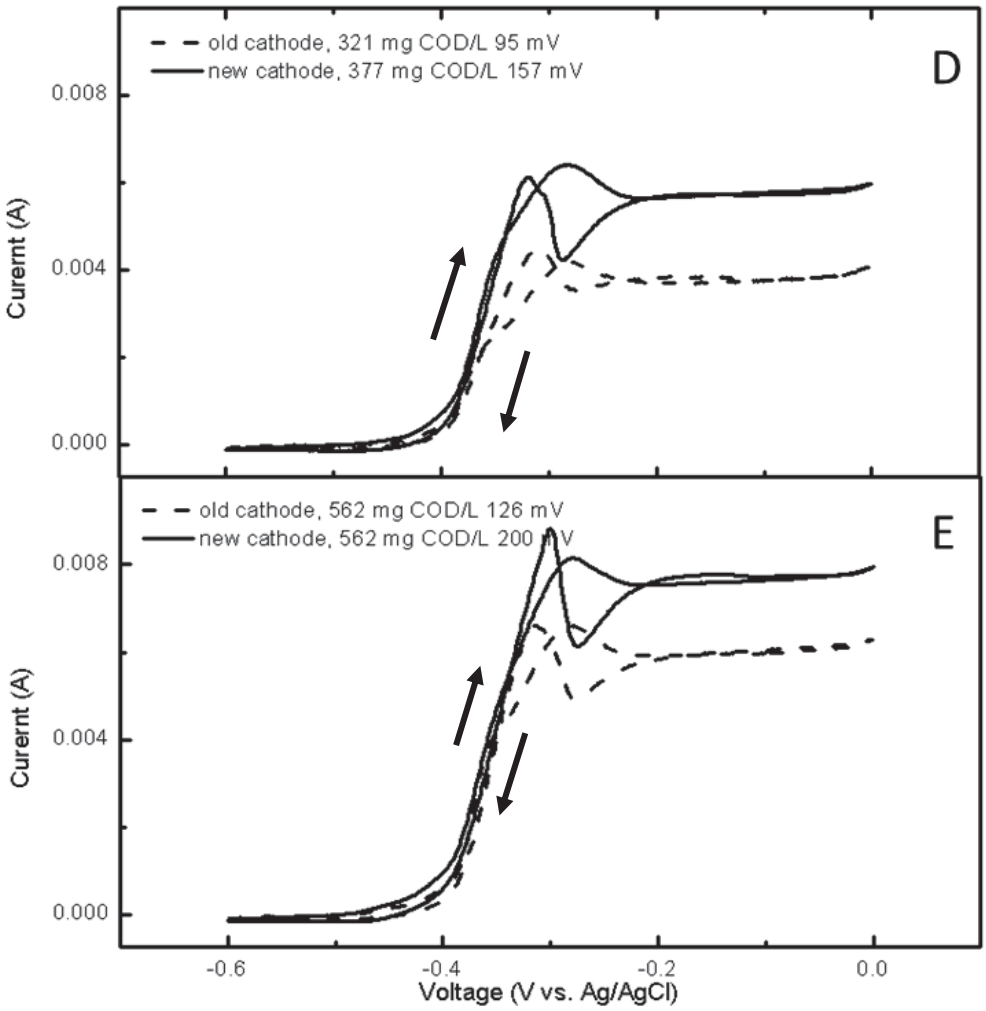

Figure 4.20 Cyclic voltammetry curves of MFCs operated with new (solid lines) and used (dashed lines) cathodes and supplied with leachate diluted to approximately: (A) 56 mg COD/L, (B) 110 mg COD/L, (C) 1013 mg COD/L, (D) 377 mg COD/L, and (E) 562 mg COD/L.

4.3.5 Effects of Substrate Concentration on P_d and R_{int} in the Trial 1 Continuous-Flow Experiment

LSV tests were performed on the continuous-flow MFC during Trial 1 to evaluate the impact of S and OLR on P_d and R_{int}. The resulting P_d curves are shown in Figure 4.21. As

expected, the maximum P_d (1.28 W/m^2 or 2.2 W/m^3) was obtained at the highest OLR (2.5 g COD/L·d). P_d decreased with decreasing S.

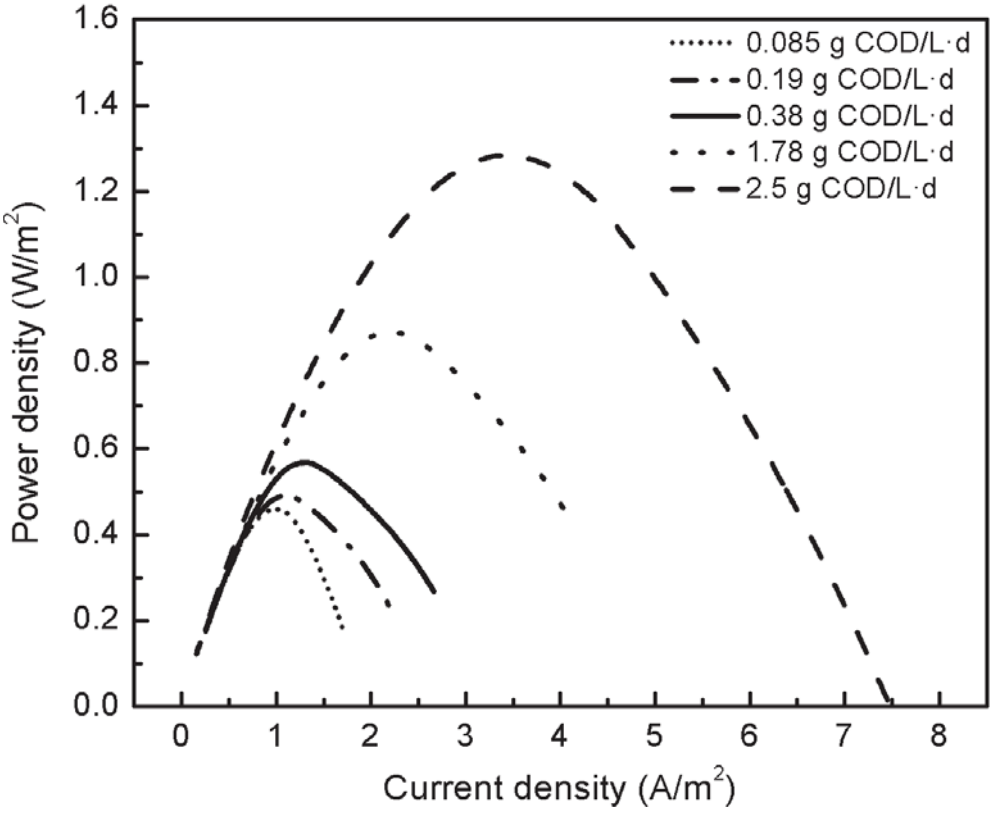

Figure 4.21 P_d curves obtained for the continuous-flow MFC operated at different OLRs during Trial 1

4.3.5.1 Internal resistance vs. OLR

The polarization curves obtained in Trial 1 are shown in Figure 4.22. As discussed previously, the slope of the linear portion of the polarization curve is equal to the total R_{int}, which decreased with OLR. EIS tests were performed on the MFC 30 min after running

LSV analysis at each OLR. An example of the Nyquist and Bode plots obtained from the EIS are shown in Figure 4.23.

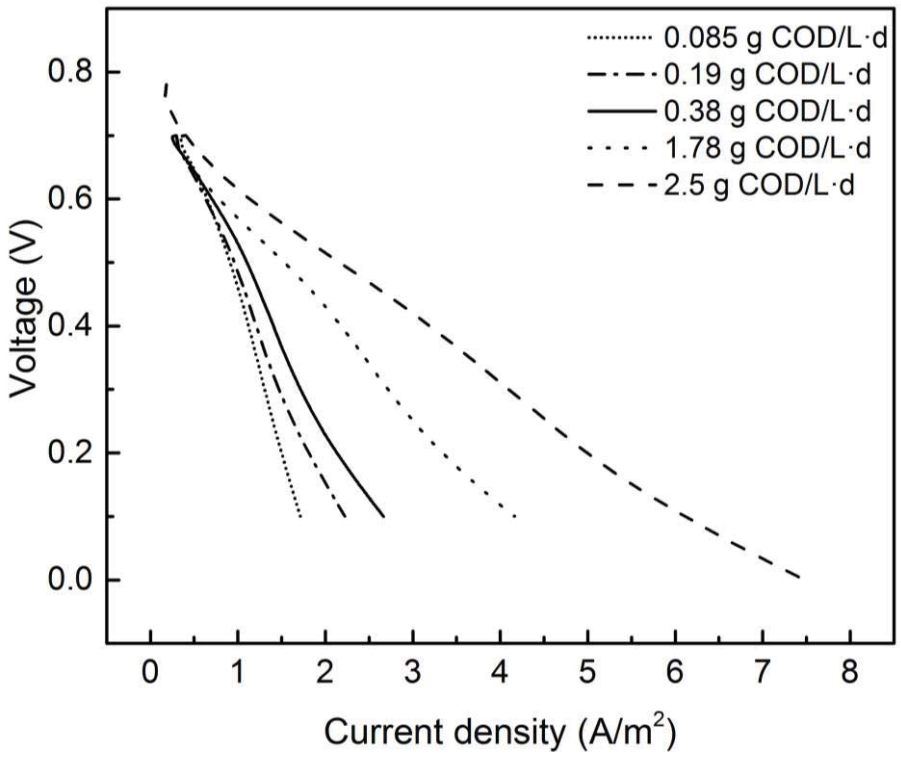

Figure 4.22 Polarization curves obtained for the continuous-flow MFC operated at different OLRs during Trial 1.

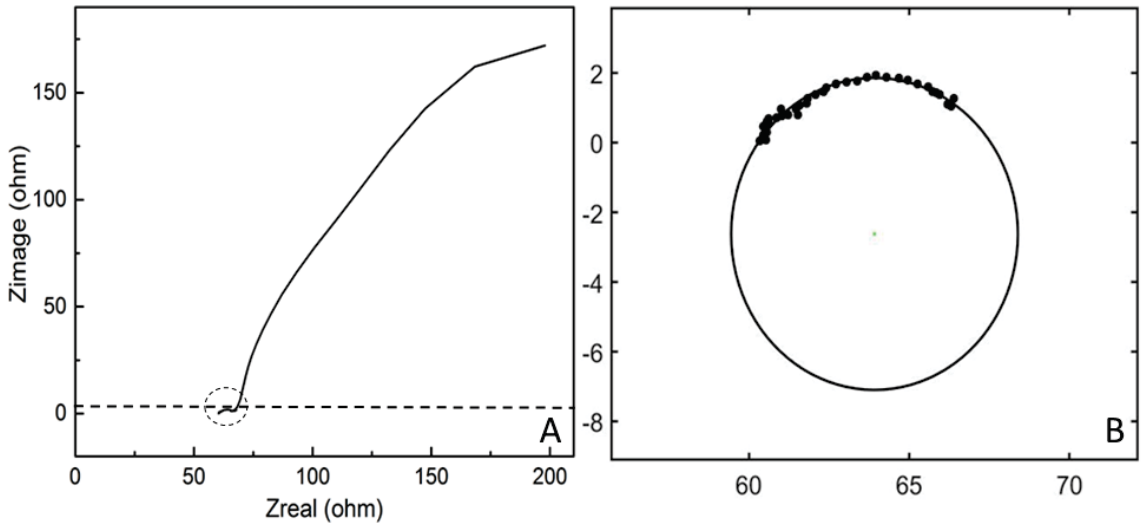

Figure 4.23 Example EIS results obtained using the continues-flow MFC operated on leachate diluted to 0.19 g COD/L·d. (A) The Nyquist plot and (B) Bode (circle fit) plot performed on the curved section of the Nyquist plot to estimate charge transfer resistance. In panel A, a dashed circle identifies the portion of the Nyquist plot analyzed in the circle fit plot (panel B). In panel B, each data point represents data of the dashed circle and the solid line represents the best circle fit to the data.

The $R_{solution}$ (64 Ω) was found at the x-axis intercept of the curve in the Nyquist plot. The circle-fit method in MATLAB was used to estimate the R_{charge}. The diameter of the fitted circle is 9 Ω. The $R_{diffusion}$ and R_{other} (515 Ω) was then calculated according to Equation 3-3. This analysis was repeated at each OLR.

Figure 4.24 shows total internal resistance, solution resistance, charge transfer resistance, and diffusion plus other resistances as a function of S. Total internal resistance decreased with increasing S. The $R_{solution}$ was fairly constant at all of the tested loading conditions. This was expected because the conductivity was kept constant at 11.25 ± 0.37 mS/cm for all leachate dilutions. The R_{charge} was only a minor component of the total $R_{int.}$. Therefore, the decrease in the total R_{int} with increasing S primarily reflected the trends in the diffusion

plus other resistance. There are at least two possible explanations for the observed decreases in the diffusion plus other resistances with increasing S. First, the driving force for substrate diffusion to electrodes grows with increases in S. Second, the rate of substrate utilization by ARB is a function of S. Therefore, increased rates of diffusion and/or microbial substrate utilization could explain the trends in R_{int} as a function of S.

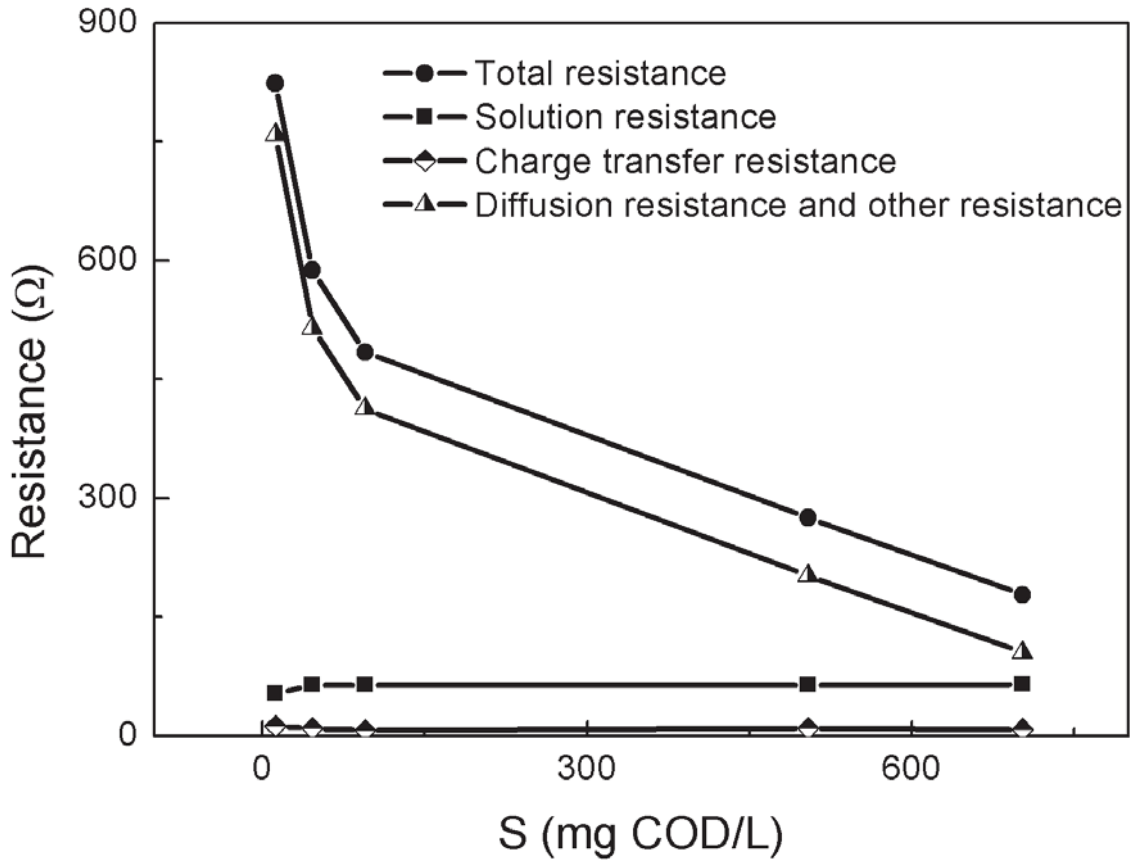

Figure 4.24 Characterization of Rint in the continuous-flow MFC operated at different substrate concentrations during Trial 1

4.3.6 Effects of Substrate Concentration on CE, COD and BOD removal in the Trial 1 Continuous-Flow Experiment

CE was calculated for the continuous-flow MFC at each S and ranged from a high of 70% at an S of 46 mg COD/L to a low of 25% at an S of 702 mg COD/L (Figure 4.25). In an earlier study, an inverse relationship between CE and OLR was observed and was attributed to high levels of sulfate reduction and/or methane generation at high OLRs [22]. Presumably, at lower S, sulfate-reducing bacteria and methanogens are unable to compete with ARB for acetate and other substrates due to their slower substrate utilization kinetics, but at higher S, they may be able to grow on the excess substrate. It is interesting to note that the CE at an OLR of 0.085 g COD/L·d was lower than that calculated at 0.19 g COD/L·d. Lower CEs at dilute S was also observed in another study [111] and was attributed to the poor performance of ARB under substrate-limited conditions. The maximum CE obtained in this study is higher than in most MFCs fed with landfill leachate. The highest CE reported in the literature is 57% and was obtained with a two-chambered, continuous-flow MFC supplied with "young" landfill leachate fed and equipped with new Ti-TiO_2 electrodes at an OLR of 1 g COD/L·d [22]. Presumably, the CE in the current study was relatively high because the leachate was produced by highly biodegradable organic wastes (paper and food products). In contrast, leachate derived from actual landfills can contain relatively high concentrations of nonbiodegradable material.

Overall, the COD and BOD removal decreased with OLR (Figure 4.25). The maximum BOD and COD removals were 67% and 57%, respectively, and were achieved

at an S of 12 mg COD/L. At an S of 702 mg COD/L, the COD removal was only 11%, which was believed to result from the insufficient amount of active bacteria in the MFC [42].

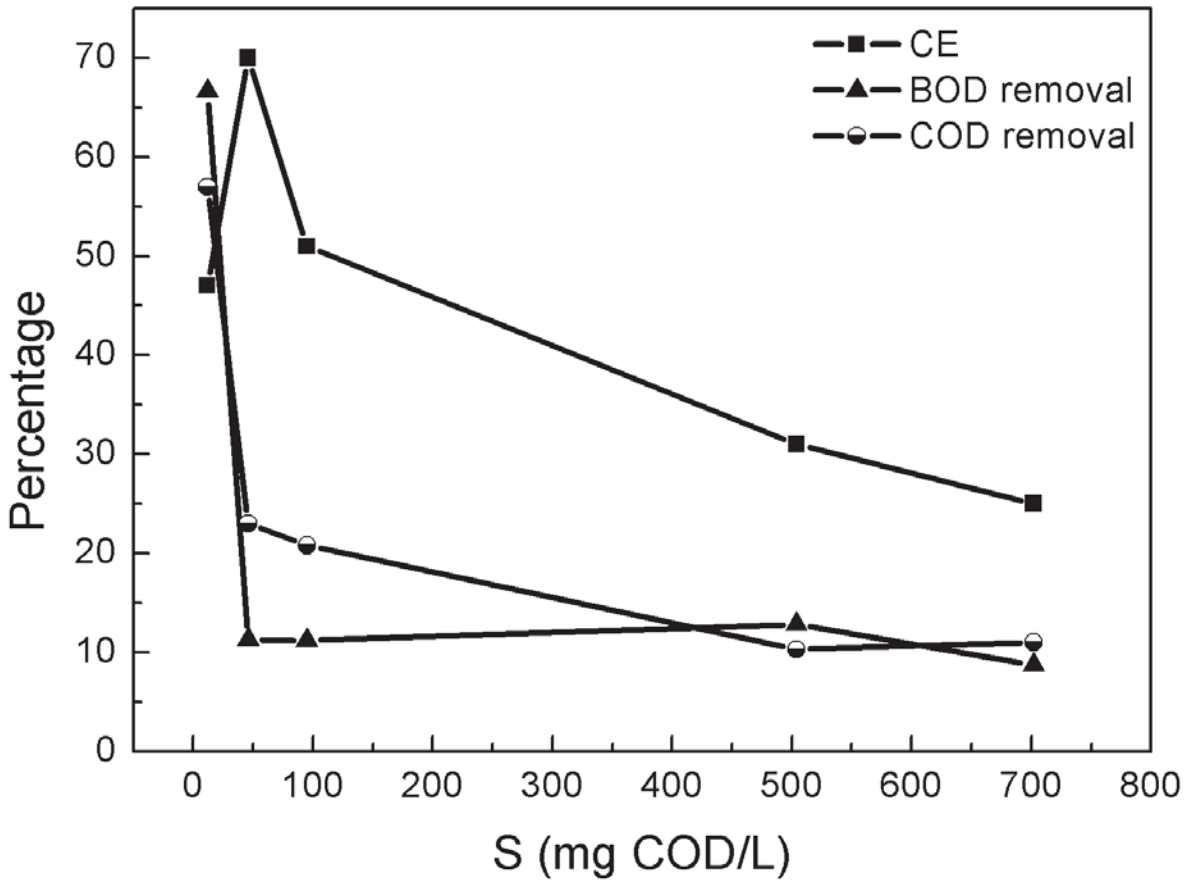

Figure 4.25 Characterization of BOD and COD removal and CE in the continuous-flow MFC operated at different substrate concentrations during Trial 1

References

1. United States Environmental Protection Agency, *Municipal Solid Waste Generation, Recycling, and Disposal in the United States: Facts and Figures for 2012*. 2014.
2. Christensen T. H., P. Kjeldsen, P. L. Bjerg, D. L. Jensen, J. B. Christensen, A. Baun, H. J. Albrechtsen, and G. Heron, *Biogeochemistry of landfill leachate plumes.* Applied Geochemistry, 2001. **16**(7-8): p. 659-718.
3. Kjeldsen P., M. A. Barlaz, A. P. Rooker, A. Baun, A. Ledin, and T. H. Christensen, *Present and long-term composition of MSW landfill leachate: A review.* Critical Reviews in Environmental Science and Technology, 2002. **32**(4): p. 297-336.
4. Li H. S, S. Q Zhou, Y. B Sun, P. Feng, and J. D Li, *Advanced treatment of landfill leachate by a new combination process in a full-scale plant.* Journal of Hazardous Materials, 2009. **172**(1): p. 408-415.
5. Tugtas A. E., P. Cavdar, and B. Calli, *Bio-electrochemical post-treatment of anaerobically treated landfill leachate.* Bioresour Technol, 2013. **128**: p. 266-72.
6. Johannessen Lars Mikkel, *Guidance note on leachate management for municipal solid waste landfills*. 1999: World Bank.
7. *Municipal Solid Waste Landfills Economic Impact Analysis for the Proposed New Subpart to the New Source Performance Standards*, O.o.A.a.R. U.S. Environmental Protection Agency, Office of Air Quality Planning and Standards, Research Triangle Park, Editor. 2014: http://www.epa.gov/ttnecas1/eia.html.
8. International Environmental Business, *U.S. Solid Waste Industry Reaches $55 Billion in Revenues - Innovative conversion technologies poised to shake up the industry*. 2012: http://ebionline.org/updates/1244-us-solid-waste-industry-reaches-55-billion-in-revenuesinnovative-conversion-technologies-poised-to-shake-up-the-industry.
9. Janicek Anthony, Yanzen Fan, and Hong Liu, *Design of microbial fuel cells for practical application: a review and analysis of scale-up studies.* Biofuels, 2014. **5**(1): p. 79-92.
10. Allen R. M. and H. P. Bennetto, *MICROBIAL FUEL-CELLS - ELECTRICITY PRODUCTION FROM CARBOHYDRATES.* Applied Biochemistry and Biotechnology, 1993. **39**: p. 27-40.
11. Kim H. J., H. S. Park, M. S. Hyun, I. S. Chang, M. Kim, and B. H. Kim, *A mediator-less microbial fuel cell using a metal reducing bacterium, Shewanella putrefaciense.* Enzyme and Microbial Technology, 2002. **30**(2): p. 145-152.
12. Logan Bruce E., *Microbial Fuel Cells*. 2008, Hoboken, NJ: John Wiley & Sons, Inc.
13. Reimers C. E., L. M. Tender, S. Fertig, and W. Wang, *Harvesting energy from the marine sediment--water interface.* Environ Sci Technol, 2001. **35**(1): p. 192-5.

14. Min Booki and Bruce E Logan, *Continuous electricity generation from domestic wastewater and organic substrates in a flat plate microbial fuel cell.* Environmental science & technology, 2004. **38**(21): p. 5809-5814.
15. Patil S. A., V. P. Surakasi, S. Koul, S. Ijmulwar, A. Vivek, Y. S. Shouche, and B. P. Kapadnis, *Electricity generation using chocolate industry wastewater and its treatment in activated sludge based microbial fuel cell and analysis of developed microbial community in the anode chamber.* Bioresource Technology, 2009. **100**(21): p. 5132-5139.
16. Heilmann J. and B. E. Logan, *Production of electricity from proteins using a microbial fuel cell.* Water Environment Research, 2006. **78**(5): p. 531-537.
17. Ieropoulos I. A., P. Ledezma, A. Stinchcombe, G. Papaharalabos, C. Melhuish, and J. Greenman, *Waste to real energy: the first MFC powered mobile phone.* Physical Chemistry Chemical Physics, 2013. **15**(37): p. 15312-15316.
18. Yuan H. R., L. F. Deng, T. Lu, and Y. Chen, *Hydrothermal Synthesis of Nanostructured Manganese Oxide as Cathodic Catalyst in a Microbial Fuel Cell Fed with Leachate.* Scientific World Journal, 2014: p. 6.
19. Choi J. D. and Y. Ahn, *Enhanced bioelectricity harvesting in microbial fuel cells treating food waste leachate produced from biohydrogen fermentation.* Bioresource Technology, 2015. **183**: p. 53-60.
20. Wu D., T. Wang, X. H. Huang, J. Dolfing, and B. Xie, *Perspective of harnessing energy from landfill leachate via microbial fuel cells: novel biofuels and electrogenic physiologies.* Applied Microbiology and Biotechnology, 2015. **99**(19): p. 7827-7836.
21. Yuan Haoran, Lifang Deng, and Yong Chen, *Optimization of biodrying pretreatment of municipal solid waste and microbial fuel cell treatment of leachate.* Biotechnology and Bioprocess Engineering, 2014. **19**(4): p. 668-675.
22. Ozkaya B., A. Y. Cetinkaya, M. Cakmakci, D. Karadag, and E. Sahinkaya, *Electricity generation from young landfill leachate in a microbial fuel cell with a new electrode material.* Bioprocess and Biosystems Engineering, 2013. **36**(4): p. 399-405.
23. Ganesh K. and J. R. Jambeck, *Treatment of landfill leachate using microbial fuel cells: Alternative anodes and semi-continuous operation.* Bioresource Technology, 2013. **139**: p. 383-387.
24. Ren Lijiao, Yongtae Ahn, and Bruce E. Logan, *A two-stage microbial fuel cell and anaerobic fluidized bed membrane bioreactor (MFC-AFMBR) system for effective domestic wastewater treatment.* Environ Sci Technol, 2014. **48**(7): p. 4199-206.
25. Mangimbulude Jubhar C., Boris M. Van Breukelen, Agna S. Krave, Nico M. Van Straalen, and Wilfred F. M. Röling, *Seasonal dynamics in leachate hydrochemistry and natural attenuation in surface run-off water from a tropical landfill.* Waste Management, 2009. **29**(2): p. 829-838.
26. Rikame Satish S., Alka A. Mungray, and Arvind K. Mungray, *Electricity generation from acidogenic food waste leachate using dual chamber mediator less*

microbial fuel cell. International Biodeterioration & Biodegradation, 2012. **75**: p. 131-137.
27. Christensen Thomas H., Peter Kjeldsen, Poul L. Bjerg, Dorthe L. Jensen, Jette B. Christensen, Anders Baun, Hans-Jørgen Albrechtsen, and Gorm Heron, *Biogeochemistry of landfill leachate plumes.* Applied Geochemistry, 2001. **16**(7–8): p. 659-718.
28. Qasaimeh Ahmad, *Intelligent MSW Biocell Approach for Efficient Methane Production.* Computational Water, Energy, and Environmental Engineering, 2012. **Vol.01No.02**: p. 7.
29. Hilger H. Hilger Morton A. Barlaz, *Anaerobic decomposition of refuse in landfills and methane oxidation in landfill cover soils*, in *Manual of Environmental Microbiology*. 2002, ASM Press: Washington, DC.
30. Christensen Thomas, *Sanitary landfilling: process, technology and environmental impact*. 2012: Elsevier.
31. Pohland Frederick George, *Sanitary landfill stabilization with leachate recycle and residual treatment.* 1973.
32. Renou S., J. G. Givaudan, S. Poulain, F. Dirassouyan, and P. Moulin, *Landfill leachate treatment: Review and opportunity.* Journal of Hazardous Materials, 2008. **150**(3): p. 468-493.
33. Omar Hecham and Sohrab Rohani, *Treatment of landfill waste, leachate and landfill gas: A review.* Frontiers of Chemical Science and Engineering, 2015. **9**(1): p. 15-32.
34. Laloui-Carpentier Wassila, Tianlun Li, Vassilia Vigneron, Laurent Mazéas, and Théodore Bouchez, *Methanogenic diversity and activity in municipal solid waste landfill leachates.* Antonie van Leeuwenhoek, 2006. **89**(3-4): p. 423-434.
35. Ledakowicz Stanislaw and Katarzyna Kaczorek, *Laboratory simulation of anaerobic digestion of municipal solid waste.* Journal of Environmental Science and Health, Part A, 2004. **39**(4): p. 859-871.
36. Huang L. N., H. Zhou, Y. Q. Chen, S. Luo, C. Y. Lan, and L. H. Qu, *Diversity and structure of the archaeal community in the leachate of a full-scale recirculating landfill as examined by direct 16S rRNA gene sequence retrieval.* FEMS Microbiol Lett, 2002. **214**(2): p. 235-40.
37. Reinhart Debra R. and Basel A. Al-Yousfi, *THE IMPACT OF LEACHATE RECIRCULATION ON MUNICIPAL SOLID WASTE LANDFILL OPERATING CHARACTERISTICS.* Waste Management & Research, 1996. **14**(4): p. 337-346.
38. Shoener B. D., I. M. Bradley, R. D. Cusick, and J. S. Guest, *Energy positive domestic wastewater treatment: the roles of anaerobic and phototrophic technologies.* Environmental Science: Processes & Impacts, 2014. **16**(6): p. 1204-1222.
39. Lee Y., L. Martin, P. Grasel, K. Tawfiq, and G. Chen, *Power generation and nitrogen removal of landfill leachate using microbial fuel cell technology.* Environ Technol, 2013. **34**(17-20): p. 2727-36.

40. Vázquez-Larios Ana Line, Omar Solorza-Feria, Héctor M. Poggi-Varaldo, Rosa De Guadalupe González-Huerta, María Teresa Ponce-Noyola, Elvira Ríos-Leal, and Noemí Rinderknecht-Seijas, *Bioelectricity production from municipal leachate in a microbial fuel cell: Effect of two cathodic catalysts.* International Journal of Hydrogen Energy, 2014. **39**(29): p. 16667-16675.
41. Puig S., M. Serra, M. Coma, M. Cabre, M. D. Balaguer, and J. Colprim, *Microbial fuel cell application in landfill leachate treatment.* Journal of Hazardous Materials, 2011. **185**(2-3): p. 763-767.
42. You S. J., Q. L. Zhao, J. Q. Jiang, J. N. Zhang, and S. Q. Zhao, *Sustainable approach for leachate treatment: Electricity generation in microbial fuel cell.* Journal of Environmental Science and Health Part a-Toxic/Hazardous Substances & Environmental Engineering, 2006. **41**(12): p. 2721-2734.
43. Franks Ashley E and Kelly P Nevin, *Microbial fuel cells, a current review.* Energies, 2010. **3**(5): p. 899-919.
44. Kim J. R., J. Dec, M. A. Bruns, and B. E. Logan, *Removal of odors from Swine wastewater by using microbial fuel cells.* Appl Environ Microbiol, 2008. **74**(8): p. 2540-3.
45. Pant Deepak, Gilbert Van Bogaert, Ludo Diels, and Karolien Vanbroekhoven, *A review of the substrates used in microbial fuel cells (MFCs) for sustainable energy production.* Bioresource Technology, 2010. **101**(6): p. 1533-1543.
46. Clauwaert P., K. Rabaey, P. Aelterman, L. De Schamphelaire, T. H. Ham, P. Boeckx, N. Boon, and W. Verstraete, *Biological denitrification in microbial fuel cells.* Environmental Science & Technology, 2007. **41**(9): p. 3354-3360.
47. Logan B. E., B. Hamelers, R. A. Rozendal, U. Schrorder, J. Keller, S. Freguia, P. Aelterman, W. Verstraete, and K. Rabaey, *Microbial fuel cells: Methodology and technology.* Environmental Science & Technology, 2006. **40**(17): p. 5181-5192.
48. Logan B. E. and J. M. Regan, *Microbial fuel cells--challenges and applications.* Environ Sci Technol, 2006. **40**(17): p. 5172-80.
49. Holmberg Sunshine, Alexandra Perebikovsky, Lawrence Kulinsky, and Marc Madou, *3-D Micro and Nano Technologies for Improvements in Electrochemical Power Devices.* Micromachines, 2014. **5**(2): p. 171-203.
50. Oh Sang-Eun and Bruce E Logan, *Proton exchange membrane and electrode surface areas as factors that affect power generation in microbial fuel cells.* Applied Microbiology and Biotechnology, 2006. **70**(2): p. 162-169.
51. Cheng Shaoan and Bruce E. Logan, *Ammonia treatment of carbon cloth anodes to enhance power generation of microbial fuel cells.* Electrochemistry Communications, 2007. **9**(3): p. 492-496.
52. Cheng S., H. Liu, and B. E. Logan, *Increased power generation in a continuous flow MFC with advective flow through the porous anode and reduced electrode spacing.* Environmental Science & Technology, 2006. **40**(7): p. 2426-2432.

53. Janicek Anthony, Yanzhen Fan, and Hong Liu, *Performance and stability of different cathode base materials for use in microbial fuel cells.* Journal of Power Sources, 2015. **280**(0): p. 159-165.
54. Hutchinson Adam J., Justin C. Tokash, and Bruce E. Logan, *Analysis of carbon fiber brush loading in anodes on startup and performance of microbial fuel cells.* Journal of Power Sources, 2011. **196**(22): p. 9213-9219.
55. Lanas V. and B. E. Logan, *Evaluation of multi-brush anode systems in microbial fuel cells.* Bioresour Technol, 2013. **148**: p. 379-85.
56. Kumar G. G., V. G. S. Sarathi, and K. S. Nahm, *Recent advances and challenges in the anode architecture and their modifications for the applications of microbial fuel cells.* Biosensors & Bioelectronics, 2013. **43**: p. 461-475.
57. Cai Hui, Juan Wang, Yunfei Bu, and Qin Zhong, *Treatment of carbon cloth anodes for improving power generation in a dual-chamber microbial fuel cell.* Journal of Chemical Technology & Biotechnology, 2013. **88**(4): p. 623-628.
58. Lowy Daniel A. and Leonard M. Tender, *Harvesting energy from the marine sediment–water interface: III. Kinetic activity of quinone- and antimony-based anode materials.* Journal of Power Sources, 2008. **185**(1): p. 70-75.
59. Feng Yujie, Qiao Yang, Xin Wang, and Bruce E. Logan, *Treatment of carbon fiber brush anodes for improving power generation in air–cathode microbial fuel cells.* Journal of Power Sources, 2010. **195**(7): p. 1841-1844.
60. Oh S. E. and B. E. Logan, *Voltage reversal during microbial fuel cell stack operation.* Journal of Power Sources, 2007. **167**(1): p. 11-17.
61. Zhang Fang, Shaoan Cheng, Deepak Pant, Gilbert Van Bogaert, and Bruce E. Logan, *Power generation using an activated carbon and metal mesh cathode in a microbial fuel cell.* Electrochemistry Communications, 2009. **11**(11): p. 2177-2179.
62. Choi J. and Y. Ahn, *Continuous electricity generation in stacked air cathode microbial fuel cell treating domestic wastewater.* Journal of Environmental Management, 2013. **130**: p. 146-152.
63. Cheng Shaoan, Hong Liu, and Bruce E. Logan, *Power Densities Using Different Cathode Catalysts (Pt and CoTMPP) and Polymer Binders (Nafion and PTFE) in Single Chamber Microbial Fuel Cells.* Environmental Science & Technology, 2006. **40**(1): p. 364-369.
64. Kim J. R., B. Min, and B. E. Logan, *Evaluation of procedures to acclimate a microbial fuel cell for electricity production.* Appl Microbiol Biotechnol, 2005. **68**(1): p. 23-30.
65. Li Xiao Min, Ka Yu Cheng, Ammaiyappan Selvam, and Jonathan W. C. Wong, *Bioelectricity production from acidic food waste leachate using microbial fuel cells: Effect of microbial inocula.* Process Biochemistry, 2013. **48**(2): p. 283-288.
66. Wagner Rachel C., Douglas F. Call, and Bruce E. Logan, *Optimal Set Anode Potentials Vary in Bioelectrochemical Systems.* Environmental Science & Technology, 2010. **44**(16): p. 6036-6041.

67. Wang Xin, Yujie Feng, Nanqi Ren, Heming Wang, He Lee, Nan Li, and Qingliang Zhao, *Accelerated start-up of two-chambered microbial fuel cells: Effect of anodic positive poised potential.* Electrochimica Acta, 2009. **54**(3): p. 1109-1114.
68. Ahn Y. and B. E. Logan, *Saline catholytes as alternatives to phosphate buffers in microbial fuel cells.* Bioresour Technol, 2013. **132**: p. 436-9.
69. Li X. M., K. Y. Cheng, and J. W. C. Wong, *Bioelectricity production from food waste leachate using microbial fuel cells: Effect of NaCl and pH.* Bioresource Technology, 2013. **149**: p. 452-458.
70. Wang Xi, Shaoan Cheng, Xiaoyuan Zhang, Xiao-Yan Li, and Bruce E. Logan, *Impact of salinity on cathode catalyst performance in microbial fuel cells (MFCs).* International Journal of Hydrogen Energy, 2011. **36**(21): p. 13900-13906.
71. Liu Hong, Shaoan Cheng, and Bruce E Logan, *Power generation in fed-batch microbial fuel cells as a function of ionic strength, temperature, and reactor configuration.* Environmental science & technology, 2005. **39**(14): p. 5488-5493.
72. Miyahara Morio, Atsushi Kouzuma, and Kazuya Watanabe, *Effects of NaCl concentration on anode microbes in microbial fuel cells.* AMB Express, 2015. **5**: p. 34.
73. Lefebvre O., Z. Tan, S. Kharkwal, and H. Y. Ng, *Effect of increasing anodic NaCl concentration on microbial fuel cell performance.* Bioresour Technol, 2012. **112**: p. 336-40.
74. Damiano Lisa, Jenna R Jambeck, and David B Ringelberg, *Municipal solid waste landfill leachate treatment and electricity production using microbial fuel cells.* Applied biochemistry and biotechnology, 2014. **173**(2): p. 472-485.
75. Li Yan, Anhuai Lu, Hongrui Ding, Xin Wang, Changqiu Wang, Cuiping Zeng, and Yunhua Yan, *Microbial fuel cells using natural pyrrhotite as the cathodic heterogeneous Fenton catalyst towards the degradation of biorefractory organics in landfill leachate.* Electrochemistry Communications, 2010. **12**(7): p. 944-947.
76. Gil G. C., I. S. Chang, B. H. Kim, M. Kim, J. K. Jang, H. S. Park, and H. J. Kim, *Operational parameters affecting the performannce of a mediator-less microbial fuel cell.* Biosens Bioelectron, 2003. **18**(4): p. 327-34.
77. Rabaey Korneel, Geert Lissens, Steven D Siciliano, and Willy Verstraete, *A microbial fuel cell capable of converting glucose to electricity at high rate and efficiency.* Biotechnology letters, 2003. **25**(18): p. 1531-1535.
78. He Zhen, Shelley D. Minteer, and Largus T. Angenent, *Electricity Generation from Artificial Wastewater Using an Upflow Microbial Fuel Cell.* Environmental Science & Technology, 2005. **39**(14): p. 5262-5267.
79. Galvez A., J. Greenman, and I. Ieropoulos, *Landfill leachate treatment with microbial fuel cells; scale-up through plurality.* Bioresour Technol, 2009. **100**(21): p. 5085-91.
80. Lee Hyung-Sool, Cesar I. Torres, and Bruce E. Rittmann, *Effects of Substrate Diffusion and Anode Potential on Kinetic Parameters for Anode-Respiring Bacteria.* Environmental Science & Technology, 2009. **43**(19): p. 7571-7577.

81. Liu Hong and Bruce E Logan, *Electricity generation using an air-cathode single chamber microbial fuel cell in the presence and absence of a proton exchange membrane.* Environmental science & technology, 2004. **38**(14): p. 4040-4046.
82. Liu Hong, Shaoan Cheng, and Bruce E. Logan, *Production of Electricity from Acetate or Butyrate Using a Single-Chamber Microbial Fuel Cell.* Environmental Science & Technology, 2005. **39**(2): p. 658-662.
83. Zhang Jiqiang, Ping Zheng, Meng Zhang, Hui Chen, Tingting Chen, Zuofu Xie, Jing Cai, and Ghulam Abbas, *Kinetics of substrate degradation and electricity generation in anodic denitrification microbial fuel cell (AD-MFC).* Bioresource Technology, 2013. **149**: p. 44-50.
84. Quanrud D. M., S. M. Carroll, C. P. Gerba, and R. G. Arnold, *Virus removal during simulated soil-aquifer treatment.* Water Research, 2003. **37**(4): p. 753-762.
85. William F. Koch George Marinenko, Robert C. Paule, *Development of a standard reference material for rainwater analysis.* Journal of Research of the National Bureau of Standards, 1986. **91**(1): p. 33-41.
86. Beaster Tristan T, *A Two-Stage Microbial Fuel Cell System to Convert Solid Organic Waste to Electricity*, in *Civil and Environmental Enginerring*. 2013, Michigan Technological University.
87. Liu Chunmei, Jun Li, Xun Zhu, Liang Zhang, Dingding Ye, Robert Keith Brown, and Qiang Liao, *Effects of brush lengths and fiber loadings on the performance of microbial fuel cells using graphite fiber brush anodes.* International Journal of Hydrogen Energy, 2013. **38**(35): p. 15646-15652.
88. Timmis Kenneth N, T Mcgenity, Jr Van Der Meer, and V De Lorenzo, *Handbook of hydrocarbon and lipid microbiology*. 2010: Springer Berlin/Heidelberg.
89. Kim Jung Rae, Booki Min, and Bruce E. Logan, *Evaluation of procedures to acclimate a microbial fuel cell for electricity production.* Applied Microbiology and Biotechnology, 2005. **68**(1): p. 23-30.
90. Atlas Ronald M . *Handbook of Media for Environmental Microbiology*. Second ed. 2005: CRC Press.
91. Wang Xin, Shaoan Cheng, Yujie Feng, Matthew D. Merrill, Tomonori Saito, and Bruce E. Logan, *Use of Carbon Mesh Anodes and the Effect of Different Pretreatment Methods on Power Production in Microbial Fuel Cells.* Environmental Science & Technology, 2009. **43**(17): p. 6870-6874.
92. Cheng Shaoan, Hong Liu, and Bruce E. Logan, *Increased performance of single-chamber microbial fuel cells using an improved cathode structure.* Electrochemistry Communications, 2006. **8**(3): p. 489-494.
93. Middaugh Joshua *How to Make Cathodes with a Diffusion Layer for Single-Chamber Microbial Fuel Cells*. 2006.
94. Venkata Mohan S., R. Saravanan, S. Veer Raghavulu, G. Mohanakrishna, and P. N. Sarma, *Bioelectricity production from wastewater treatment in dual chambered microbial fuel cell (MFC) using selectively enriched mixed microflora: Effect of catholyte.* Bioresource Technology, 2008. **99**(3): p. 596-603.

95. Oh S., B. Min, and B. E. Logan, *Cathode performance as a factor in electricity generation in microbial fuel cells.* Environ Sci Technol, 2004. **38**(18): p. 4900-4.
96. Logan B., S. Cheng, V. Watson, and G. Estadt, *Graphite fiber brush anodes for increased power production in air-cathode microbial fuel cells.* Environ Sci Technol, 2007. **41**(9): p. 3341-6.
97. Klemm Sara, *Bioenhanced Dissolution of a Tetrachloroethene (PCE) Pool in a Sand Tank Aquifer System*, in *Department of Civil and Environmental Engineering*. 2016, Michigan Technological University.
98. American Public Health Association American Water Works Association, Water Environment Federation, *Standard Methods for the Examination of Water and Wastewater*. 20th ed. 1998, Washington, DC: American Public Health Association.
99. Watson Valerie J. and Bruce E. Logan, *Analysis of polarization methods for elimination of power overshoot in microbial fuel cells.* Electrochemistry Communications, 2011. **13**(1): p. 54-56.
100. Nam J. Y., H. W. Kim, K. H. Lim, H. S. Shin, and B. E. Logan, *Variation of power generation at different buffer types and conductivities in single chamber microbial fuel cells.* Biosens Bioelectron, 2010. **25**(5): p. 1155-9.
101. Torres C. I., A. Kato Marcus, and B. E. Rittmann, *Kinetics of consumption of fermentation products by anode-respiring bacteria.* Applied Microbiology and Biotechnology, 2007. **77**(3): p. 689-697.
102. Torres C. I., A. K. Marcus, H. S. Lee, P. Parameswaran, R. Krajmalnik-Brown, and B. E. Rittmann, *A kinetic perspective on extracellular electron transfer by anode-respiring bacteria.* Fems Microbiology Reviews, 2010. **34**(1): p. 3-17.
103. Marsili E., J. B. Rollefson, D. B. Baron, R. M. Hozalski, and D. R. Bond, *Microbial biofilm voltammetry: direct electrochemical characterization of catalytic electrode-attached biofilms.* Appl Environ Microbiol, 2008. **74**(23): p. 7329-37.
104. Bonanni P. Sebastian, Dan F. Bradley, Germán D. Schrott, and Juan Pablo Busalmen, *Limitations for Current Production in Geobacter sulfurreducens Biofilms.* ChemSusChem, 2013. **6**(4): p. 711-720.
105. Richter Hanno, Kelly P. Nevin, Hongfei Jia, Daniel A. Lowy, Derek R. Lovley, and Leonard M. Tender, *Cyclic voltammetry of biofilms of wild type and mutant Geobacter sulfurreducens on fuel cell anodes indicates possible roles of OmcB, OmcZ, type IV pili, and protons in extracellular electron transfer.* Energy & Environmental Science, 2009. **2**(5): p. 506.
106. He Weihua, Jia Liu, Da Li, H. M. Wang, Youpeng Qu, Xin Wang, and Yujie Feng, *The electrochemical behavior of three air cathodes for microbial electrochemical system (MES) under meter scale water pressure.* Journal of Power Sources, 2014. **267**: p. 219-226.
107. Ahn Yongtae, Fang Zhang, and Bruce E. Logan, *Air humidity and water pressure effects on the performance of air-cathode microbial fuel cell cathodes.* Journal of Power Sources, 2014. **247**(0): p. 655-659.

108. Rismani-Yazdi Hamid, Sarah M Carver, Ann D Christy, and Olli H Tuovinen, *Cathodic limitations in microbial fuel cells: an overview.* Journal of Power Sources, 2008. **180**(2): p. 683-694.
109. Li Lianhua, Xiaoying Kong, Yongming Sun, Zhenhong Yuan, and Ying Li. *Performance of microbial fuel cell in different anode and cathode electrode sizes*. in *Remote Sensing, Environment and Transportation Engineering (RSETE), 2011 International Conference on*. 2011.
110. Li Da, Jia Liu, Youpeng Qu, Haiman Wang, and Yujie Feng, *Analysis of the effect of biofouling distribution on electricity output in microbial fuel cells.* Rsc Advances, 2016. **6**(33): p. 27494-27500.
111. Huang Liping, Shaoan Cheng, Farzaneh Rezaei, and Bruce E. Logan, *Reducing organic loads in wastewater effluents from paper recycling plants using microbial fuel cells.* Environmental Technology, 2009. **30**(5): p. 499-504.